

SAMPLING METHODS FOR PARAMETRIC NON-BANDLIMITED SIGNALS: EXTENSIONS AND APPLICATIONS

THÈSE N° 3058 (2004)

PRÉSENTÉE À LA FACULTÉ INFORMATIQUE ET COMMUNICATIONS

Institut de systèmes de communication

SECTION DES SYSTÈMES DE COMMUNICATION

ÉCOLE POLYTECHNIQUE FÉDÉRALE DE LAUSANNE

POUR L'OBTENTION DU GRADE DE DOCTEUR ÈS SCIENCES

PAR

Irena MARAVIC

M.Sc. in Electrical Engineering, California Institute of Technology, Etats-Unis
et de nationalité serbe et monténégrine

acceptée sur proposition du jury:

Prof. M. Vetterli, directeur de thèse

Dr T. Blu, rapporteur

Prof. U. Mitra, rapporteur

Prof. K. Ramchandran, rapporteur

Lausanne, EPFL
2004

THESE NO. 3058 (2004)

*Thèse présentée à la faculté informatique et communications
pour l'obtention du grade de Docteur ès Sciences.*

Prof. Martin Vetterli

Directeur de thèse

Prof. Kannan Ramchandran

Rapporteur

Prof. Urbashi Mitra

Rapporteur

Dr. Thierry Blu

Rapporteur

Sous la présidence du Prof. Emre Telatar, le 5 Juillet 2004.

ECOLE POLYTECHNIQUE FEDERALE DE LAUSANNE, 2004.

Abstract

Sampling theory has experienced a strong research revival over the past decade, which led to a generalization of Shannon's original theory and development of more advanced formulations with immediate relevance to signal processing and communications. For example, it was recently shown that it is possible to develop exact sampling schemes for a large class of non-bandlimited signals, namely, certain signals with finite rate of innovation. A common feature of such signals is that they have a parametric representation with a finite number of degrees of freedom and can be perfectly reconstructed from a finite number of samples.

The goal of this thesis is to advance the sampling theory for signals of finite rate of innovation and consider its possible extensions and applications. In the first part of the thesis, we revisit the sampling problem for certain classes of such signals, including non-uniform splines and piecewise polynomials, and develop improved schemes that allow for stable and precise reconstruction in the presence of noise. Specifically, we develop a subspace approach to signal reconstruction, which converts a nonlinear estimation problem into the simpler problem of estimating the parameters of a linear model. This provides an elegant and robust framework for solving a large class of sampling problems, while offering more flexibility than the traditional scheme for bandlimited signals. In the second part of the thesis, we focus on applications of our results to certain classes of nonlinear estimation problems encountered in wideband communication systems, most notably ultra-wideband (UWB) systems, where the bandwidth used for transmission is much larger than the bandwidth or rate of information being sent. We develop several frequency domain methods for channel estimation and synchronization in UWB systems, which yield high-resolution estimates of all relevant channel parameters by sampling a received signal below the traditional Nyquist rate. We also propose algorithms that are suitable for identification of more realistic UWB channel models, where a received signal is made up of pulses with different pulse shapes. Finally, we extend our results to multidimensional signals, and develop exact sampling schemes for certain classes of parametric non-bandlimited 2-D signals, such as sets of 2-D Diracs, polygons or signals with polynomial boundaries.

Résumé

La théorie de l'échantillonnage a récemment été l'objet d'un nouveau intérêt de la part de la communauté scientifique. Nombreuses contributions ont amené à une généralisation de la théorie classique de Shannon avec un impact direct pour le traitement du signal et les systèmes de communications. Par exemple, il a été démontré qu'une large classe de signaux à bande non limitée peuvent être reconstruits à partir d'un nombre fini d'échantillons. Il s'agit de signaux à taux fini d'innovation, qui ont la caractéristique commune d'avoir une représentation paramétrique avec un nombre fini de degrés de liberté, et de pouvoir être reconstruits à partir d'un nombre fini d'échantillons.

Ce travail de thèse apporte une contribution à la théorie d'échantillonnage pour les signaux à taux d'innovations fini et il explore les extensions et applications de cette théorie. Dans sa première partie, nous présentons la théorie de d'échantillonnage pour une sous classe des signaux à taux fini d'innovation, incluant des splines non uniformes et des polynômes par morceaux, ainsi que des méthodes robustes pour leur reconstruction précise à partir de données bruitées. Une attention particulière est consacrée à la méthode par sous espaces, qui permet de transformer la reconstruction du signal d'un problème non linéaire à un problème linéaire. Nous obtenons ainsi une approche élégante et robuste pour résoudre une large classe de problèmes de reconstruction à partir d'un jeu fini d'échantillons, sans se restreindre aux signaux à bande limitée.

Dans la deuxième partie de ce manuscrit nous appliquons les résultats de notre approche à l'échantillonnage aux problèmes d'estimation dans les systèmes de communication à large bande, et en particulier aux systèmes "ultra-wideband" (UWB). Dans ces derniers, la bande utilisée pour la transmission est considérablement plus large que le taux d'information envoyée. Nous développons diverses méthodes fréquentielles pour l'estimation du canal et sa synchronisation dans les systèmes UWB. Celle-ci permettent d'obtenir des estimées à haute résolution des paramètres le plus relevant du canal, à partir d'un échantillonnage à une fréquence bien inférieure à celle classique de Nyquist. Nous proposons aussi des algorithmes qui sont adaptés à l'identification de modèles de canal UWB plus réalistes, où le signal reçu est composé de pulses de formes différentes.

Pour conclure, nous présentons une extension de nos résultats aux signaux multidimensionnels et nous développons des méthodes de reconstruction parfaites pour certaines classes de signaux paramétriques 2-D à bande non limitée, comme les Diracs 2-D, les polygones ou les signaux à enveloppes polynomiales.

Acknowledgements

I would like to thank:

My advisor, Martin Vetterli, for his guidance, support and his incredible patience with my ever-changing mood.

My LCAV/LCM colleagues, especially Paolo, Pietro, Rajesh, Nino and Chris, for their friendship, and Jocelyne Plantefol for all her help.

My Caltech advisor, Demetri Psaltis, for his early guidance and support over the years, and two great ladies, Lucinda Acosta and Yayun Liu, who made me feel at home.

My “other” friends, George, Bojan, Milos, Ivanuska, Dragana and Xiaolin, for their love and support.

And finally, my family, for all of the above and much more.

Lausanne, July 2004.

Contents

Abstract	i
Résumé	iii
Acknowledgements	v
List of Figures	xi
1 Introduction	1
1.1 Motivation	1
1.2 Problem Statement	3
1.2.1 Sampling schemes in the presence of noise	4
1.2.2 Alternative computational tools and methods for resolution improvement	4
1.2.3 Communication applications	5
1.2.4 Extension to two-dimensions	6
1.3 Related Work	6
1.3.1 Sampling theory and model-based signal analysis	6
1.3.2 Two-dimensional sampling theory	8
1.3.3 Applications to wideband communications	8
1.4 Thesis Outline	9
List of Acronyms	1
2 Fundamentals of Sampling Theory for Signals with Finite Rate of Innovation	11
2.1 Signals with Finite Rate of Innovation	12
2.2 Periodic Stream of Diracs: Continuous-Time Case	13
2.2.1 Frequency domain formulation	13
2.2.2 Annihilating filter method	14
2.3 Subspace-Based Approach	17
2.3.1 Subspace solution based on the shift-invariance property	17
2.3.2 Relation between the subspace and the polynomial estimator	20
2.4 Performance Evaluation	21
2.5 Extensions of the Subspace Methods	23
2.5.1 Estimation of closely spaced Diracs: increasing the resolution	23
2.5.2 Constructing enhanced data matrix	25
2.6 Simulation Results	26
2.7 Conclusion	28

3	Sampling Methods in the Presence of Noise	31
3.1	Sampling Schemes in the Presence of Noise: Problem Statement . . .	32
3.2	Sampling Periodic Nonuniform Splines and Piecewise Polynomials . . .	34
3.2.1	Periodic nonuniform splines	34
3.2.2	Piecewise polynomials	35
3.2.3	Model mismatch	37
3.3	Aperiodic Signals of Finite Rate of Innovation	38
3.3.1	Streams of Diracs	38
3.3.2	Nonuniform splines	40
3.3.3	Piecewise polynomials	41
3.3.4	Practical realization of the Gaussian sampling schemes	41
3.4	Simulation Results	42
3.4.1	Periodic signals	42
3.4.2	Finite length signals	44
3.4.3	Model mismatch	45
3.5	Conclusion	47
4	High-Resolution Synchronization and Channel Estimation in Ultra-Wideband Systems	51
4.1	Channel Estimation at Low Sampling Rate	52
4.1.1	Problem statement	52
4.1.2	Bandpass sampling scheme	54
4.1.3	Subspace-based approach to channel estimation	55
4.2	Estimating More Realistic Channel Models	57
4.2.1	Theory	57
4.2.2	Algorithm outline	58
4.3	Improvements of the Subspace Method	59
4.3.1	Filter bank approach	59
4.3.2	Estimation from non-adjacent bands	59
4.4	Numerical Performance and Complexity	61
4.4.1	Analysis of noise sensitivity	61
4.4.2	Computational complexity and alternative solutions	63
4.5	Low-Complexity Rapid Acquisition in UWB Localizers	64
4.5.1	System model	64
4.5.2	Two-step estimation	65
4.6	Simulation Results	66
4.6.1	Timing performance	66
4.6.2	Two-step estimation	70
4.6.3	Estimation from non-adjacent bands	70
4.6.4	Timing in the case of a non-ideal channel	71
4.6.5	Higher-rank channel models	72
4.6.6	Joint pulse shape and delay estimation	73
4.7	Application to CDMA systems	75
4.7.1	Channel estimation	75
4.7.2	Joint time delay and angle estimation	76
4.7.3	Channel estimation in W-CDMA systems: simulation results	77
4.8	Conclusion	78

5	Sampling Methods for Classes of Periodic Non-Bandlimited 2-D Signals	81
5.1	Problem Statement	82
5.1.1	2-D Signals of Finite Complexity	83
5.2	Periodic Set of 2-D Diracs in Continuous Space	83
5.2.1	Fourier series	83
5.2.2	Annihilating filter approach: the separable case	84
5.2.3	Algorithm outline	85
5.3	Sampling schemes in the non-separable case	87
5.3.1	Subspace-based approach	88
5.3.2	Outline of the ACMP algorithm	88
5.4	Extension to Lines and Polygons	91
5.4.1	Line of finite length	91
5.4.2	Polygonal line	92
5.4.3	Bilevel 2-D signals	93
5.5	Numerical Performance and Algorithms in the Presence of Noise	93
5.5.1	Complexity	94
5.5.2	Noisy case	94
5.5.3	Estimation of the model order and model mismatch	95
5.6	Simulation Results	95
5.7	Conclusion	100
6	Extension to Aperiodic and Radon Transform Case	103
6.1	Gaussian Sampling Scheme	104
6.1.1	Point spread function	105
6.1.2	Noisy case	106
6.2	Sampling the Radon transform	108
6.3	Extension to More Complex Classes of Signals	111
6.3.1	Bilevel polygon	111
6.3.2	Bilevel signal with piecewise polynomial boundary	112
6.4	Conclusion	114
7	Conclusion	115
7.1	Summary	115
7.2	Future Research	117
	Bibliography	121
	Curriculum Vitae	129

List of Figures

2.1	<p>Periodic stream of Diracs <i>A periodic signal of length 10000, made up of 7 weighted Diracs, is passed through a lowpass filter and sampled uniformly at the critical rate, determined by the filter bandwidth. We considered 3 different filter bandwidths: $B_1 = [-500, 500]$, $B_2 = [-1000, 1000]$ and $B_3 = [-1250, 1250]$. (a) Magnitude of the signal spectrum and bands used for estimation. (b) MSE of location estimates versus SNR. Solid lines correspond to the case when the locations are randomly chosen according to a uniform distribution over the interval $[1, 10000]$, while dashed lines correspond to the MSE in the case when the average spacing between components is 20 (i.e. 0.2% of the signal period).</i></p>	27
2.2	<p>Periodic stream of Diracs: Improving the Resolution (a) MSE of location estimates for the original method and the matrix-shifting method vs. SNR. For the latter method, the error is plotted for different values of the shift parameter p. (b) MSE of location estimates vs. average spacing between the components. The MSE of the original method is compared to the MSE's of the interleaving technique and the subspace-shifting approach.</p>	29
2.3	<p>Annihilating filter method <i>We consider a periodic signal made up of $K = 7$ Diracs, randomly distributed over the interval $[1, 10000]$. The signal is filtered through a lowpass filter $B_1 = -[500, 500]$ and a uniform set of $N_t = 1000$ samples is taken from its lowpass version. (a) MSE of location estimates obtained by the subspace method vs. MSE obtained using the annihilating filter approach. In the latter case, we show the MSE for different values of the filter order. (b) MSE of the annihilating filter approach vs. the filter order, shown for two values of SNR.</i></p>	30
3.1	<p>Approximation of the derivatives of a Gaussian kernel (a) Magnitude of the first three terms in the Taylor series expansion of $H_\sigma^{(1)}(\omega)$. (b) First derivative Gaussian kernel and its approximated version. (c) Second derivative Gaussian kernel and its approximation. (d) Third derivative Gaussian kernel and its approximation.</p>	43
3.2	<p>Periodic nonuniform splines and piecewise polynomials (a) Noisy nonuniform spline (SNR=27dB) of degree $R = 1$ and reconstructed signal. The signal is reconstructed with an error of $MSE=0.0135$. The error is defined as $MSE = E\{(x_{est} - x)^2\}/E\{x^2\}$, where x_{est} and x denote respectively, the estimated signal and the original signal in one period. (b) Noisy piecewise linear signal (SNR=15dB) and reconstructed signal. MSE of reconstruction is $MSE=0.015$.</p>	44

3.3	<p>Aperiodic stream of Diracs: We consider a signal of length 1000, made up of K weighted Diracs (K is varied between 2 and 12), and sampled with the Gaussian kernel $e^{-t^2/2\sigma^2}$. Average spacing between the components is assumed to be $t_s = 60$. (a) MSE of position estimates vs. SNR, for $K = 6$, $\sigma = 35$. The MSE of the original method (i.e. with no weighting of the data matrix) is compared to the MSE obtained by the method from Section 3.3.1. (b) MSE of reconstruction vs. the width of the Gaussian kernel. The error is plotted as a function of the parameter σ/t_s (and is shown for different values of SNR), indicating a sensitivity of the method to the choice of the width σ. (c) MSE vs. σ/t_s, for different values of K. (d) MSE vs. number of Diracs K. For each value of K, we chose the optimal value of the kernel width σ, that is, the one which minimizes a reconstruction error. Dashed lines correspond to the MSE obtained by sampling the signal over two smaller time windows and finding local reconstruction in each window.</p>	46
3.4	<p>Aperiodic piecewise constant signal (a) <i>Noisy piecewise constant signal (SNR=25dB)</i>. (b) <i>Gaussian kernel</i>. (c) <i>Filtered signal</i>. (d) <i>Noisy signal and reconstructed piecewise constant signal. The signal is reconstructed from $N = 160$ samples, with an error of $MSE = 6 \cdot 10^{-3}$</i>. (e) <i>Reconstruction error vs. SNR for different number of samples. The error is defined as $MSE = E\{(x_{est} - x)^2\}/E\{x^2\}$</i>.</p>	48
3.5	<p>Model mismatch: unknown model order (a) <i>The periodic signal made up of 15 weighted Dirac pulses, with 8 pulses being dominant</i>. (b) <i>Reconstructed dominant components</i>.</p>	49
3.6	<p>Model mismatch: unknown signal model (a) <i>Piecewise polynomial signal, noisy signal and the piecewise constant approximation</i>. (b) <i>Original signal and reconstructed lowpass version using Shannon's interpolation formula</i>.</p>	49
4.1	<p><i>Receiver block diagram</i></p>	53
4.2	<p><i>Estimation from multiple bands: receiver block diagram</i></p>	61
4.3	<p>System model (a) <i>The transmitted (single) UWB pulse is assumed to have an ideal first-derivative Gaussian shape. We considered the channel model (4.1), with six propagation paths and one dominant path (containing 70% of the total power). The received pulse is made up of six attenuated and delayed replicas of the transmitted pulse</i>. (b) <i>A coded sequence of 127 UWB impulses (red) is periodically transmitted over multiple cycles, while the sequence duration spans approximately 20% of the cycle time T_c. Coding is achieved with a PN sequence of length 127, and the relative delay between the transmitted pulses is 20 samples. The received signal (blue) is dominated by noise. In this case, the received signal-to-noise ratio is SNR=-15dB</i>.</p>	67
4.4	<p>Timing recovery in UWB systems (a) <i>Root-mean square error (RMSE) of delay estimation (in terms of number of samples) vs. SNR, for the case with one dominant path. We compare performances of the SVD-based algorithm and the Power method for several values of the sampling rate N_s. N_n denotes the Nyquist rate</i>. (b) <i>RMSE of t-delay estimation (SNR=0dB) for the annihilating filter and the SVD-based method, and this for different values of Q, which denotes the polynomial degree (annihilating filter method) or the number of columns in the data matrix \mathbf{Y}_s (SVD-based method). N is the total number of samples used for estimation</i>.</p>	68

4.5	Timing recovery: the case with two dominant paths (a)	<i>RMSE of delay estimation of the two dominant components vs. relative time delay (i.e. peak-to-peak delay) between the pulses. We show the performance of the original subspace algorithm ($d = 1$) and the modified (subspace-shifting) algorithm from Section 4.1.3 ($d = 8, 12, 16$), assuming that $N_s = N_n/5$ and $SNR = -5dB$. (b) <i>RMSE of delay estimation vs. received SNR, and this for the original algorithm ($d = 1$) and the subspace-shifting method ($d = 8$). The sampling rate is $N_s = N_n/5$, while the relative delay between the dominant components equals the pulse duration. In both cases, we plot the RMSE obtained with the SVD-based method and the method of Orthogonal iteration.</i></i>	69
4.6	Two-step delay estimation (a)	<i>Coarse synchronization is obtained by sampling the received signal uniformly (over the entire cycle) at a low rate $N_l = N_n/20$. For low SNR's (less than -5dB) the samples are averaged over multiple cycles (dashed line). Once a rough estimate of the sequence timing is obtained, fine synchronization follows: the signal is sampled only within a narrow window, yet at a higher rate $N_h = N_n/2$. RMSE of time delay estimation is compared to the RMSE obtained with high-rate uniform sampling over the entire cycle. (b) <i>RMSE of delay estimation for different combinations of N_l (the sampling rate for coarse synchronization) and N_h (the sampling rate for fine synchronization). N_c denotes the number of averaging cycles during each phase, chosen such that the total power consumption remains constant.</i></i>	71
4.7	Estimation from non-adjacent bands (a)	<i>Normalized power spectral density (PSD) of the received pulse and frequency bands used for estimation. (b) <i>The channel is estimated from bands B_1 and B_2 (no interference) and the delay estimation performance is compared to the case when B_1 and B_3 are sampled (strong interference in B_2).</i></i>	72
4.8	Timing recovery in non-ideal channels (a)	<i>Received waveform (single pulse, including multipaths) and transmitted pulse. (b) <i>Normalized power spectral density (PSD) of the received pulse and frequency bands used for estimation. (c) <i>Timing estimation performances of the SVD-based method and the matched filter approach. The sampling rate for the SVD approach is $N_s = 0.1N_n$ (the band B_1 is sampled), $N_s = 0.2N_n$ (B_1 and B_2 are sampled) and $N_s = 0.3N_n$ (B_2 and B_3 are sampled), while for the matched filter $N_s = N_n$.</i></i></i>	73
4.9	Higher-rank channel models (a)	<i>Received UWB signal made up of 70 pulses, with 8 components being dominant (containing approximately 85% of the total power). (b) <i>RMSE of delay estimation of the dominant components vs. SNR.</i>(c) <i>Effects of quantization on the RMSE of delay estimation for 4-7 bit receiver architectures. The results are compared to the case when the number of bits is $n_b = 32$. The sampling rate is one fourth the Nyquist rate ($N_s = N_n/4$).</i></i>	74

4.10	Joint pulse shape and delay estimation (a) Received noisy signal (blue) and the noiseless signal made up of three short pulses having different shapes (red). (b) Estimated shape of the first pulse. (c) Estimated shape of the second pulse. (d) Estimated shape of the third pulse. The received signal is sampled at one fifth the Nyquist rate ($N_s = N_n/5$). We used a polynomial of order $R = 20$ to approximate the DFT coefficients of the received signal. (e) Estimated second pulse in the case when the sampling rate is increased to $N_n = N_n/3$. No spectral extrapolation is used. (f) Estimated second pulse from (e) using spectral extrapolation along with the exponential weighting of the approximated DFT coefficients.	79
4.11	Channel estimation in CDMA systems Average timing synchronization error (normalized to T_c) in the multiuser case vs. sampling rate. We assumed a non-fading channel. The signature sequence is of length 511. (d) Comparison of timing estimation errors in single-path and multipath channels (3 received components of equal power).	80
4.12	Channel estimation in CDMA systems - Joint angle and delay estimation (a) Normalized angle and delay estimation errors vs. number of sensors in the antenna array S . The signature sequence assigned to a user is of length 511. (b) Normalized angle and delay estimation errors vs. sampling rate.	80
5.1	Sampling Setup Analog signal $g(x, y)$ is prefiltered with $h(x, y) = \varphi(-x, -y)$ (anti-aliasing step). The sampled signal is given by $g_s(p, q) = \sum_{p, q \in \mathbb{Z}} g_f(x, y) \delta(x - p, y - q)$	82
5.2	The Annihilating Filter Method. (a) Two-dimensional signal made up of $M = 9$ weighted Diracs (b) 2-D sinc sampling kernel of bandwidth $[-M\omega_0, M\omega_0] \times [-\omega_0, \omega_0]$ (c) Lowpass approximation obtained by convolving the signal with the sinc function (d) Reconstructed signal.	96
5.3	The ACMP algorithm. (a) Signal made up of $M = 9$ weighted Diracs that have common components along both directions (b) Sinc sampling kernel of bandwidth $[-M\omega_0, M\omega_0] \times [-M\omega_0, M\omega_0]$ used in the algorithm (c) Lowpass approximation of the signal.	97
5.4	Numerical Performance vs. Average Spacing of the Diracs. The numerical behavior of the algorithms is tested for different values of the average spacing (normalized to one period) of M Diracs in the set, as well as for different values of M . (a) Average reconstruction error for the annihilating filter algorithm (b) Average reconstruction error for the ACMP algorithm.	98
5.5	Model mismatch (a) Set of $M = 8$ weighted Diracs with $K = 5$ Diracs being dominant, all having the same weights $a_n = 10$, while the rest have weights $a_n = 3$. (b) Reconstructed signal. We assumed that the model order is $M = 5$ and used the ACMP algorithm to reconstruct the signal. Only the dominant components are extracted, with the reconstruction error of $RMSE=0.006$. (c) Average reconstruction error for different values of the ratio of amplitudes $\frac{A_{\text{dominant}}}{A_{\text{non-dominant}}}$ as well as for different number of non-dominant components in the set for the ACMP method	99

5.6	Performance in the presence of noise. <i>RMSE versus SNR for different values of the oversampling factor. We consider the signal made up of 8 Diracs with equal weights. The method was tested for different values of SNR and different values of the bandwidth of the sampling kernel B_s.</i>	100
5.7	Set of Finite Lines. (a) <i>Signal made up of two finite lines</i> (b) <i>Lowpass approximation obtained by convolving the signal with the sinc kernel of bandwidth $[-4\omega_0, 4\omega_0] \times [-\omega_0, \omega_0]$</i> (c) <i>Reconstructed set of lines.</i>	101
5.8	Bilevel Polygon. (a) <i>Bilevel pentagon. The signal has $2M = 10$ degrees of freedom</i> (b) <i>Lowpass approximation obtained by convolving the signal with the sinc kernel of bandwidth $[-2M\omega_0, 2M\omega_0] \times [-\omega_0, \omega_0]$</i> (c) <i>Polygonal line reconstructed with the annihilating filter method and the original polygonal line.</i> (d) <i>Polygonal line reconstructed with the state space method. In this case the line is reconstructed with an RMSE of less than 10^{-4}.</i>	102
6.1	Finite Set of 2-D Diracs. (a) <i>Two-dimensional signal made up of $M = 17$ weighted Diracs</i> (b) <i>Gaussian sampling kernel</i> (c) <i>Convolution of the signal with the sampling kernel</i> (d) <i>Reconstructed signal with an RMSE of less than 10^{-8}.</i>	105
6.2	Numerical Precision vs. Width of the Gaussian Kernel. <i>The signal from Figure 6.1(a) is sampled with the Gaussian kernel $e^{-\frac{x^2+y^2}{2\sigma^2}}$. The parameter σ is varied between $0.03T$ and $25T$, where T denotes the spacing between adjacent samples. The reconstruction error is plotted as a function of $\frac{\sigma}{T}$, indicating a strong sensitivity to the choice of the width σ.</i>	106
6.3	Point spread function. (a) <i>Two-dimensional signal made up of $M = 17$ weighted Diracs, convolved with a Gaussian PSF.</i> (d) <i>Reconstructed signal with an RMSE of less than 10^{-7}.</i>	107
6.4	Performance of the 2-D Gaussian sampling scheme. <i>RMSE of location estimates versus SNR for different values of the oversampling factor. We consider the signal made up of 8 Diracs with equal weights, randomly distributed over $[1, 100] \times [1, 100]$, sampled with the 2-D Gaussian kernel, with parameter $\sigma = 7$. The method was tested for different values of SNR and different values of the oversampling factor.</i>	108
6.5	Radon transform of the set of Diracs <i>The projection of a set of M weighted 2-D Diracs onto an arbitrary line is a stream of at most M weighted 1-D Diracs.</i>	109
6.6	Reconstruction of the Set of 2-D Diracs. (a) <i>2-D signal consisting of $M = 3$ weighted Diracs</i> (b) <i>Reconstruction of the signal from projecting lines obtained by sampling the Radon transform of the signal with a Gaussian kernel. Points where exactly $M + 1 = 4$ lines intersect correspond to the Diracs in the set.</i>	110
6.7	Bilevel polygon <i>The projection of a bilevel polygon is a piecewise linear signal. For the signal with M vertices, $2M$ sample values of the Radon transform taken from each of its $M + 1$ different projections uniquely define the signal.</i>	112
6.8	Reconstruction of a bilevel triangle. (a) <i>Bilevel triangle</i> (b) <i>Reconstructed (and original) boundary. The reconstructed boundary is obtained by taking a set of filtered projections with a Gaussian kernel along $M + 1 = 4$ different directions.</i>	113

Chapter 1

Introduction

1.1 Motivation

Sampling theory treats a very fundamental problem, with so many practical repercussions, that it lies at the core of signal processing and communications. Sampling is all about representing a continuous-time signal $x(t)$ by a discrete set of values $x[n]$, $n \in \mathbb{Z}$. Often, in practice, instead of sampling the waveform itself, one has access only to its filtered version. If $x(t)$ is the original waveform, its filtered version is given by $y(t) = x(t) * \tilde{h}(t)$, where $\tilde{h}(t) = h(-t)$ is the convolution kernel. Then, uniform sampling with a sampling interval T_s yields samples $y(nT_s)$, which can be expressed as

$$y(nT_s) = \langle x(t), h(t - nT_s) \rangle = \int_{-\infty}^{\infty} x(t)h(t - nT_s)dt. \quad (1.1)$$

Now the key question that arises is the following. Under what conditions is the original signal $x(t)$ uniquely defined by its samples $y(nT_s)$? The crucial result was stated by Shannon in 1949, in the form of the following sampling theorem [71] [72]:

Theorem 1. [*Shannon's Sampling Theorem*] If $x(t)$ is bandlimited to ω_m , that is, $X(\omega) = 0$, $|\omega| > \omega_m$, then $x(t)$ is uniquely determined by its samples taken at twice ω_m or $x(n\pi/\omega_m)$.

The reconstruction formula that complements the sampling theorem is given by

$$x(t) = \sum_{n \in \mathbb{Z}} y(nT_s) \text{sinc}(t/T_s - n), \quad (1.2)$$

where the uniform samples of $y(nT_s)$ can be interpreted as coefficients of basis functions obtained by appropriate shifting and scaling of the sinc function $\text{sinc}(t) = \sin(\pi t)/(\pi t)$.

While Shannon must get full credit for formalizing this result and realizing its potential for communication theory and signal processing, equivalent forms of the theorem had already appeared in the mathematical literature at the time, in particular, in the work of Whittaker [91] and Kotel'nikov [36] [37]. Although this result is very elegant and has proven to be extremely fruitful, there are two

main problems associated with it. First, it is an idealization: real world signals or images are rarely bandlimited. And secondly, the reconstruction formula (1.2) is almost never used in practice, especially with images, due to the slow decay of the sinc function [60]. Instead, most of the reconstruction methods that are currently in use, rely on simpler techniques such as linear interpolation [7] [8].

Recently, sampling theory has experienced a strong research revival, mainly due to the intense activity taking place around wavelets, which led researchers to reexamine some of the foundations of Shannon's original theory and develop more advanced formulations with immediate relevance to signal processing and communications. For example, a modern, Hilbert-space formulation reinterprets the standard sampling system as an orthogonal projection operator that computes the minimum error bandlimited approximation of an input signal that is not necessarily bandlimited. This concept also extends to the class of spline-like or shift-invariant spaces, spanned by a generating function and its uniform shifts [80]. That is, by replacing the $\text{sinc}(t)$ function in (1.2) by a more general template or the *generating function* $\varphi(t)$, one can specify the basic approximation space V as

$$V(\varphi) = \{f(t) = \sum_{n \in \mathcal{Z}} c(n)\varphi(t - n)\}. \quad (1.3)$$

This means that any function $f(t) \in V(\varphi)$ is characterized by a sequence of coefficients $c(n)$, that is, its discrete representation [80]. A direct consequence of the above formulation is that signals that belong to the space V can be perfectly reconstructed, which can be considered as a more abstract formulation of Shannon's theorem. However, this result cannot be extended to the general case of non-bandlimited signals, and typically, only the projection of the signal onto a specific subspace can be reconstructed.

In recent work by Vetterli, Marziliano and Blu [85], it was shown that it is possible to develop exact sampling schemes for some classes of signals that are neither bandlimited nor live on shift-invariant spaces, namely, certain signals with *finite rate of innovation*. Examples include streams of Diracs, non-uniform splines and piecewise polynomials. A common feature of such signals is that they have a parametric representation with a finite number of degrees of freedom per unit of time, or finite rate of innovation ρ , and can be perfectly reconstructed from a set of samples taken at a rate $R \geq \rho$, after appropriate smoothing. The key in all constructions is to identify the innovative part of a signal, such as time instants of Diracs, using an annihilating or locator filter, a well-known tool from spectral analysis [74] or error correction coding [6]. This allows for standard computational procedures for solving the sampling problem for a wide class of non-bandlimited signals and leads to some interesting results.

The notion of "rate of innovation" can be also related to the classical Shannon bandwidth [54], which defines the dimension of the subspace (per unit of time) that allows one to represent the space of signals of interest. For example, in the case of bandpass signals, where the Nyquist rate can be very large, Shannon bandwidth is the correct notion [20]. Still, there are some differences between the two concepts. In systems that use pulse position modulation (PPM) [62], Shannon bandwidth is proportional to the number of possible positions inside a given interval, whereas the rate of innovation is fixed, and is related to the number of degrees of freedom of the signal per interval.

The above discussion indicates that one of the most promising applications of the new sampling results can be found in communication systems with bandwidth expansion, such as ultra-wideband (UWB) systems, where the bandwidth used to transmit the information is much larger than the rate of information being sent. UWB systems use trains of pulses of very short duration, typically on the order of a nanosecond, thus spreading the signal energy over a bandwidth of up to a few gigahertz. However, due to the extreme bandwidths involved, the design of digital UWB receivers can be a very challenging task, as it would require very fast and expensive A/D converters (operating in the gigahertz range) and thus lead to prohibitively high costs in terms of power consumption and receiver complexity. Yet the rate of innovation of a received UWB signal is related to the symbol rate, which can be orders of magnitude lower than the Nyquist rate. Thus, using the new sampling results, one can sample the received signal at a rate that is lower than the Nyquist rate, and still be able to recover the signal. Similar arguments can be used to sample a filtered stream of Diracs, known as shot noise, which may be of interest not only to communications, but to biological signal processing as well. For example, in neurophysiology, signals are often modeled as shot noise, and one can expect to be able to recover the signal by sampling it at a low rate.

One can even look further and try to generalize the results to multidimensional signals, specifically to images, where the bandlimited property almost never holds. In particular, one can consider classes of signals with “finite complexity”, and develop sampling schemes that allow for perfect reconstruction from a finite set of samples. Compared to existing multidimensional sampling techniques, such an approach will provide a more elegant solution to the sampling problem for some classes of parametric non-bandlimited signals, but would also lead to an efficient representation for such signals. One possible application can be found in super-resolution videogrammetry, where the position of 3-D objects can be determined with a sub-pixel precision by locating some clearly marked features, such as points or edges, using a set of low-resolution 2-D images taken from various angles. Other possible applications include astronomical image processing, tomography, medical imaging and image compression.

These and similar problems suggest that the subject of sampling is far from being closed and that its importance will most likely grow in the future with the increasing trend to replace analog systems with digital ones.

1.2 Problem Statement

The discussion from the previous section presents a strong motivation for advancing the sampling theory for signals that belong to finite-dimensional non-linear spaces, and more importantly, for exploring its possible applications. The results outlined so far obviously raise a number of questions. What algorithms can be used to reconstruct a signal from the set of its samples and are those methods computationally feasible and stable? What other computational tools, potentially more efficient than the annihilating filter, can be used to identify innovation? What are possible extensions of these results and practical problems encountered in certain applications?

The first question was partially addressed in [85], since the authors considered only the class of deterministic noiseless signals. In such a case, the problem

of numerical instability of the developed schemes was not an issue. However, the potential problem with ill-conditioning in the presence of noise, along with other problems we mentioned, calls for novel constructions that can be efficiently used in practice. In particular, our aim in this thesis is following:

- Revisit the sampling problem for signals of finite rate of innovation and develop improved sampling schemes that allow for stable and precise reconstruction in the presence of noise.
- Develop alternative computational tools that can extract relevant information about the signal more efficiently and with higher precision.
- Explore applications of the new sampling results to communication problems.
- Extend the results to the two-dimensional case.

To provide more insight into the subject we studied, in the sequel, we briefly explain the relevant problems related to each of these topics.

1.2.1 Sampling schemes in the presence of noise

In order to prove sampling theorems, Vetterli et al. considered only a class of deterministic, noiseless signals. While in such a case the developed schemes lead to perfect reconstruction by sampling the signal at (or above) the rate of innovation, many of those methods involve steps that can result in numerical ill-conditioning in the presence of noise. For example, it was shown that the problem of reconstructing non-uniform splines can be reduced to the problem of reconstructing streams of Diracs (which allows for an elegant mathematical solution) by taking a sufficient number of signal derivatives. However, when noise is present, such an approach often results in an ill-conditioned problem, where standard techniques, including oversampling and solving various systems using the singular value decomposition, are not sufficient for improving the numerical performance. In the case of piecewise polynomials, the method from [85] uses derivation as well, leading to a sum of derivatives of Diracs. In addition to noise amplification, such an approach requires identification of multiple roots of the annihilating filter, a task that is difficult even in the noiseless case. This naturally calls for a revision of some of the techniques presented in [52] [85] and development of alternative algebraic approaches and computational tools that can solve the problem of ill-conditioning in the presence of noise and lead to precise reconstruction.

1.2.2 Alternative computational tools and methods for resolution improvement

The sampling methods developed [85] rely on identifying the innovative part of a signal using an annihilating (or prediction) filter, where the exact information about the discontinuities can be extracted from the zeros of the annihilating filter, modeled as an FIR filter. This converts a nonlinear estimation problem to the linear parameter estimation problem of the polynomial model. The polynomial realization of the estimator was first suggested by Prony in 1975 [63], and

has received much attention in the spectral estimation literature. However, such an approach has certain limitations. In particular, in order to reduce sensitivity of the parameter estimates to noise, typically a high order polynomial must be used [32], which imposes a significant computational burden since it is necessary to find roots of a large size polynomial in order to extract a small number of signal poles. In addition to increased computational requirements, overmodeling gives rise to spurious filter zeros, which can be incorrectly identified as signal poles. We will thus develop an alternative, subspace algorithm for signal reconstruction, based on state space modeling [65], which avoids root finding and relies only on a proper deployment of matrix manipulations. We will show that such an approach yields robust parameter estimates, not by overmodeling, but by appropriately exploiting the algebraic structure of the signal subspace.

Another problem that we investigated in the context of model-based spectral estimation is the possibility of improving the resolution performance in the case when the signal contains closely spaced frequencies. This problem arises, for example, in applications such as time delay estimation in multipath channels, where both statistical analysis and practice have shown that the estimation performance of parametric methods can degrade significantly if a received signal has closely spaced components. It is thus of interest to explore techniques that can improve the resolution capability of existing methods, without increasing their computational complexity. Namely, since the performance of parametric methods depends strongly on the eigenstructure of an associated data matrix, the idea is to use alternative ways for constructing such a matrix from the same data set. This can improve matrix conditioning and yield better estimation accuracy.

1.2.3 Communication applications

One of the most interesting applications of the new sampling framework is in certain classes of non-linear estimation problems in ultra-wideband communication systems. Ultra-wideband technology has recently received much attention due to the benefits of an extremely wide transmission bandwidth, such as very fine time resolution for accurate ranging and positioning and multipath fading mitigation in indoor wireless networks [16] [25] [94]. The same properties that make UWB a promising candidate for a variety of new applications also bring new challenges to both the analysis and practice of reliable systems. One of the main design challenges is rapid synchronization, as its accuracy and complexity directly affect the system performance. In this context, it is of interest to explore low-complexity methods for channel estimation and synchronization in digital ultra-wideband receivers, which would yield high-resolution estimates of all relevant channel parameters by sampling a received signal below the Nyquist rate. Such an approach would allow for faster acquisition compared to proposed digital solutions and potentially reduce power consumption and complexity of digital UWB receivers significantly. In addition, it is of interest to develop algorithms that are suitable for identification of more realistic UWB channel models, where a received signal is made up of pulses with different pulse shapes.

1.2.4 Extension to two-dimensions

The new sampling framework led to many interesting results for the 1-D case and the next logical step was to generalize the concept to multidimensional signals. Compared to existing multidimensional sampling techniques, such an approach can provide a more elegant solution to the sampling problem for some classes of parametric signals, and also lead to efficient representation for such signals. However, the problem becomes more complex when going to higher dimensions and does not necessarily allow for direct extensions of 1-D formulations. Still, we will show that it is possible to develop exact sampling schemes and reconstruction formulas for some classes of non-bandlimited signals, such as sets of 2-D Diracs, polygons or signals with piecewise polynomial boundaries. We will focus on developing sampling schemes for signals with M degrees of freedom that require on the order of M (or at most $\mathcal{O}(M^2)$) samples, and algorithms that can recover such signals with high numerical precision, regardless of the signal complexity (e.g. the value of the parameter M) or signal structure.

1.3 Related Work

Perhaps one of the most appealing aspects of the subject of this thesis is its interdisciplinary nature. Topics that we cover range from sampling theory and model-based signal analysis, to some system-design problems such as channel estimation and synchronization in communication systems. These topics have been traditionally studied by different communities, yet, we will take a signal processing point of view and put the emphasis on developing practical algorithmic solutions.

1.3.1 Sampling theory and model-based signal analysis

The first part of the thesis is related to sampling theory for classes of non-bandlimited signals with finite rate of innovation. In this context, this part is a follow-up to the work of Vetterli, Marziliano and Blu [85] [52], where it was shown that certain classes of such signals allow for uniform sampling after appropriate smoothing and perfect reconstruction from a set of samples. In particular, the authors concentrated on noiseless, deterministic signals like streams of Diracs, nonuniform splines and piecewise polynomials, and derived exact reconstruction formulas from a set of samples taken at the rate of innovation. Some extensions of these results to other classes of signals, including piecewise bandlimited signals, are presented in [52].

At this point, it is interesting to note that the concept of sampling “at the rate of innovation” is not entirely new. In 1977, Papoulis introduced a powerful generalization of Shannon’s sampling theory, showing that a bandlimited signal can be perfectly reconstructed from the samples of the response of m linear shift-invariant systems, sampled at $1/m$ -th of the Nyquist rate [59]. The basis for this kind of formulation is that there are many different ways to extract the information about the signal, provided that the number of measurements is greater than or equal to the number of degrees of freedom of the signal. Typical cases of generalized sampling are interlaced and derivative sampling [43] [90]. Djokovic and Vaidyanathan applied similar ideas for the reconstruction of functions in certain wavelet spaces [21]. A further step was taken by Unser and

Zerubia, who generalized the concept to the reconstruction in shift-invariant spaces $V(\varphi)$, with no constraint on the input signal [79]. However, instead of obtaining perfect reconstruction, which is not possible for signals that do not belong to $V(\varphi)$, they looked for an approximate solution that is consistent in the sense that it yields the same measurements when reinjected in the system.

The sampling problem considered in [85] apparently differs from other problems in sampling theory in the following way: the space of signals which was considered, and for which perfect reconstruction schemes were developed, is not a shift-invariant vector space (e.g. the bandlimited space or spline spaces), but rather a union of shift-invariant spaces of finite dimension [45]. As a result, reconstruction methods rely on identifying the innovative part of a signal from the set of samples obtained after appropriate smoothing. In particular, the idea is to use algebraic transformations that convert the samples into a sum of exponentials (complex or real), and reduce the problem of reconstructing the unknown signal parameters into the classical spectral estimation problem, that is, the problem of estimating the parameters of superimposed exponentials. Such a problem is a prototype of a class of nonlinear estimation problems that appear in a vast range of signal processing applications, including power spectrum estimation of a stochastic process, time delay estimation, direction finding of a narrowband source, among others [58] [74] [65]. For these and closely related problems, model-based methods provide an elegant tool for exposing the structure of an underlying signal [65] [74]. Such methods assume that the signal satisfies a generating model of known functional form, and then proceed in estimating the parameters of the assumed model.

There are several classes of model-based estimation algorithms that have received a considerable attention in the literature. In [65] [74], a polynomial realization of the estimator is discussed, where the signal parameters are estimated from zeros of the so-called prediction or annihilating filter. In [65], a state space method is proposed, which provides an elegant and numerically robust tool for parameter estimation using a subspace-based approach. The ESPRIT algorithm is developed in [58], which can be viewed as a generalization of the state space method applicable to general antenna arrays. In [33], several subspace techniques for estimating generalized eigenvalues of matrix pencils are addressed, such as Direct matrix pencil algorithm, Pro-ESPRIT and its improved version TLS-ESPRIT.

Model-based techniques have been also extended to two-dimensional signals and used in communication applications, for example in joint time delay and angle of arrival estimation. However, the problem of estimating 2-D exponentials is a much more involved task than in the case of 1-D signals, since it is not generally separable. Among the earliest spectral estimation techniques that addressed the non-separable case was the MEMP algorithm (Matrix Enhancement and Matrix Pencil) [34]. The method introduces two so-called “enhanced matrices”, from which the sets of frequencies in each dimension could be obtained separately, yet an additional step is required to form the correct pairs of 2-D frequencies. This often involves a costly minimization procedure, making this algorithm unattractive due to its computational cost. In response to that, there has been a lot of work toward developing high-resolution methods that would link the estimation problems in both dimensions [28] [69] [81]-[84]. Among them are the ACMP algorithm (Algebraic Coupling of Matrix Pencils), and the so-called 2-D ESPRIT [69].

1.3.2 Two-dimensional sampling theory

Most of the work on two-dimensional sampling theory is related to bandlimited signals. For instance, in [11], it was shown that Papoulis' generalized sampling theory can be extended to multidimensional bandlimited signals as well. While the problem of image reconstruction from a regularly sampled data is relatively straightforward, other types of sampling require more complex reconstruction procedures. One such example is the problem of reconstructing a signal from non-uniformly spaced samples, where the exact analysis becomes quite involved [3]. A different approach, which arises in the tomographic imaging problem, is concerned with sampling the Radon transform of the signal, rather than the signal itself [9] [67]. Specifically, the idea is to reconstruct an image from a set of its line-integral projections at different angles [18], and existing reconstruction methods are typically based on the so-called Fourier slice theorem [18] [55]. Such methods use interpolation in order to transform the Fourier projection data from the polar to Cartesian grid, from which the reconstruction can be obtained by an inverse FFT. Recently, Basu and Bresler proposed a fast reconstruction algorithm which can be considered as an improved version of the standard "filtered backprojection" (FBP) algorithm, as it uses a hierarchical decomposition of the backprojection operator [2]. However, all the algorithms we mentioned are developed primarily for bandlimited signals and assume that signal projections are available for a large number of directions.

Discrete tomography represents another whole area of research, which we mention here only briefly to make the connection with some of the topics addressed in the thesis. For example, in [29], the authors consider the problem of reconstructing plane figures from only two projections, and formulate the necessary and sufficient conditions for a unique reconstruction. Namely, the argument is based on the limit process from the reconstruction for the discrete approximation by small squares. We should note that the discrete version of this problem falls in the category of combinatorial theory, known as reconstruction of binary matrices, that is, the problem of finding a matrix with only two entries, 0 and 1, given the number of non-zero elements in each row and each column. As a result, all existing algorithms are iterative in nature and may (or may not) converge to the exact solution. In this thesis, we will investigate alternative, non-iterative reconstruction algorithms that allow for perfect reconstruction from a finite number of projections and a finite number of samples in each direction.

1.3.3 Applications to wideband communications

The use of subspace techniques for certain problems in wideband communication systems, such as channel estimation in code division multiple access (CDMA) systems has appeared in the literature [4] [23] [61] [78]. Yet almost all existing methods solve for the desired parameters from a sample estimate of the covariance matrix and resort to the Nyquist sampling rate (or even use fractional sampling). Clearly, applying such techniques to ultra-wideband systems would require sampling rates on the order of GHz and computational requirements not affordable in most UWB applications. Similarly, conventional techniques based on sliding correlators would require very fast and expensive A/D converters (operating in the gigahertz range) and thus high power consumption.

Besides, implementation of such techniques in digital systems would have almost unaffordable complexity in real systems as well as slow convergence time, since one has to perform exhaustive search over thousands of fine bins, each at the nanosecond level.

In order to improve the acquisition speed, several modified timing recovery schemes have been proposed, such as a bit reversal search [30], or the correlator-type approach which exploits properties of beacon sequences [25]. Even though some of these methods have already been in use in certain analog UWB systems, the need for very high sampling rates, along with the search-based nature of these methods, makes them less attractive for digital implementation. Recently, a family of blind synchronization techniques was developed [89], which takes advantage of the so-called cyclostationarity of UWB signaling, that is, the fact that every information symbol is made up of UWB pulses that are periodically transmitted (one per frame) over multiple frames. While such an approach relies on frame-rate rather than Nyquist rate sampling, it still requires large data sets in order to achieve good synchronization performance.

Another challenge arises from the fact that the design of an optimal UWB receiver must take into account certain frequency-dependent effects on the received waveform. That is, due to the broadband nature of UWB signals, the components propagating along different paths typically undergo different frequency-selective distortions [16] [94]. As a result, a received signal is made up of pulses with different pulse shapes, which makes the problem of optimal receiver design a much more delicate task than in other wideband systems [4] [61] [78]. In previous work [16], an array of sensors is used to spatially separate the multipath components, which is then followed by identification of each path using an adaptive method, the so-called Sensor-CLEAN algorithm. Due to the complexity of the method and the need for an antenna array, the method has been mainly used for UWB propagation experiments. Thus, developing simpler and faster algorithms for handling realistic channels which can be used in low-complexity UWB transceivers is still an open problem.

1.4 Thesis Outline

The thesis is organized as follows. In Chapter 2, we begin with defining classes of signals with finite rate of innovation and reviewing some basic sampling results for such signals, developed in [85]. We analyze in detail a signal made up of a periodic stream of Diracs, discuss some existing, and develop novel algorithmic tools that will be used in all our subsequent constructions. While some of the techniques we present, such as annihilating filters or subspace methods, have been already encountered in spectral estimation framework, we further explore preconditioning methods that lead to improved resolution performance in the case when the signal contains closely spaced components. Finally, we present performance analysis and show some simulation results.

In Chapter 3, we generalize the concept to more complex classes of periodic and finite-length signals with finite rate of innovation. We revisit the problem from [85] and propose improved, more robust methods that have better numerical conditioning in the presence of noise and yield more accurate reconstruction. For classes of periodic signals, such as piecewise polynomials and nonuniform splines, we propose novel algebraic approaches that solve the sampling problem

in the Laplace domain, after appropriate windowing. Building on the results for periodic signals, we extend our analysis to finite-length signals and develop schemes based on a Gaussian kernel, which avoid the problem of ill-conditioning by proper weighting of the data matrix.

In Chapter 4, we focus on applications of the new sampling framework to certain nonlinear estimation problems encountered in wideband communication systems. In particular, we consider the problem of low-complexity channel estimation and synchronization in digital ultra-wideband receivers. We develop a frequency domain framework that yields high-resolution estimates of all relevant channel parameters by sampling a received signal below the traditional Nyquist rate. Our framework allows for faster acquisition compared to current digital UWB receivers and potentially reduces power consumption and complexity of digital UWB receivers significantly. Furthermore, we show that it can be used for identification of more realistic channel models, where different propagation paths undergo different frequency-selective mitigation. We also extend our results to the case when the channel parameters are estimated from multiple frequency bands with the highest signal-to-noise ratio, which allows one to maximize the estimation performance, given a constraint on the acceptable sampling rate in a system. Finally, we present a multiresolution version of our framework and discuss its application to rapid acquisition in ultra-wideband localizers, showing unique advantages over existing techniques in terms of complexity, acquisition speed and power requirements.

In Chapter 5, we consider possible extensions of the new sampling results to the two-dimensional case. We focus on classes of parametric non-bandlimited 2-D signals that have a parametric representation with a finite number of degrees of freedom. While there are many such parametric signals, it is often difficult to propose practical sampling schemes, therefore, we concentrate on those classes for which we are able to give exact sampling algorithms and reconstruction formulas. We analyze in detail a periodic set of 2-D Diracs and extend the results to more complex objects such as lines and polygons. Unlike most multidimensional sampling schemes, the methods we propose perfectly reconstruct such signals from a finite number of samples in the noiseless case. Similarly to the 1-D case, some of the techniques we use are already encountered in the context of high-resolution harmonic retrieval. In particular, SVD-based methods and the annihilating filter approach are both explored as inherent parts of the developed algorithms.

In Chapter 6, we consider the problem of sampling aperiodic signals of finite complexity using a Gaussian sampling kernel. We also propose an alternative approach, which exploits the properties of a signal in the Radon transform domain. In particular, we show that by taking a finite number of “filtered” line integrals, the problem can be reduced to its one-dimensional equivalent, which is more convenient for algorithmic implementation. Such an approach allows us to develop exact sampling results for 2-D Diracs, polygons or signals with polynomial boundaries. That is, we demonstrate that by using an appropriate sampling kernel, one can perfectly reconstruct the signal from a finite set of samples of its Radon transform, which reduces the computational load compared to “true” two-dimensional schemes and allows for simpler reconstruction algorithms.

Finally, we conclude in Chapter 7 with a summary of our work and an outlook on future research.

Chapter 2

Fundamentals of Sampling Theory for Signals with Finite Rate of Innovation

In this chapter, we present some key sampling results for signals with finite rate of innovation and establish the mathematical framework that will be used as a basis in all subsequent developments. We review some of the techniques presented in [85], and develop alternative mathematical tools for solving the sampling problem, which allow for simpler reconstruction and better numerical performance in the presence of noise.

Some of the techniques we will be using are already encountered in the context of parametric spectral estimation [33] [58] [74] and model-based signal analysis [65]. In particular, we use algebraic methods that reduce a set of samples into a sum of exponentials, thus, the reconstruction problem can be broadly considered as the one of estimating the parameters of superimposed exponentials. This problem has been studied extensively in the literature and several classes of high-resolution or subspace methods have been already developed [65] [58] [74]. We focus on state space parameterization of a signal subspace [65], which allows us to use high-resolution techniques based on eigendecomposition of certain well-conditioned matrices [33] [65].

The outline of this chapter is as follows. In Section 2.1, we review classes of signals of finite rate of innovation that will be treated in the sequel. In Section 2.2, we consider the problem of sampling a periodic continuous-time signal made up of a stream of Diracs. Although this signal has a relatively simple parametric representation, it provides a basis for all the constructions that will be discussed later. In particular, we present a frequency domain formulation of the sampling problem and review the annihilating filter approach from [85]. In Section 2.3.1, we develop a new frequency domain framework that relies on subspace parameter estimation [65], and prove a relation between the subspace approach and the polynomial realization of the estimator [33] [85]. In Section 2.4, we present a brief analysis of the numerical performance of the subspace estimator and give exact performance bounds in some simple cases. In Section 2.5, we discuss techniques for improving the resolution performance in the case of closely spaced components, without increasing the computational complexity

of the method. We also propose an improved version of the subspace method, which uses an appropriate “enhanced” data matrix and allows for better estimation performance. In Section 2.6, we show simulation results that illustrate the numerical performances of the proposed techniques, and finally, in Section 2.7, we conclude with a summary of our results.

2.1 Signals with Finite Rate of Innovation

A class of signals with finite rate of innovation can be informally defined as a class of parametric signals having a finite number of degrees of freedom per unit of time, or finite *rate of innovation* [52] [85]. For example, consider a known function $\varphi(t)$ and signals of the form

$$x(t) = \sum_{n \in \mathbb{Z}} c_n \varphi\left(\frac{t - nT_s}{T_s}\right). \quad (2.1)$$

It is clear that the only degrees of freedom in $x(t)$ are the coefficients c_n , thus, the rate of innovation is $\rho = 1/T_s$. There are many examples of such signals: e.g. $\varphi(t)$ can be a scaling function in a wavelet multiresolution framework [46] [87], or when $\varphi(t) = \text{sinc}(t)$, we obtain the class of bandlimited signals. In the case of bandlimited signals, it is well-known that this rate corresponds to the minimum sampling rate that allows perfect reconstruction in the noiseless case. However, as we will see in the following, this will hold not only for bandlimited signals, but for other classes of signals as well.

A more general case appears when we allow arbitrary shifts t_n , that is,

$$x(t) = \sum_{n \in \mathbb{Z}} c_n \varphi\left(\frac{t - t_n}{T_s}\right). \quad (2.2)$$

For example, when $c_n = 1$, $\varphi(t) = \delta(t)$ and $t_n - t_{n-1}$ are i.i.d. random variables with exponential density, we have the Poisson process of rate $1/T$. Furthermore, by allowing a set of known functions $\{\varphi_r(t)\}_{r=0, \dots, R}$ and arbitrary shifts, we obtain

$$x(t) = \sum_{n \in \mathbb{Z}} \sum_{r=0}^R c_{nr} \varphi_r\left(\frac{t - t_n}{T_s}\right). \quad (2.3)$$

Clearly, in this case, the only degrees of freedom are the time instants t_n and the coefficients c_{nr} . By introducing a counting function $C_x(t_1, t_2)$ that counts the number of degrees of freedom of $x(t)$ in the interval $[t_1, t_2]$, the rate of innovation can be defined as

$$\rho = \lim_{\tau \rightarrow \infty} \frac{1}{\tau} C_x\left(-\frac{\tau}{2}, \frac{\tau}{2}\right). \quad (2.4)$$

Thus, we have the following definition [85]:

Definition 1: A signal with a finite rate of innovation is a signal whose parametric representation is given by (2.2) or (2.3), and which has a finite ρ , as defined in (2.4).

The reason for introducing the rate of innovation ρ is that one can expect to relate it to the minimum sampling rate that allows perfect reconstruction in the

absence of noise. We know that this is true in the case of bandlimited signals, however, it turns out to be true for more general classes of signals given by (2.2) and (2.3), as we will show in the sequel.

2.2 Periodic Stream of Diracs: Continuous-Time Case

In this section, we consider the problem of sampling and reconstructing a periodic stream of weighted Diracs. We will show that in the absence of noise, this signal can be reconstructed uniquely from its projection onto a subspace of dimension that is greater than or equal to the number of degrees of freedom of the signal. We will consider a lowpass approximation of the signal, which is one possible choice of the subspace, and present two high-resolution frequency domain methods for signal reconstruction from its lowpass version. One is a polynomial method, which uses the concept of annihilating filters [74] and requires polynomial rooting to obtain parameters of interest. The other is a subspace-based method, which allows for a more robust parameterization using the state space approach [65].

2.2.1 Frequency domain formulation

Consider a periodic signal $x(t)$ of period T , given by a sum of weighted Diracs,

$$x(t) = \sum_n \sum_{k=0}^{K-1} c_k \delta(t - t_k - nT), \quad (2.5)$$

where $0 \leq t_k < T$ and $t_k \neq t_l$, for $k \neq l$. This signal is not bandlimited, however, note that $x(t)$ has only $2K$ degrees of freedom, that is, time delays $\{t_k\}_{k=0}^{K-1}$ and weighting coefficients $\{c_k\}_{k=0}^{K-1}$. Therefore, it seems intuitive that by taking only $2K$ measurements of the signal, one can perfectly estimate all the unknown parameters. In [85], it was proved to be possible, provided that the signal is first filtered with an appropriate filter. For example, one can use an ideal lowpass filter of minimum bandwidth B , where B is greater than or equal to the rate of innovation ρ . In order to show how this can be achieved, consider the frequency domain representation of the signal.

Since $x(t)$ is periodic, it can be represented through its Fourier series

$$x(t) = \sum_{m=-\infty}^{\infty} X[m] e^{jm\omega_0 t}, \quad \text{where } \omega_0 = 2\pi/T. \quad (2.6)$$

The Fourier series coefficients $X[m]$ are given by

$$\begin{aligned} X[m] &= \frac{1}{T} \int_0^T x(t) e^{-jm\omega_0 t} dt = \frac{1}{T} \int_0^T \sum_{k=0}^{K-1} c_k \delta(t - t_k) e^{-jm\omega_0 t} dt \\ &= \frac{1}{T} \sum_{k=0}^{K-1} c_k \int_0^T \delta(t - t_k) e^{-jm\omega_0 t} dt = \frac{1}{T} \sum_{k=0}^{K-1} c_k e^{-jm\omega_0 t_k} \\ &= \frac{1}{T} \sum_{k=0}^{K-1} c_k z_k^m. \end{aligned} \quad (2.7)$$

Note that the coefficients $X[m]$ are given by a sum of K complex exponentials $z_k^m = e^{-jm\omega_0 t_k}$, where z_k are usually referred to as signal poles [65] [74]. Therefore, if one has access to $N_t \geq 2K$ adjacent Fourier series coefficients of the signal, the problem of estimating the parameters $\{t_k\}_{k=0}^{K-1}$ and $\{c_k\}_{k=0}^{K-1}$ can be reduced to the classical harmonic retrieval problem, well-studied in spectral estimation [74] and model-based signal analysis [65]. In [85], the signal parameters are estimated from the Fourier series coefficients corresponding to the lowpass approximation of the signal, using the method based on annihilating filters, which belongs to the class of high-resolution parametric methods for harmonic retrieval [74]. In the following, we give an overview of the method, while a more detailed discussion can be found in [65] [74] [85].

2.2.2 Annihilating filter method

The annihilating filter approach exploits the fact that in the absence of noise, each exponential $\{e^{-jn\omega_0 t_k}\}_{n \in \mathbb{Z}}$ can be “nulled out” or annihilated by a first order FIR filter $H_k(z) = (1 - e^{-j\omega_0 t_k} z^{-1})$, that is,

$$e^{-jn\omega_0 t_k} * [1, -e^{-j\omega_0 t_k}] = 0.$$

Consider thus a K -th order FIR filter $H(z) = \sum_{m=0}^K H[m]z^{-m}$, having K zeros at $z_k = e^{-j\omega_0 t_k}$,

$$H(z) = \prod_{k=1}^K (1 - e^{-j\omega_0 t_k} z^{-1}) = \sum_{m=0}^K H[m]z^{-m}. \quad (2.8)$$

Note that $H(z)$ is the convolution of K elementary filters with coefficients $[1, -e^{-j\omega_0 t_k}]$, $l = 1, \dots, K$. Since $X[n]$ is the sum of complex exponentials, each will be annihilated by one of the roots of $H(z)$, thus we have

$$(H * X)[n] = \sum_{k=0}^K H[k]X[n-k] = 0, \quad \text{for } n \in \mathbb{Z}. \quad (2.9)$$

Assuming without loss of generality that $H[0] = 1$, at critical sampling (2.9) becomes

$$\sum_{m=1}^K H[m]X[n-m] = -X[n], \quad n = 1, \dots, K. \quad (2.10)$$

Once the filter coefficients $H[m]$ have been found, the information about the time delays t_k can be extracted from the roots of the filter $H(z)$. The corresponding weighting coefficients c_k are then estimated by solving the system of linear equations (2.7).

From the above analysis, it becomes clear that in order to find K filter coefficients $H[m]$, $m = 1, \dots, K$ from (2.10), one requires $2K$ Fourier series coefficients $X[m]$, where $m \in [-K+1, K]$. Therefore, in the following, we show how to obtain these coefficients from a set of $N_t \geq 2K$ uniform samples of the lowpass version. Assume that the signal $x(t)$ is sampled with a sinc sampling kernel $\varphi(t)$ of bandwidth $[-K\omega_0, K\omega_0]$, and that the sampling period T_s is chosen such that $N_t = T/T_s \geq 2K+1$ with $N_t \in \mathbb{N}$. The sample values

$y_n = \langle \varphi(t - nT_s), x(t) \rangle$ are then given by

$$\begin{aligned}
y_n &= \langle \varphi(t - nT_s), \sum_m X[m] e^{jm\omega_0 t} \rangle \\
&= \sum_m X[m] \langle \varphi(t - nT_s), e^{jm\omega_0 t} \rangle \\
&= \sum_m X[m] \Phi(m\omega_0) e^{jm\omega_0 nT_s} \\
&= \sum_m X[m] e^{jm\omega_0 nT_s}, \tag{2.11}
\end{aligned}$$

where $\Phi(\omega)$ is the Fourier transform of $\varphi(t)$, which satisfies

$$\Phi(\omega) = \begin{cases} 1, & |\omega| \leq K\omega_0, \\ 0, & \text{otherwise.} \end{cases} \tag{2.12}$$

If the sampling period satisfies the above requirement, this system of equations is invertible and will yield a unique solution for $X[m]$, $m \in [-K, K]$. In particular, when $N_t = 2K + 1$, $\{y_n\}_{n=1}^{N_t}$ represent the inverse discrete-time Fourier transform of $X[m]$.

The algorithm can be thus summarized as follows:

Outline of the annihilating filter algorithm

1. Compute the set of at least $2K$ Fourier series coefficients $X[m]$ from a set of $N_t \geq 2K + 1$ uniform samples $y_n = \langle \varphi(t - nT_s), x(t) \rangle$.
2. Find the coefficients $H[k]$ of the annihilating filter

$$H(z) = \prod_{k=1}^K (1 - e^{-j\omega_0 t_k} z^{-1}) = \sum_{k=0}^K H[k] z^{-k}, \tag{2.13}$$

which satisfies (2.9), that is,

$$(H * X)[n] = 0, \text{ for } n \in \mathbb{Z}.$$

By setting $H[0] = 1$, at critical sampling (2.9) becomes

$$\begin{pmatrix} X[0] & X[-1] & \cdots & X[-K+1] \\ X[1] & X[0] & \cdots & X[-K+2] \\ \vdots & \vdots & \ddots & \vdots \\ X[K-1] & X[K-2] & \cdots & X[0] \end{pmatrix} \cdot \begin{pmatrix} H[1] \\ \vdots \\ H[K] \end{pmatrix} = - \begin{pmatrix} X[1] \\ X[2] \\ \vdots \\ X[K] \end{pmatrix}. \tag{2.14}$$

This system of equations is usually referred to as a high-order Yule-Walker system [74].

3. Find the values of t_k by finding the roots of $H(z)$.

4. Solve for the coefficients c_k by solving the system of linear equations in (2.7), that is:

$$\begin{pmatrix} X[0] \\ X[1] \\ \vdots \\ X[K-1] \end{pmatrix} = \frac{1}{T} \begin{pmatrix} 1 & 1 & \dots & 1 \\ z_0 & z_1 & \dots & z_{K-1} \\ \vdots & \vdots & \dots & \vdots \\ z_0^{K-1} & z_1^{K-1} & \dots & z_{K-1}^{K-1} \end{pmatrix} \cdot \begin{pmatrix} c_0 \\ c_1 \\ \vdots \\ c_{K-1} \end{pmatrix}. \quad (2.15)$$

This is a Vandermonde system, which has a unique solution since the t_k 's are assumed to be distinct.

We have seen that in the absence of noise, it suffices to use only $2K$ adjacent Fourier series coefficients $X[m]$ to obtain perfect estimates of all the unknown parameters. While in the noiseless case the critically sampled scheme leads to perfect estimates of all the parameters, in the presence of noise, such an approach can suffer from poor numerical performance. In particular, any least-square procedure that determines the filter coefficients directly from (2.14) has poor numerical precision. In practice, this problem can be dealt with by over-sampling and using standard techniques from noisy spectral estimation, such as the singular value decomposition (SVD). That is, one should consider an extended system of equations (2.14)

$$\begin{pmatrix} X[0] & X[-1] & \dots & X[-K+1] \\ X[1] & X[0] & \dots & X[-K+2] \\ \vdots & \vdots & \ddots & \vdots \\ X[K_1-1] & X[K_1-2] & \dots & X[K_1-K] \end{pmatrix} \cdot \begin{pmatrix} H[1] \\ \vdots \\ H[K] \end{pmatrix} = - \begin{pmatrix} X[1] \\ X[2] \\ \vdots \\ X[K_1] \end{pmatrix} \\ \iff \mathbf{Y} \cdot \mathbf{h} = -\mathbf{X}, \quad (2.16)$$

where $K_1 > K$, and find the singular value decomposition of the matrix \mathbf{X}

$$\mathbf{X} = \mathbf{U}_s \mathbf{S}_s \mathbf{V}_s^H + \mathbf{U}_n \mathbf{S}_n \mathbf{V}_n^H. \quad (2.17)$$

The first term corresponds to the best (in the Frobenius-norm sense) rank K approximation of the matrix \mathbf{X} . The filter coefficients \mathbf{h} are then computed as

$$\mathbf{h} = -\mathbf{V}_s \mathbf{S}_s^{-1} \mathbf{U}_s^H \cdot \mathbf{X}. \quad (2.18)$$

However, even though such an approach improves numerical accuracy on the estimates of the filter coefficients, it is not sufficient for good overall performance of the algorithm. Specifically, both theoretical analysis and practice have shown that in order to reduce sensitivity of time-delay estimates to noise, the filter order should be chosen according to the length of the data set, rather than the number of unknown signal components [32] [49]. That is, even though the number of components may be relatively low, typically, a high-order filter must be used, which imposes a significant computational burden since it is necessary to find roots of a large size polynomial in order to extract a small number of signal poles [65].

This brings us to a more practical version of the model-based approach, the so-called subspace estimator, which avoids the root finding step and relies only on some matrix factorizations. It takes advantage of the so-called shift-invariant subspace property and leads to robust estimates without overmodeling, by properly exploiting the algebraic structure of the signal subspace [32] [65].

2.3 Subspace-Based Approach

2.3.1 Subspace solution based on the shift-invariance property

Consider the set of Fourier series coefficients $X[m]$, given by (2.7), and construct a Hankel¹ data matrix \mathbf{X} of size $M \times N$, where $M, N > K$,

$$\mathbf{X} = \begin{pmatrix} X[0] & X[1] & \dots & X[N-1] \\ X[1] & X[2] & \dots & X[N] \\ \vdots & & & \\ X[M-1] & X[M] & \dots & X[M+N-2] \end{pmatrix}. \quad (2.19)$$

For simplicity, we have constructed the data matrix using only the coefficients $X[m]$ with non-negative indices m . In Section 2.5.2, we will show that the method can be directly extended to the case when the coefficients with negative indices are used as well.

Note that in the absence of noise, \mathbf{X} can be decomposed as $\mathbf{X} = \mathbf{U}\mathbf{S}\mathbf{V}^H$, where \mathbf{U} and \mathbf{V} are Vandermonde matrices given by

$$\mathbf{U} = \begin{pmatrix} 1 & 1 & 1 & \dots & 1 \\ z_0 & z_1 & z_2 & \dots & z_{K-1} \\ \vdots & & & & \\ z_0^{M-1} & z_1^{M-1} & z_2^{M-1} & \dots & z_{K-1}^{M-1} \end{pmatrix}, \quad (2.20)$$

$$\mathbf{V} = \begin{pmatrix} 1 & 1 & 1 & \dots & 1 \\ z_0^* & z_1^* & z_2^* & \dots & z_{K-1}^* \\ \vdots & & & & \\ z_0^{*N-1} & z_1^{*N-1} & z_2^{*N-1} & \dots & z_{K-1}^{*N-1} \end{pmatrix}, \quad (2.21)$$

while \mathbf{S} is a diagonal matrix

$$\mathbf{S} = \text{diag}(c_0 \ c_1 \ c_2 \ \dots \ c_{K-1}). \quad (2.22)$$

At this point, it is important to note that the above factorization is not unique. That is, if $\mathbf{X} = \mathbf{U}\mathbf{S}\mathbf{V}^H$, then $\mathbf{X} = \mathbf{U}\mathbf{P} \cdot \mathbf{P}^{-1}\mathbf{S}\mathbf{Q} \cdot \mathbf{Q}^{-1}\mathbf{V}^H$ is another possible factorization, for every choice of $K \times K$ non-singular matrices \mathbf{P} and \mathbf{Q} . However, as we will show in the following, any such factorization can be used to estimate the signal parameters.

Consider first the matrix \mathbf{U} , given by (2.20). Since \mathbf{U} has a Vandermonde structure, it can be written in the following, more compact form:

$$\mathbf{U} = \begin{pmatrix} \mathbf{b} \\ \mathbf{b} \cdot \Phi \\ \mathbf{b} \cdot \Phi^2 \\ \vdots \\ \mathbf{b} \cdot \Phi^{M-1} \end{pmatrix}, \quad (2.23)$$

where \mathbf{b} is a row vector of length K , given by $\mathbf{b} = [1 \ 1 \ \dots \ 1]$, while Φ is a $K \times K$ diagonal matrix containing the signal poles on the main diagonal, i.e.

¹A Hankel matrix is a matrix in which the (i, j) -th entry depends only on the sum $i + j$.

$\Phi = \text{diag}(z_k)$. Similarly, due to the Vandermonde structure of the matrix \mathbf{V} (2.21), it can be written as

$$\mathbf{V} = \begin{pmatrix} \mathbf{b} \\ \mathbf{b} \cdot \Phi_{\mathbf{h}} \\ \mathbf{b} \cdot \Phi_{\mathbf{h}}^2 \\ \vdots \\ \mathbf{b} \cdot \Phi_{\mathbf{h}}^{N-1} \end{pmatrix}, \quad (2.24)$$

where $\Phi_{\mathbf{h}} = \Phi^H$.

The subspace approach takes advantage of two properties of the data matrix \mathbf{X} . The first property is that in the case of noiseless data, \mathbf{X} has rank K . This will allow us to reduce the noise level by approximating the noisy data matrix with a rank K matrix. The second property is the so-called shift-invariant subspace property. That is, if we consider the matrices \mathbf{U} and \mathbf{V} , given by (2.20) and (2.21), they satisfy the following relations:

$$\overline{\mathbf{U}} = \underline{\mathbf{U}} \cdot \Phi \quad \text{and} \quad \overline{\mathbf{V}} = \underline{\mathbf{V}} \cdot \Phi^H, \quad (2.25)$$

where $\overline{(\cdot)}$ and $\underline{(\cdot)}$ denote the operations of omitting the first and the last row of (\cdot) respectively, while Φ is a diagonal matrix having the signal poles z_k 's on the main diagonal. Note that the shift-invariance property is satisfied not only by \mathbf{U} and \mathbf{V} , but also by all matrices \mathbf{UP} and \mathbf{VQ} , where, as already mentioned, \mathbf{P} and \mathbf{Q} are any non-singular $K \times K$ matrices. In order to prove this property, consider, for example, the matrix \mathbf{UP} . This matrix can be expressed as

$$\mathbf{UP} = \begin{pmatrix} \mathbf{bP} \\ \mathbf{bP} \cdot \mathbf{P}^{-1} \Phi \mathbf{P} \\ \mathbf{bP} \cdot \mathbf{P}^{-1} \Phi^2 \mathbf{P} \\ \vdots \\ \mathbf{bP} \cdot \mathbf{P}^{-1} \Phi^{M-1} \mathbf{P} \end{pmatrix}, \quad (2.26)$$

where we have inserted \mathbf{PP}^{-1} between \mathbf{b} and Φ^k , $k = 0, \dots, M-1$. Given that $(\mathbf{P}^{-1} \Phi \mathbf{P})^k = \mathbf{P}^{-1} \Phi^k \mathbf{P}$, it becomes obvious that \mathbf{UP} satisfies the shift-invariance property as well, that is,

$$\overline{\mathbf{UP}} = \underline{\mathbf{UP}} \cdot \mathbf{P}^{-1} \Phi \mathbf{P}. \quad (2.27)$$

Since the matrix $\mathbf{P}^{-1} \Phi \mathbf{P}$ in (2.27) is related to Φ by a similarity transformation, it has the same eigenvalues as Φ , i.e. $\{z_k\}_{k=0}^{K-1}$. Similarly, it can be proved that the matrix \mathbf{VQ} , where \mathbf{Q} is any $K \times K$ non-singular matrix, will satisfy the following relation:

$$\overline{\mathbf{VQ}} = \underline{\mathbf{VQ}} \cdot \mathbf{Q}^{-1} \Phi_{\mathbf{h}} \mathbf{Q}. \quad (2.28)$$

In practice, the data matrix \mathbf{X} will be decomposed using the SVD as

$$\mathbf{X} = \mathbf{U}_s \mathbf{S}_s \mathbf{V}_s^H + \mathbf{U}_n \mathbf{S}_n \mathbf{V}_n^H, \quad (2.29)$$

where the columns of \mathbf{U}_s and \mathbf{V}_s are K principal left and right singular vectors of \mathbf{X} respectively, while the second term contains remaining non-principals. Since the presence of additive white noise has little effect on the principal singular

vectors², the singular vectors \mathbf{U}_s and \mathbf{V}_s , corresponding to the K dominant singular values, will be good estimates of the singular vectors of the original, noiseless matrix \mathbf{X} . Since both \mathbf{U}_s and \mathbf{V}_s are matrices of rank K (as well as \mathbf{U} and \mathbf{V} in (2.20) and (2.21)), there will exist $K \times K$ non-singular matrices \mathbf{Q} and \mathbf{R} such that $\mathbf{U}_s = \mathbf{U} \cdot \mathbf{Q}$ and $\mathbf{V}_s = \mathbf{V} \cdot \mathbf{R}$. As a result, both matrices \mathbf{U}_s and \mathbf{V}_s will satisfy the shift-invariance property, and therefore, the time instants of Diracs $\{t_k\}_{k=0}^{K-1}$ can be uniquely determined from the eigenvalues λ_k of an operator that maps $\underline{\mathbf{U}}_s$ onto $\overline{\mathbf{U}}_s$ (or $\underline{\mathbf{V}}_s$ onto $\overline{\mathbf{V}}_s$), that is,

$$t_k = -\frac{T \angle \lambda_k}{2\pi}. \quad (2.30)$$

At this point, it is important to note that when the signal poles are estimated from the left singular vectors \mathbf{U}_s , the minimum required size of the data matrix \mathbf{X} in the noiseless case is $(K+1) \times K$. Alternatively, if the right singular vectors \mathbf{V}_s are used for estimation, the minimum size of \mathbf{X} is $K \times (K+1)$. Once the signal poles have been estimated, the weighting coefficients c_k can be found as a least-squares solution to (2.7). In the following, we give a summary of the algorithm.

Subspace-based algorithm

1. Given a set of the Fourier series coefficients $X[m]$, construct an $M \times N$ matrix data \mathbf{X} as in (2.19), where $M, N > K$.
2. Compute the singular value decomposition of \mathbf{X} , that is, $\mathbf{X} = \mathbf{U}\mathbf{S}\mathbf{V}^H$. Find the principal left and right singular vectors, \mathbf{U}_s and \mathbf{V}_s , as the singular vectors corresponding to the K largest singular values of \mathbf{X} .
3. Estimate the signal poles $z_k = e^{-j\omega_0 t_k}$ by computing the eigenvalues of a matrix \mathbf{Z} , defined as

$$\mathbf{Z} = \underline{\mathbf{U}}_s^+ \cdot \overline{\mathbf{U}}_s. \quad (2.31)$$

Note that if \mathbf{V}_s is used in (2.31), one would estimate complex conjugates of z_k 's, since in the singular value decomposition of \mathbf{X} , \mathbf{V}_s is used with the Hermitian transpose.

4. Find the coefficients c_k as a least-squares solution to the Vandermonde system (2.7), that is,

$$X[m] = \sum_{k=0}^{K-1} c_k e^{-jn\omega_0 t_k} + \mathcal{N}[m].$$

The method can be further modified to improve its numerical performance, specifically in the low SNR regime. For example, since in the noiseless case $\underline{\mathbf{U}}_s$ and $\overline{\mathbf{U}}_s$ span the same column space, we can extract K principal components from $\underline{\mathbf{U}}_s$ and $\overline{\mathbf{U}}_s$ by computing the joint SVD

$$[\underline{\mathbf{U}}_s, \overline{\mathbf{U}}_s] = \mathbf{U}_s \mathbf{S}_s [\mathbf{V}_{s1}^H, \mathbf{V}_{s2}^H]. \quad (2.32)$$

²This is true under the assumption that the smallest singular value corresponding to the signal is not dominated by noise.

The signal poles $z_k = e^{-j\omega_0 t_k}$ are then estimated from generalized eigenvalues of a $K \times K$ matrix pencil $\mathbf{V}_{s1} - z\mathbf{U}_{s2}$ [33]. While this approach typically leads to better estimation accuracy than the original state space algorithm, it requires that the SVD of the two matrices \mathbf{X} and $[\underline{\mathbf{U}}_s, \overline{\mathbf{U}}_s]$ is computed.

2.3.2 Relation between the subspace and the polynomial estimator

In the above case, where the coefficients $X[m]$ are given by a linear combination of exponentials, it is possible to find a decomposition of the matrix $\mathbf{X} = \mathbf{U}\mathbf{S}\mathbf{V}^H$, where both \mathbf{U} and \mathbf{V} are Vandermonde matrices. This allowed us to exploit the shift-invariance property (2.25), and estimate the signal poles as the eigenvalues of the operator \mathbf{Z} that maps one signal subspace onto another, “shifted” subspace. However, in the case when the coefficients $X[m]$ have more complex structure (e.g. in the case of piecewise polynomial signals), finding an exact algebraic expression for matrices obtained by any such decomposition becomes much more involved task, whereas the polynomial parameterization may still allow for an intuitive and relatively simple solution. Therefore, in this section, we prove a general relation between the annihilating filter approach [85] and the subspace estimator, which will allow us to extend the subspace method to other classes of signals. To avoid any confusion about notation, in the following, lowercase bold and uppercase bold will denote respectively, a column/row vector and a matrix.

Given a set of Fourier series coefficients $X[n]$, we first define the state vector [65] of length K as:

$$\mathbf{x}[n] = (X[n-1] \ X[n-2] \ X[n-3] \ \cdots \ X[n-K])^T. \quad (2.33)$$

From the system (2.10), one can see that each coefficient $X[n]$ can be predicted from its K past values, thus we can write,

$$X[n] = (-H[1] \ -H[2] \ -H[3] \ \cdots \ -H[K]) \mathbf{x}[n] \Leftrightarrow X[n] = \mathbf{h} \mathbf{x}[n]. \quad (2.34)$$

Combining (2.33) and (2.34), we obtain:

$$\begin{pmatrix} X[n] \\ X[n-1] \\ X[n-2] \\ \vdots \\ X[n-K+1] \end{pmatrix} = \begin{pmatrix} -H[1] & -H[2] & -H[3] & \cdots & -H[K] \\ 1 & 0 & 0 & \cdots & 0 \\ 0 & 1 & 0 & \cdots & 0 \\ \vdots & \vdots & \vdots & \vdots & \vdots \\ 0 & 0 & \cdots & 1 & 0 \end{pmatrix} \begin{pmatrix} X[n-1] \\ X[n-2] \\ X[n-3] \\ \vdots \\ X[n-K] \end{pmatrix}, \quad (2.35)$$

or in matrix form

$$\mathbf{x}[n+1] = \mathbf{H} \mathbf{x}[n]. \quad (2.36)$$

Therefore, the state space representation of the polynomial estimator is given by

$$X[n] = \mathbf{h} \mathbf{x}[n], \quad (2.37)$$

$$\mathbf{x}[n+1] = \mathbf{H} \mathbf{x}[n]. \quad (2.38)$$

Starting with (2.37) and (2.38), we can write:

$$X[n] = \mathbf{h} \mathbf{H}^n \mathbf{x}[0]. \quad (2.39)$$

Now let us show how the above relations can be used to find a subspace-based solution to the estimation problem. Similarly to the approach from Section 2.3.1, one should first construct a Hankel data matrix \mathbf{X} as in (2.19), of size $M \times N$, where $M, N \geq K$. Using (2.38) and (2.39), the matrix \mathbf{X} in (2.19) can be factored as follows:

$$\mathbf{X} = \begin{pmatrix} \mathbf{h} \\ \mathbf{h} \mathbf{H} \\ \mathbf{h} \mathbf{H}^2 \\ \vdots \\ \mathbf{h} \mathbf{H}^{M-1} \end{pmatrix} (\mathbf{x}[0] \quad \mathbf{H} \mathbf{x}[0] \quad \mathbf{H}^2 \mathbf{x}[0] \quad \dots \quad \mathbf{H}^{N-1} \mathbf{x}[0]) \Leftrightarrow \mathbf{L} \mathbf{R}^T. \quad (2.40)$$

Thus, one can think of \mathbf{H} as being an operator that maps $\underline{\mathbf{L}}$ onto $\overline{\mathbf{L}}$ (or, alternatively, $\underline{\mathbf{R}}$ onto $\overline{\mathbf{R}}$). Now the key is to observe that the characteristic polynomial of \mathbf{H} is given by

$$\det(\lambda \mathbf{I} - \mathbf{H}) = \lambda^K + \sum_{i=1}^K H[i] \lambda^{K-i}. \quad (2.41)$$

By comparing (2.41) with an expression for the annihilating filter (2.8), that is, $H(z) = 1 + \sum_{m=1}^K H[m] z^{-m}$, it follows that the eigenvalues of the operator \mathbf{H} (i.e. the zeros of its characteristic polynomial) are identical to the zeros of the annihilating filter. Note that this relation holds in the general case and allows one to obtain the subspace estimator once the annihilating filter has been determined, and vice versa. As already discussed in Section 2.3.1, there will be no difference whether \mathbf{H} is obtained from the matrix \mathbf{L} in (2.40), or from another matrix $\mathbf{L}\mathbf{Q}$, where \mathbf{Q} is any non-singular matrix. The corresponding estimates of \mathbf{H} are related by similarity transformation and thus have the same eigenvalues. This property also holds in the case when \mathbf{H} is computed from the matrix \mathbf{R} or, alternatively, $\mathbf{Q}\mathbf{R}$. In practice, since the matrix \mathbf{X} will be decomposed using the singular value decomposition as $\mathbf{X} = \mathbf{U}_s \mathbf{S}_s \mathbf{V}_s^H + \mathbf{U}_n \mathbf{S}_n \mathbf{V}_n^H$, with the first term corresponding to the principal components, the operator \mathbf{H} can be found either from the matrix \mathbf{U}_s or from the matrix \mathbf{V}_s . This leads us to the following proposition.

Proposition 2.1: Consider a Hankel matrix \mathbf{X} with entries $X[m]$ (2.19), and let $\mathbf{X} = \mathbf{U}_s \mathbf{S}_s \mathbf{V}_s^H + \mathbf{U}_n \mathbf{S}_n \mathbf{V}_n^H$ denote its singular value decomposition. Assume next that $X[m]$ can be annihilated by an FIR filter $H(z) = \sum_{k=0}^K H[k] z^{-k}$, that is, $(H * X)[m] = \sum_{k=0}^K H[k] X[m-k] = 0, \forall m \in \mathbb{Z}$, where K is chosen such that $H(z)$ is of minimum order. Then, in the noiseless case, the roots of the filter $H(z)$ are identical to the eigenvalues of a matrix $\mathbf{H} = \underline{\mathbf{U}}_s^+ \cdot \overline{\mathbf{U}}_s$.

2.4 Performance Evaluation

The statistical properties of the estimates obtained using high-resolution methods have been studied extensively, mainly in the context of estimating the frequencies of superimposed complex sinusoids from noisy measurements [32] [33] [66] [65]. Expressions for the mean square error (MSE) of the frequency estimates [32] indicate that the numerical performance of such methods is very close to the Cramer-Rao bound [77], which represents the lowest achievable MSE by any unbiased estimator. In the following, we present some of the key ideas used

in the statistical analysis of the state space approach, while more on this topic can be found in [32] [65].

Consider the data matrix \mathbf{X} and denote by $\mathbf{R}_c = \mathbf{X}\mathbf{X}^H$ the corresponding covariance matrix. We will analyze the subspace approach which uses the eigendecomposition of the covariance matrix \mathbf{R}_c . However, note that the same analysis applies to our method, based on the singular value decomposition of the matrix \mathbf{X} , since the left singular vectors (\mathbf{U}_s) of \mathbf{X} are the eigenvectors of \mathbf{R}_c , that is, $\mathbf{R}_c = \mathbf{U}_s\mathbf{S}_s\mathbf{U}_s^H$. Let $\tilde{\mathbf{U}}_s = \mathbf{U}_s + \Delta\mathbf{U}_s$, where $\Delta\mathbf{U}_s$ is the error in the eigenvectors corresponding to the signal subspace. Then, $\Delta\mathbf{U}_s$ can be written as $\Delta\mathbf{U}_s = \mathbf{P}_s\Delta\mathbf{U}_s + \mathbf{P}_n\Delta\mathbf{U}_s$, where $\mathbf{P}_s = \mathbf{U}_s\mathbf{U}_s^H$ is the unique orthogonal projection matrix onto the signal subspace, that is, if \mathbf{x} belongs to the signal subspace, then $\mathbf{P}_s\mathbf{x} = \mathbf{x}$. Similarly, $\mathbf{P}_n = \mathbf{I} - \mathbf{P}_s$ is a projection operator onto the noise subspace. Now the key is to observe that only $\mathbf{P}_n\Delta\mathbf{U}_s$ contributes to the error in the eigenvalue estimates [65], which simplifies the analysis considerably.

The first step in the analysis is to relate $\Delta\mathbf{R}_c$, the error in the covariance matrix, to $\mathbf{P}_n\Delta\mathbf{U}_s$,

$$\mathbf{P}_n\Delta\mathbf{U}_s = \mathbf{P}_n\Delta\mathbf{R}_c\mathbf{U}_s\mathbf{S}_s^{-1}. \quad (2.42)$$

Next, we consider how $\mathbf{P}_n\Delta\mathbf{U}_s$ affects $\mathbf{H}_s = \underline{\mathbf{U}}_s^+\overline{\mathbf{U}}_s$ as well as its eigenvalues. By denoting $\tilde{\mathbf{H}}_s = \mathbf{H}_s + \Delta\mathbf{H}_s$, it can be shown [65] that

$$\Delta\mathbf{H}_s = -\underline{\mathbf{U}}_s^+(\Delta\underline{\mathbf{U}}_s\mathbf{H}_s - \Delta\overline{\mathbf{U}}_s), \quad (2.43)$$

while the error in \mathbf{H}_s can be related to the error of its eigenvalue z_k through the following relation:

$$\Delta z_k = \mathbf{p}_k\Delta\mathbf{H}_s\mathbf{q}_k, \quad (2.44)$$

where \mathbf{p}_k and \mathbf{q}_k are left and right eigenvectors of \mathbf{H}_s corresponding to the eigenvalue z_k . Finally, by combining (2.42)-(2.44), we obtain:

$$\Delta z_k = -z_k\varepsilon_k^H\Delta\mathbf{R}_c\mathbf{U}_s\mathbf{S}_s^{-1}\mathbf{q}_k, \quad (2.45)$$

where $\varepsilon_k^H = -p_k\underline{\mathbf{U}}_s^+(\mathbf{W}_1 - z_k^*\mathbf{W}_2)$, with $\mathbf{W}_1 = [\mathbf{I}_{(K-1)\times(K-1)}, 0]$ and $\mathbf{W}_2 = [0, \mathbf{I}_{(K-1)\times(K-1)}]$.

Therefore, starting from (2.45) and using the statistics of $\Delta\mathbf{R}_c$, one can compute the mean-square-error (MSE) of Δz_k . However, due to the complex dependency of $\Delta\mathbf{R}_c$ on the data, the general expressions are quite involved. Therefore, we give simplified expressions for the MSE of the frequency estimate in the case of a single exponential, which in our framework corresponds to the estimate of the time delay t_1 of one Dirac impulse.

Consider for simplicity the case of a periodic signal with period T . Let the data matrix \mathbf{X} be of size $M \times N$, and let $N_t = M + N - 1$ be the total number of samples used for estimation. Assuming that the signal and noise are uncorrelated, the optimum performance is achieved when $N = N_t/3$ or $N = 2N_t/3$, resulting in the MSE of time delay estimation [32]:

$$E\{\Delta t_1^2\} \approx \frac{1}{\omega_0^2} \frac{27}{4N_t^3} \frac{1}{\text{SNR}}. \quad (2.46)$$

where $\omega_0 = 2\pi/T$. This is close to the Cramer-Rao bound (CRB) [77], given by

$$\text{CRB} = \frac{1}{\omega_0^2} \frac{6}{N_t^3} \frac{1}{\text{SNR}}. \quad (2.47)$$

which indicates desirable numerical performances of the subspace-based approach.

Similar performance can be obtained with the annihilating filter method [32], where the minimum MSE is given by

$$E\{\Delta t_1^2\} \approx \frac{1}{\omega_0^2} \frac{9}{N_t^3} \frac{1}{\text{SNR}}, \quad (2.48)$$

The minimum MSE is achieved for $N = N_t/3$ or $N = 2N_t/3$ as well, however, in this case, N corresponds to the polynomial degree. As we alluded to earlier, a choice of the polynomial degree directly affects the estimation performance.

2.5 Extensions of the Subspace Methods

2.5.1 Estimation of closely spaced Diracs: increasing the resolution

Model-based parameter estimation using subspace methods has received significant attention in the literature [33] [38] [65]. In many problems encountered in practice, such as finding a direction of arrival (DOA), frequency estimation, channel estimation and others, subspace-based methods provide an attractive alternative to a more complex maximum likelihood (ML) estimator, as they yield accurate estimates at a reasonable computational cost. However, the problem encountered in all model-based methods is that their performance typically degrades if the signal contains closely spaced components. This can become critical in certain applications, such as channel estimation in ultra-wideband systems [49], where one has to estimate many closely spaced components in a very low signal-to-noise ratio regime. In the following, we present two different techniques that improve the resolution performance of the developed scheme without increasing the data set used for estimation.

Consider again the data matrix \mathbf{X} , defined in (2.19). In order to estimate the signal poles z_k 's, we have exploited the shift-invariant subspace property (2.25), that is, $\overline{\mathbf{U}} = \underline{\mathbf{U}} \cdot \Phi$, or alternatively, $\overline{\mathbf{V}} = \underline{\mathbf{V}} \cdot \Phi$, where Φ is a diagonal matrix with z_k 's along the main diagonal. However, the Vandermonde structure of \mathbf{U} and \mathbf{V} allows for a more general version of (2.25), specifically,

$$\overline{\mathbf{U}}^p = \underline{\mathbf{U}}_p \cdot \Phi^p \quad \text{and} \quad \overline{\mathbf{V}}^p = \underline{\mathbf{V}}_p \cdot \Phi^p, \quad (2.49)$$

where $\overline{(\cdot)}^p$ and $\underline{(\cdot)}_p$ denote the operations of omitting the first p rows and last p rows of (\cdot) respectively [78]. In this case, the matrix Φ^p has elements $z_k^p = e^{-j\omega_0 p t_k}$ on its main diagonal. Therefore, the advantage of using the values of p larger than $p = 1$, is that the effective separation among the estimated time delays is increased p times, which in turn improves the resolution capabilities of the method [49]. In the sequel, this approach will be referred to as the subspace-shifting approach.

Another way to improve the performance in the case of closely spaced components is the following. Instead of constructing the data matrix \mathbf{X} as in (2.19),

one can construct another data matrix \mathbf{X}_i as

$$\mathbf{X}_i = \begin{pmatrix} X[0] & X[1] & \dots & X[N-1] \\ X[p] & X[p+1] & \dots & X[p+N-1] \\ X[2p] & X[2p+1] & \dots & X[2p+N-1] \\ \vdots & \ddots & & \\ X[1] & X[2] & \dots & X[N] \\ X[p+1] & X[p+2] & \dots & X[p+N] \\ X[2p+1] & X[2p+2] & \dots & X[2p+N] \\ \vdots & \ddots & & \\ X[p-1] & X[p] & \dots & X[p+N-2] \\ X[2p-1] & X[2p] & \dots & X[2p+N-2] \\ \vdots & & & \end{pmatrix}. \quad (2.50)$$

That is, \mathbf{X}_i is obtained by interleaving the rows of the original matrix \mathbf{X} in (2.19). Similarly to the approach from Section 2.3.1, in the noiseless case, the matrix \mathbf{X}_i can be decomposed as $\mathbf{X}_i = \mathbf{U}_i \mathbf{S}_i \mathbf{V}_i^H$, where \mathbf{S}_i and \mathbf{V}_i are the matrices given by (2.22) and (2.21) respectively, while the matrix \mathbf{U}_i is now given by

$$\mathbf{U}_i = \begin{pmatrix} 1 & 1 & 1 & \dots & 1 \\ z_0^p & z_1^p & z_2^p & \dots & z_{K-1}^p \\ z_0^{2p} & z_1^{2p} & z_2^{2p} & \dots & z_{K-1}^{2p} \\ \vdots & \ddots & & & \\ z_0 & z_1 & z_2 & \dots & z_{K-1} \\ z_0^{p+1} & z_1^{p+1} & z_2^{p+1} & \dots & z_{K-1}^{p+1} \\ z_0^{2p+1} & z_1^{2p+1} & z_2^{2p+1} & \dots & z_{K-1}^{2p+1} \\ \vdots & \ddots & & & \\ z_0^{p-1} & z_1^{p-1} & z_2^{p-1} & \dots & z_{K-1}^{p-1} \\ z_0^{2p-1} & z_1^{2p-1} & z_2^{2p-1} & \dots & z_{K-1}^{2p-1} \\ \vdots & & & & \end{pmatrix}. \quad (2.51)$$

Note that each column k of the matrix \mathbf{U}_i is made up of p blocks that contain consecutive powers of the signal pole z_k . Therefore, in order to estimate z_k 's, one can exploit the following shift-invariance property:

$$\overline{\mathbf{U}_i}^{p,b} = \underline{\mathbf{U}_i}_{p,b} \cdot \mathbf{\Phi}^p, \quad (2.52)$$

where in this case $\overline{(\cdot)}^{p,b}$ and $\underline{(\cdot)}_{p,b}$ denote the operations of omitting the first row and last row in each block of (\cdot) respectively. Note that the matrix $\mathbf{\Phi}^p$ is the same diagonal matrix as before, with elements $z_k^p = e^{-j\omega_0 p t_k}$ on its main diagonal. However, since the matrix \mathbf{X}_i has better conditioning than the original data matrix \mathbf{X} , the interleaving approach results in better resolution performance, as we will show in Section 2.6. Therefore, we can state the following proposition.

Proposition 2.2: Consider the matrices \mathbf{X} and \mathbf{X}_i defined in (2.19) and (2.50) respectively, and let $\mathbf{X} = \mathbf{U}\mathbf{S}\mathbf{V}^H$ and $\mathbf{X}_i = \mathbf{U}_i \mathbf{S}_i \mathbf{V}_i^H$ denote their singular value decompositions. Then, the following holds:

1. If $\{z_k\}_{k=0}^{K-1}$ are eigenvalues of the matrix $\mathbf{Z}_1 = \underline{\mathbf{U}}^+ \cdot \overline{\mathbf{U}}$, then $\{z_k^p\}_{k=0}^{K-1}$ are eigenvalues of the matrix $\mathbf{Z}_2 = \underline{\mathbf{U}}_p^+ \cdot \overline{\mathbf{U}}^p$.
2. The matrices $\mathbf{Z}_2 = \underline{\mathbf{U}}_p^+ \cdot \overline{\mathbf{U}}^p$ and $\mathbf{Z}_3 = \underline{\mathbf{U}}_{i_{p,b}}^+ \cdot \overline{\mathbf{U}}_i^{p,b}$ have identical eigenvalues.
3. If $\{t_k\}_{k=0}^{K-1}$ are the time locations of Diracs estimated from the eigenvalues $\{z_k\}_{k=0}^{K-1}$, then $\{pt_k\}_{k=0}^{K-1}$ are the locations estimated from $\{z_k^p\}_{k=0}^{K-1}$, that is, the separation between each two components is increased p times.

Finally, we would like to note that since we are considering periodic signals, estimates of the time locations t_k obtained from the powers of the signal poles z_k^p are not unique. That is, for each computed eigenvalue z_k^p , there exists a set of p possible corresponding time delays \tilde{t}_k , given by $\tilde{t}_k = t_k + nT/p$, where $n = 0, 1, \dots, p-1$. In order to avoid this ambiguity, one can first find an approximate location of the cluster of Diracs, by estimating only one principal component, using the original method from Section 2.3.1, since it is well-known that the largest signal-space singular vector is relatively insensitive to signal separation [41]. This information can be used later to select a proper set of the locations t_k , once the values of z_k^p have been estimated.

2.5.2 Constructing enhanced data matrix

In the subspace approach presented in Section 2.3.1, we have considered only the Fourier series coefficients $X[m]$ corresponding to non-negative frequencies $m\omega_0$, and proved that in the noiseless case it is possible to obtain perfect estimates of the time delays and weights of Diracs from only $2K$ adjacent coefficients $X[m]$. However, using only the positive coefficients implies that the bandwidth of the sinc sampling kernel must be at least twice the critical bandwidth, originally used in the annihilating filter method, meaning that the sampling rate is at least twice the critical sampling rate. In this section, we show how the subspace method can be modified so as to use the coefficients with negative indices in the reconstruction algorithm as well. As we will see in the sequel, the benefit of such an approach is that one could use lower sampling rates for obtaining the same performance, or alternatively, one can improve the estimation performance for a given sampling rate.

As in our previous analysis, consider periodic stream of K weighted Diracs, $x(t) = \sum_n \sum_{k=0}^{K-1} c_k \delta(t - t_k - nT)$, filtered with a lowpass filter of bandwidth $[-K\omega_0, K\omega_0]$, and sampled uniformly at a critical rate. From a set of samples, taken over one period, one can compute the Fourier series coefficients $X[m]$, $m \in [-K, K]$, given by (2.7). Construct next a Hankel data matrix \mathbf{X} as:

$$\mathbf{X} = \begin{pmatrix} X[-K+1] & X[-K+2] & \dots & X[0] \\ X[-K+2] & X[-K+2] & \dots & X[1] \\ \vdots & & & \\ X[1] & X[2] & \dots & X[K] \end{pmatrix}. \quad (2.53)$$

Note that \mathbf{X} is of size $(K+1) \times K$, however, we could have constructed the matrix of size $K \times (K+1)$ as well. The only difference is that in the first case,

we will estimate the signal poles from the left singular vectors of \mathbf{X} , while in the latter case, we would estimate them from the right singular vectors.

By analogy to the derivation from 2.3.1, one possible decomposition of noise-free \mathbf{X} is $\mathbf{X} = \mathbf{U}\mathbf{S}\mathbf{V}^H$, with \mathbf{U} , \mathbf{S} and \mathbf{V} given by

$$\mathbf{U} = \begin{pmatrix} z_0^{-K+1} & z_1^{-K+1} & z_2^{-K+1} & \cdots & z_{K-1}^{-K+1} \\ z_0^{-K+2} & z_1^{-K+2} & z_2^{-K+2} & \cdots & z_{K-1}^{-K+2} \\ \vdots & & & & \\ 1 & 1 & 1 & \cdots & 1 \\ z_0 & z_1 & z_2 & \cdots & z_{K-1} \end{pmatrix}, \quad (2.54)$$

$$\mathbf{S} = \text{diag}(c_0 \quad c_1 \quad c_2 \quad \cdots \quad c_{K-1}). \quad (2.55)$$

$$\mathbf{V} = \begin{pmatrix} 1 & 1 & 1 & \cdots & 1 \\ z_0^* & z_1^* & z_2^* & \cdots & z_{K-1}^* \\ \vdots & & & & \\ z_0^{*K-1} & z_1^{*K-1} & z_2^{*K-1} & \cdots & z_{K-1}^{*K-1} \end{pmatrix}, \quad (2.56)$$

Following the argument from Section 2.3.1, the matrix \mathbf{U} can be written in a more compact form as:

$$\mathbf{U} = \begin{pmatrix} \mathbf{b}\Phi^{-K+1} \\ \mathbf{b} \cdot \Phi^{-K+2} \\ \mathbf{b} \cdot \Phi^{-K+3} \\ \vdots \\ \mathbf{b} \\ \mathbf{b} \cdot \Phi \end{pmatrix}, \quad (2.57)$$

where, as before, \mathbf{b} is a row vector of length K , $\mathbf{b} = [1 \ 1 \ \dots \ 1]$, and Φ is a $K \times K$ diagonal matrix $\Phi = \text{diag}(z_k)$. Therefore, one can use the same shift-invariance property as in (2.25) to estimate the signal poles z_k ,

$$\overline{\mathbf{U}} = \underline{\mathbf{U}} \cdot \Phi. \quad (2.58)$$

As already discussed in Section 2.3.1, in practice, when noise is present, the matrix \mathbf{X} will be decomposed using the SVD as

$$\mathbf{X} = \mathbf{U}_s \mathbf{S}_s \mathbf{V}_s^H + \mathbf{U}_n \mathbf{S}_n \mathbf{V}_n^H, \quad (2.59)$$

and the signal poles z_k can be uniquely determined from the eigenvalues λ_k of an operator that maps $\underline{\mathbf{U}}_s$ onto $\overline{\mathbf{U}}_s$ that is,

$$t_k = -\frac{T\angle\lambda_k}{2\pi}. \quad (2.60)$$

Once the signal poles have been estimated, the weighting coefficients c_k can be found as a least-squares solution to (2.7).

2.6 Simulation Results

In this section, we illustrate the performances of the developed schemes with simulation results. Experiments are done in discrete-time, with a very long block size in order to simulate continuous time.

We first consider a length 10000 signal made up of a periodic stream of $K = 7$ weighted Diracs, and analyze the following cases: the locations of Diracs are chosen randomly according to a uniform distribution over the interval $[1, 10000]$; the first component is chosen randomly over $[1, 10000]$, while the spacing between the components is a Gaussian random variable with mean $m = 20$ and standard deviation $d = 1$. The signal is filtered with a lowpass filter, having one of the following bandwidths: $B_1 = [-500, 500]$, $B_2 = [-1000, 1000]$ and $B_3 = [-1250, 1250]$, and in each case, a lowpass version of the signal is sampled uniformly at a critical rate. The spectrum of the signal and the bandwidths used for estimation are illustrated in Figure 2.1(a). In Figure 2.1(b), we plot the mean-square error (MSE) of the position estimates versus signal-to-noise (SNR) ratio. The error is computed as an average MSE over 100 different trials and normalized to the signal period. The results indicate that the performance of the method can be improved by increasing the bandwidth and estimating the parameters from a larger set of samples. Yet, such an improved performance is achieved at the expense of increased computational requirements, since the complexity of the reconstruction scheme using N_t samples is on the order of $\mathcal{O}(N_t^3)$ [27]. More importantly, the performance of the method degrades in the case when the average spacing between the Diracs is small compared to the signal period. For example, when the average spacing is 20 (i.e. 0.2% of the signal period) and $\text{SNR} < 10\text{dB}$, it is no longer possible to reconstruct the signal using only the band B_1 , and one should estimate the parameters from a larger signal subspace.

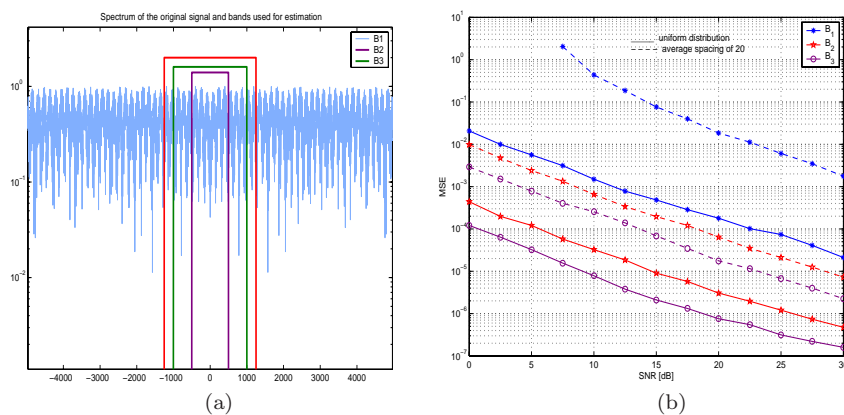


Figure 2.1: Periodic stream of Diracs A periodic signal of length 10000, made up of 7 weighted Diracs, is passed through a lowpass filter and sampled uniformly at the critical rate, determined by the filter bandwidth. We considered 3 different filter bandwidths: $B_1 = [-500, 500]$, $B_2 = [-1000, 1000]$ and $B_3 = [-1250, 1250]$. (a) Magnitude of the signal spectrum and bands used for estimation. (b) MSE of location estimates versus SNR. Solid lines correspond to the case when the locations are randomly chosen according to a uniform distribution over the interval $[1, 10000]$, while dashed lines correspond to the MSE in the case when the average spacing between components is 20 (i.e. 0.2% of the signal period).

However, a more attractive solution to this problem is the one presented in Section 2.5.1, where the resolution performance is improved by exploiting the shift-invariant subspace property in a different way, rather than by increasing the data set used for estimation. In Figure 2.2(a), we compare the MSE ob-

tained with the original method and the subspace-shifting method from Section 2.5.1. We show the estimation performance for different values of the shift parameter p , which determines the increase in the effective separation between the estimated components. Clearly, for all considered values of SNR, the latter approach results in much better numerical precision. Note that by increasing the value of p , the estimation accuracy improves, and in this particular case, the value of $p = 10$ already yields very good precision. Also note that such an approach does not increase the overall computational requirements, since the size of the data matrix is the same as in the original method. In Figure 2.2(b), we compare the estimation performances of the subspace-shifting approach and the interleaving method, also presented in Section 2.5.1, and this for different values of the average spacing between the Diracs. The value of SNR used in this set of simulations is $\text{SNR} = 10\text{dB}$. The results we obtained indicate that the interleaving technique yields better performance as the spacing between the components decreases. Besides, the numerical precision achievable by both techniques is by an order of magnitude better than the precision of the original method.

In Figure 2.3, we compare the estimation performance of the subspace method and the annihilating filter approach. We consider the case of a periodic stream of $K = 7$ Diracs, randomly distributed over the interval $[1, 10000]$, and assume that the band B_1 is used for estimation (i.e. the total number of samples is $N_t = 1000$). For the annihilating filter approach, we plot the MSE of location estimates obtained for several values of the filter order, that is, $N = 2K$, $N = 3K$, $N = 4K$ and $N = 150$. Obviously, as the filter order increases, one can obtain better estimates, and when $N = 150$, the subspace method and the annihilating filter approach yield almost the same results. However, in the latter case, one has to solve for $N \gg K$ zeros of the filter and then estimate the locations of the Diracs from $K = 7$ filter zeros closest to the unit circle [74]. This can be better seen in Figure 2.3, where we show the MSE of location estimates obtained with the annihilating filter method, and this for different values of the filter order. That is, even though the number of Diracs is $K = 7$, the size of the filter required for the “optimum” performance of the method is more than ten times larger.

2.7 Conclusion

In this chapter, we have formulated the sampling problem for signals of finite rate of innovation. We have revisited some of the results for deterministic, noiseless signals [85], and developed alternative computational tools that allow for more efficient reconstruction. Specifically, we have considered the case of a stream of Diracs and developed a subspace framework to signal reconstruction [65] [58], which provides an elegant and robust solution to the sampling problem. While some of the tools we used were borrowed from spectral analysis [74], we have developed techniques that improve resolution capabilities of the existing spectral estimation schemes in the case when the signal contains closely spaced components. In the next chapter, we will generalize the subspace framework to more complex classes of periodic signals with finite rate of innovation, such as piecewise polynomials and nonuniform splines, as well as extend the results to finite-length signals.

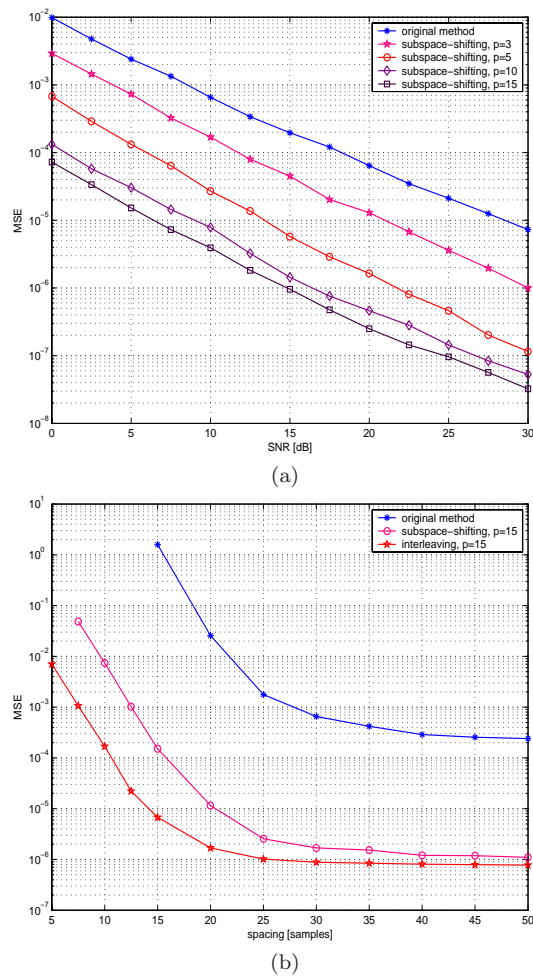
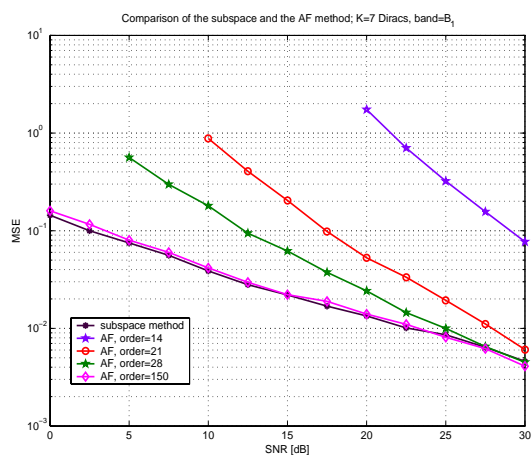
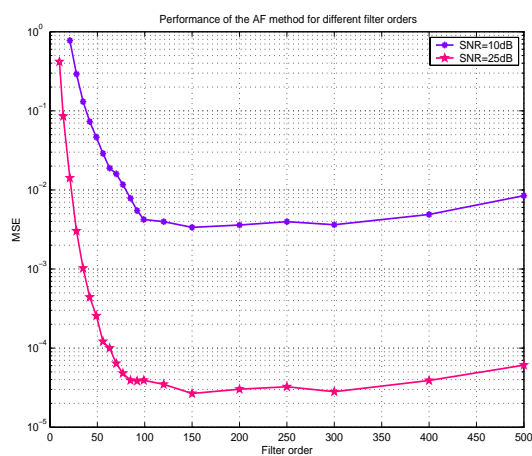


Figure 2.2: Periodic stream of Diracs: Improving the Resolution (a) MSE of location estimates for the original method and the matrix-shifting method vs. SNR. For the latter method, the error is plotted for different values of the shift parameter p . (b) MSE of location estimates vs. average spacing between the components. The MSE of the original method is compared to the MSE's of the interleaving technique and the subspace-shifting approach.



(a)



(b)

Figure 2.3: Annihilating filter method We consider a periodic signal made up of $K = 7$ Diracs, randomly distributed over the interval $[1, 10000]$. The signal is filtered through a lowpass filter $B_1 = -[500, 500]$ and a uniform set of $N_t = 1000$ samples is taken from its lowpass version. (a) MSE of location estimates obtained by the subspace method vs. MSE obtained using the annihilating filter approach. In the latter case, we show the MSE for different values of the filter order. (b) MSE of the annihilating filter approach vs. the filter order, shown for two values of SNR.

Chapter 3

Sampling Methods in the Presence of Noise

In the previous chapter, we have considered the problem of sampling a periodic stream of weighted Diracs and proved that in the absence of noise, such a signal can be perfectly reconstructed from its projection onto a subspace of dimension that is greater than or equal to the number of degrees of freedom of the signal. That is, even though this signal is not bandlimited, we showed that the minimum sampling rate required for a unique reconstruction is determined by the rate of innovation of the signal. In the presence of noise, however, one has to increase the sampling rate beyond the critical rate and estimate the signal parameters from a larger subspace in order to improve the numerical performance of the scheme.

In this chapter, we extend our results to other classes of signals with finite rate of innovation, such as non-uniform splines and piecewise polynomials. While the problem of sampling such signals in the deterministic, noiseless case was already considered in [85], many of those methods involve steps that can result in numerical ill-conditioning in the presence of noise. For example, it was shown that the problem of reconstructing non-uniform splines or piecewise polynomials can be reduced to the problem of reconstructing streams of Diracs by taking a sufficient number of signal derivatives. However, when noise is present, such an approach often results in an ill-conditioned problem, where standard techniques from noisy spectral estimation, including oversampling and solving various systems using the singular value decomposition, are not sufficient for improving the numerical performance. This naturally requires a revision of some of the techniques presented in [85] and development of alternative algebraic approaches that can solve the problem of ill-conditioning in the presence of noise and allow for precise reconstruction.

In this chapter, we develop improved, more robust methods that make use of proper preconditioning techniques and achieve good numerical performance, while retaining a linear, model-based flavor of the original sampling schemes. As in the previous chapter, we will focus on a subspace framework for signal reconstruction [65] [58], which, along with efficient noise suppression via singular value decomposition, provides an elegant and robust solution to the sampling problem.

The outline of the chapter is as follows. In Section 3.1, we review some of the related sampling results from [85], and discuss the problems that arise in the presence of noise. In Section 3.2, we extend the results from Chapter 2 to more complex classes of periodic signals of finite rate of innovation, such as nonuniform splines and piecewise polynomials, and propose novel algebraic approaches that use proper data windowing and solve the problem in the Laplace domain. We also briefly discuss the case of model mismatch. In Section 3.3, we consider the sampling problem for finite-length signals, and develop schemes that avoid the problem of ill-conditioning by appropriate weighting of a data matrix and allow for an almost local reconstruction. In particular, we investigate the possibility of developing practical sampling schemes using a Gaussian kernel. Simulation results that illustrate the numerical performances of the proposed techniques are shown in Section 3.4, and finally, in Section 3.5, we conclude with a brief summary of our work.

3.1 Sampling Schemes in the Presence of Noise: Problem Statement

Consider the following simple example. Let a signal $x(t)$ be a finite-length continuous-time signal made up of K weighted Diracs, i.e.

$$x(t) = \sum_{k=0}^{K-1} a_k \delta(t - t_k). \quad (3.1)$$

Since the signal is aperiodic, one can no longer use the frequency domain approach from the previous chapter to estimate the unknown parameters $\{t_k\}_{k=0}^{K-1}$ and $\{a_k\}_{k=0}^{K-1}$. However, if the signal is sampled with a proper sampling kernel, such as a Gaussian or a sinc sampling kernel, one can use similar techniques to solve for the parameters by exploiting the structure of the signal in the time domain [85].

In order to show the main idea behind the approach from [85], assume that the signal is filtered with the Gaussian kernel $h_g(t) = e^{-t^2/2\sigma^2}$ and that $N_t \geq 2K$ samples are taken from a filtered version,

$$y_n = \langle h_g(t - nT), x(t) \rangle, \quad n = 1, \dots, N_t. \quad (3.2)$$

In this case, the sample values are given by

$$y_n = \sum_{k=0}^{K-1} a_k e^{-(t_k - nT)^2/2\sigma^2} = \sum_{k=0}^{K-1} a_k e^{-t_k^2/2\sigma^2} \cdot e^{nt_k T/\sigma^2} \cdot e^{-n^2 T^2/2\sigma^2}. \quad (3.3)$$

If we denote by $u_n = y_n e^{n^2 T^2/2\sigma^2}$ and $c_k = a_k e^{-t_k^2/2\sigma^2}$, then (3.3) is equivalent to

$$u_n = \sum_{k=0}^{K-1} c_k e^{nt_k T/\sigma^2} = \sum_{k=0}^{K-1} c_k z_k^n, \quad (3.4)$$

where $z_k = e^{t_k T/\sigma^2}$. Note that the samples u_n are given by a linear combination of exponentials z_k^n ; thus we can reduce the problem of estimating the unknown

3.1. Sampling Schemes in the Presence of Noise: Problem Statement 33

parameters $\{t_k\}_{k=0}^{K-1}$ and $\{c_k\}_{k=0}^{K-1}$, into the classical spectral estimation problem, that is, the problem of estimating frequencies and weighting coefficients of superimposed exponentials [33] [65] [74].

In the above example, we assumed a deterministic, noiseless signal, when the presented method yields perfect estimates of all the parameters from only $2K$ samples. Yet, in the presence of noise, such an approach often gives rise to numerical ill-conditioning. To understand the main reason for performance degradation, consider a noisy version of the signal, that is, $x_n(t) = x(t) + \eta(t)$, where $\eta(t)$ is additive white Gaussian noise, and consider the set of noisy samples \tilde{y}_n , taken with the Gaussian kernel. As in the previous case, by denoting $\tilde{u}_n = \tilde{y}_n e^{n^2 T^2 / 2\sigma^2}$ and $c_k = a_k e^{-t_k^2 / 2\sigma^2}$, the set of samples \tilde{u}_n can be expressed as:

$$\tilde{u}_n = \sum_{k=0}^{K-1} c_k z_k^n + \eta_n e^{n^2 T^2 / 2\sigma^2}. \quad (3.5)$$

In this case, however, the samples of noise η_n become significantly amplified as n increases, due to the weighting of \tilde{y}_n 's with exponentially increasing terms $e^{n^2 T^2 / 2\sigma^2}$. This obviously makes the above method for reconstructing the signal from the samples \tilde{u}_n ill-conditioned.

A similar problem occurs with other classes of signals as well, such as piecewise polynomials or non-uniform splines. In [85], it was proved that in the absence of noise, the sampling problem for these signals can be reduced to the problem of sampling streams of Diracs, and this by taking a sufficient number of signal derivatives. For example, consider a periodic nonuniform spline $x(t)$ of period T and degree R , that is, a signal whose $(R+1)$ -th derivative $x^{(R+1)}(t)$ is a periodic stream of weighted Diracs [85]. If we denote by $X[m]$ and $X^{(R+1)}[m]$ the Fourier series coefficients of $x(t)$ and $x^{(R+1)}(t)$ respectively, the following relation holds:

$$X^{(R+1)}[m] = (jm\omega_0)^{(R+1)} X[m] = \frac{1}{T} \sum_{k=0}^{K-1} c_k e^{-jm\omega_0 t_k}, \quad \omega_0 = 2\pi/T. \quad (3.6)$$

Similarly to the argument for numerical ill-conditioning in the case of a set of Diracs, the problem with this approach is derivation. In particular, in order to compute the coefficients $X^{(R+1)}[m]$ and estimate the unknown parameters c_k and t_k , one first has to multiply all the coefficients $X[m]$ with $(jm\omega_0)^{(R+1)}$, which amplifies noise as frequency increases. In the case of piecewise polynomials, the method in [85] uses derivation as well, resulting in a sum of derivatives of Diracs. In addition to noise amplification, such an approach requires identification of multiple roots of the annihilating filter, a task that is difficult even in the noiseless case.

This obviously calls for an extension of the original results from [85] to solve the problems of ill-conditioning and robustness to noise, and to investigate alternative algebraic approaches that will yield numerically stable and precise reconstruction. In the following, we will show that by properly exploiting the signal structure, one can come up with more general constructions that satisfy all of the above requirements, while still being computationally reasonable.

3.2 Sampling Periodic Nonuniform Splines and Piecewise Polynomials

In this section, we consider the sampling problem for classes of periodic signals with finite rate of innovation, such as nonuniform splines and piecewise polynomials. In particular, we show how to modify methods from [85] in order to achieve good numerical performance in the noisy case.

3.2.1 Periodic nonuniform splines

We first consider the sampling problem for periodic nonuniform splines, since this case is a direct extension of the sampling problem for a stream of Diracs, which will also set the grounds for the following subsection on piecewise polynomials.

A signal $x(t)$ is a periodic nonuniform spline of period T and degree R , with knots at $\{t_k\}_{k=0}^{K-1} \in [0, T]$, if its $(R+1)$ -th derivative is a periodic stream of K weighted Diracs, that is,

$$x^{(R+1)}(t) = \sum_n \sum_{k=0}^{K-1} c_k \delta(t - t_k - nT). \quad (3.7)$$

The Fourier series coefficients $X^{(R+1)}[m]$ are given by (3.6), that is, $X^{(R+1)}[m] = \frac{1}{T} \sum_{k=0}^{K-1} c_k e^{-jm\omega_0 t_k}$, where $\omega_0 = 2\pi/T$. Therefore, by considering the coefficients that correspond to the $(R+1)$ -th derivative of the original signal $x(t)$, we can reduce the problem of estimating the unknown signal parameters to the one of estimating the parameters of superimposed complex exponentials. Note that the derivation can be done in the frequency domain, by multiplying the Fourier series coefficients $X[m]$ with $(jm\omega_0)^{(R+1)}$. Once the coefficients $X^{(R+1)}[m]$ have been computed, the signal parameters can be estimated using the method developed in Section 2.3.1. However, the problem in the presence of noise is derivation, as it enhances noise. Therefore, in the following, we present a modified version of the method from [85], which yields better performance while retaining the shift-invariant flavor of the original scheme.

Consider again the Fourier series coefficients $X[m]$, given by (3.6). Note that the term $(jm\omega_0)^{R+1}$, corresponding to the $(R+1)$ -th derivative operator in the frequency domain, grows as m^{R+1} . Thus, the idea is to weight the coefficients $X^{(R+1)}[m]$ with a multiplicative term $S[m]$, which has at least an exponential decay, in order to compensate for the polynomial growth of $(jm\omega_0)^{R+1}$. One possible solution is to choose $S[m] = e^{-sm\omega_0}$, where s is a parameter that can be adjusted according to the value of SNR (s is a positive real number) and the size of the data set used for estimation. Consider thus an expression for the new, weighted coefficients $X_s[m]$:

$$\begin{aligned} X_s[m] &= (j\omega_0 m)^{(R+1)} X[m] e^{-sm\omega_0} \\ &= \sum_{k=0}^{K-1} c_k e^{-jm\omega_0 t_k} e^{-sm\omega_0} \\ &= \sum_{k=0}^{K-1} c_k e^{-m\omega_0(s+jt_k)}. \end{aligned} \quad (3.8)$$

3.2. Sampling Periodic Nonuniform Splines and Piecewise Polynomials 35

Note that the $X_s[m]$'s are given by a sum of damped exponentials, however, the shift invariance property (2.25) still holds. Therefore, one can use the method from Section 2.3.1 to estimate the unknown parameters $\{c_k\}_{k=0}^{K-1}$ and $\{t_k\}_{k=0}^{K-1}$ from the coefficients $X_s[m]$. The only difference compared to the original approach is that the estimated eigenvalues $z_k^{(s)}$ are now given by $z_k^{(s)} = e^{-\omega_0 \sigma_k}$, where $\sigma_k^{(s)} = s + jt_k$. Given that the value of the damping factor s is known, the time instants t_k 's can be found directly from the eigenvalues $z_k^{(s)}$, while estimation of the weighting coefficients c_k follows the same procedure as before. We note that this is a general result, which holds for all classes of periodic signals considered in [85]. Namely, all the methods developed for periodic signals use the Fourier series coefficients $X[m]$ to extract the signal poles $z_k = e^{-j\omega_0 t_k}$, and thus estimate the unknown locations t_k . Alternatively, one can consider the set of weighted coefficients $X_s[m]$, and use the same techniques to estimate the scaled version of the signal poles, $z_k^{(s)} = e^{-\omega_0(s+jt_k)}$. Therefore, instead of solving the problem in the Fourier domain [85], one can solve the problem in the Laplace transform domain, which allows for the same algorithmic tools, and yet leads to better conditioning for certain classes of signals. Thus, we have the following proposition.

Theorem 3.1: Consider a periodic nonuniform spline $x(t)$ of period T and degree R , with the $(R+1)$ -th derivative of the form $x^{(R+1)}(t) = \sum_n \sum_{k=0}^{K-1} c_k \delta(t - t_k - nT)$, and Fourier series coefficients $X^{(R+1)}[m] = \frac{1}{T} \sum_{k=0}^{K-1} c_k e^{-jm\omega_0 t_k}$, $\omega_0 = 2\pi/T$. Consider a weighted set of coefficients $X_s[m] = X^{(R+1)}[m]e^{-sm\omega_0}$, $s \geq 0$. If $H(z)$ is the annihilating filter for $X[m]$, then $H(ze^{-s\omega_0})$ will be the annihilating filter for $X_s[m]$, and vice versa. An equivalent statement holds for eigenvalues obtained by the subspace approach (4.17).

While in the above proposition we made no assumption on the value of the parameter s , in practice, it should be chosen such that in a considered frequency band, the power spectral density of noise, weighted by $|(jm\omega_0)^{(R+1)}e^{-sm\omega_0}|^2$, is as uniform as possible (and does not exceed the power spectral density of a signal). However, we should note that in the general case of nonuniform splines of degree $R > 1$, the method may still be sensitive to noise, despite windowing. Namely, in the case when transitions between adjacent pieces are almost smooth, it is difficult to extract the discontinuities in the differentiated signal, even with proper windowing. In the case of piecewise polynomials, this is not an issue, since the signal itself already contains discontinuities.

3.2.2 Piecewise polynomials

Similarly to the definition of periodic nonuniform splines, a signal $x(t)$ is a periodic piecewise polynomial of period T , having K pieces of maximum degree R , if and only if its $(R+1)$ -th derivative is a periodic stream of differentiated Diracs, that is,

$$x^{(R+1)}(t) = \sum_n \sum_{k=0}^{K-1} \sum_{r=0}^{R_k-1} c_{k,r} \delta^{(r)}(t - t_k - nT). \quad (3.9)$$

The corresponding Fourier series coefficients are given by

$$X^{(R+1)}[m] = \frac{1}{T} \sum_{k=0}^{K-1} \sum_{r=0}^{R_k-1} c_{k,r}(j\omega_0 m)^r e^{-jm\omega_0 t_k}. \quad (3.10)$$

By denoting $\tilde{c}_{k,r} = (1/T)c_{k,r}(j\omega_0)^r$, we obtain

$$X^{(R+1)}[m] = \sum_{k=0}^{K-1} \sum_{r=0}^{R_k-1} \tilde{c}_{k,r} m^r e^{-jm\omega_0 t_k}. \quad (3.11)$$

As discussed in the previous section, the problem in the presence of noise is differentiation. Therefore, instead of considering the set of coefficients corresponding to the $(R+1)$ -th derivative, the idea is to consider a set of weighted coefficients $X_s^{(R+1)}[m] = X^{(R+1)}[m]e^{-j\omega_0 sm}$, given by

$$X_s^{(R+1)}[m] = \sum_{k=0}^{K-1} \sum_{r=0}^{R_k-1} \tilde{c}_{k,r} m^r e^{-m\omega_0(s+jt_k)}. \quad (3.12)$$

However, in this case, it is no longer obvious that the shift-invariant subspace property (2.25) can be exploited, since each term $e^{-m\omega_0(s+jt_k)}$ is additionally multiplied by a polynomial $\sum_{r=0}^{R_k-1} m^r$. That is, the coefficients $X_s^{(R+1)}[m]$ are given by a non-linear combination of complex exponentials. In the following, we will show that one can still obtain a closed-form subspace solution to the problem of parameter estimation from $X_s^{(R+1)}[m]$. Specifically, since the exact solution can be relatively easily obtained using the annihilating filter method [85], we will use Theorem 3.1, to find a subspace solution to the problem. This will provide a practical approach for solving a more general class of non-linear estimation problems [49], and will also extend classic high-resolution spectral estimation techniques [33] [65] [74].

Consider thus the annihilating filter $H(z) = \sum_{m=0}^N H[m]z^{-m}$, which satisfies

$$(H * X_s^{(R+1)})[n] = 0, \quad \forall n \in \mathbb{Z}. \quad (3.13)$$

In [85], it was shown that in the case when the coefficients $X_s^{(R+1)}[n]$ are given by (3.12), the annihilating filter has multiple roots at $z_k = e^{-\omega_0(s+jt_k)}$, that is,

$$H(z) = \prod_{k=0}^{K-1} (1 - e^{-\omega_0(s+jt_k)} z^{-1})^R = \sum_{m=0}^{RK} H[m]z^{-m}. \quad (3.14)$$

Namely, the key is to observe that each component $S_{k,r}^{(R+1)}[m] = m^r e^{-m\omega_0(s+jt_k)}$ in (3.12) is annihilated by a filter which has $r+1$ zeros at $z_k^{(s)} = e^{-\omega_0(s+jt_k)}$ [85], i.e.

$$H_{k,r}(z) = (1 - e^{-\omega_0(s+jt_k)} z^{-1})^{r+1}. \quad (3.15)$$

Since the filter $H_{k,R-1}(z)$ annihilates all the components $S_{k,r}^{(R+1)}[m]$, where $r = 0, \dots, R-1$, the annihilating filter for the signal $X_s^{(R+1)}[n]$ is given by

$$H(z) = \prod_{k=1}^K H_{k,R-1}(z) = \prod_{k=0}^{K-1} (1 - e^{-\omega_0(s+jt_k)} z^{-1})^R. \quad (3.16)$$

3.2. Sampling Periodic Nonuniform Splines and Piecewise Polynomials 37

Therefore, the information about the time delays t_k can be extracted from the R -th order roots z_{ks} of the filter $H(z)$, while the corresponding weights $c_{k,r}$ can be then found by solving the system of linear equations (3.10).

Let us show next how this result can be used to find a subspace solution to the estimation problem. Following the approach from Section 2.3.1, given a set of the coefficients $X_s^{(R+1)}[m]$, one first has to construct a Hankel data matrix \mathbf{X} of size $M \times N$, where $M, N \geq RK$. The second step is to compute the SVD of \mathbf{X} and extract its RK principal left singular vectors \mathbf{U}_s (or alternatively, RK principal right singular vectors \mathbf{V}_s). Once \mathbf{U}_s has been estimated, one should compute the matrix \mathbf{H} as in (4.17), that is, $\mathbf{H} = \underline{\mathbf{U}}_s^+ \cdot \overline{\mathbf{U}}_s$. From Proposition 1, it follows that the eigenvalues of \mathbf{H} are identical to the roots of the annihilating filter $H(z)$ (3.16). Specifically, since the filter has R -th order roots at $z_k^{(s)} = e^{-\omega_0(s+jt_k)}$, $k = 1, \dots, K$, the matrix \mathbf{H} will have K distinct eigenvalues at $z_k^{(s)}$, each with an algebraic multiplicity R . Thus, an equivalent statement to the one in Proposition 1, holds in this case as well. However, we note that in the presence of noise, it is desirable to estimate the signal poles from those eigenvalues $z_k^{(s)}$ closest to the circle $|z| = e^{-s\omega_0}$ [74]. Finally, we note that since the signal already contains discontinuities, the above method will generally result in better numerical performance than in the case of nonuniform splines.

3.2.3 Model mismatch

In all the methods presented so far, we assumed that both a signal model and the model order are known a priori. This allowed us to select an appropriate reconstruction technique, as well as the size of the data matrix, to ensure that all the signal parameters are reliably estimated. In the presence of noise, the low-rank subspace property is destroyed and such an increased dimension of the solution set must be dealt with carefully.

In the problem of estimating the parameters of superimposed exponentials, the model order can be obtained from the number of dominant singular values of the noisy data matrix, which is a very good estimate provided that the smallest singular value of the original, noiseless matrix dominates the noise variance. However, for low values of SNR, it is often difficult to discriminate between small singular values corresponding to the signal from extraneous ones due to noise and, typically, only dominant signal components can be reliably estimated [74]. The problem becomes more involved in the case of piecewise polynomials and non-uniform splines, since one has to take a sufficient number of signal derivatives prior to constructing the data matrix. Such an approach obviously raises the following question: how to reconstruct the signal in the case when neither the signal model nor the model order are known? While at this point we do not have a formal answer to this question, we would still like to point to one possible solution, that is, finding a piecewise constant approximation of the signal.

In order to explain the main idea behind such an approach, consider a periodic signal $x(t)$ of period T , filtered with a lowpass filter and sampled uniformly at a critical rate. In the case when the bandwidth of the filter is relatively low compared to the effective bandwidth of the original signal, one could expect that the Shannon interpolation formula would not yield a good approximation of the signal. Therefore, following the approach used for reconstruction of a stream of

Diracs from a lowpass version, one can obtain a piecewise constant approximation $x_a(t)$ of the signal. This would potentially yield a better approximation, particularly for signals with discontinuities.

Assume thus that $x_a(t)$ contains M constant pieces. In this case, $x_a(t)$ is uniquely determined by a set of transition instants $\{t_m\}_{m=1}^M$ and the corresponding amplitudes $\{a_m\}_{m=1}^M$. The key is to consider the first derivative $x_d(t)$ of the piecewise constant approximation $x_a(t)$. By denoting $c_m = a_m - a_{m-1}$, the first derivative $x_d(t)$ is given by a periodic sum of weighted pulses,

$$x_d(t) = \frac{d}{dt}x_a(t) = \sum_n \sum_{m=0}^{M-1} c_m \delta(t - t_m - nT). \quad (3.17)$$

The idea is to approximate the first derivative of $x(t)$ with the sum of weighted Diracs, instead of approximating the original signal $x(t)$. This can be done using the method developed in Section 2.2 and estimating the values of $\{t_m\}_{m=1}^M$ and $\{c_m\}_{m=1}^M$ from the following system:

$$j\omega_0 n X[n] e^{-sn\omega_0} = \sum_{m=0}^{M-1} c_m e^{-n\omega_0(s+jt_m)}. \quad (3.18)$$

where $j\omega_0 X[n]$ are the Fourier series coefficients corresponding to the first derivative of the original signal. Note that these coefficients are windowed by exponentially decaying terms $w[n] = e^{-sn\omega_0}$, in order to avoid ill-conditioning of the system (3.8).

3.3 Aperiodic Signals of Finite Rate of Innovation

So far, we have considered the sampling problem for periodic signals of finite rate of innovation and developed methods that exploit the structure of the Fourier series coefficients. The problem becomes more challenging in the aperiodic case, since the frequency domain approach cannot be used. Therefore, we will present alternative methods that solve the problem in the time domain. In particular, we will consider schemes where a signal is sampled with a Gaussian kernel, since in such a case the signal samples have an algebraic structure that can be easily exploited (3.3)-(3.4) [85].

3.3.1 Streams of Diracs

Consider first the basic problem discussed in Section 3.1, that is, the problem of sampling the finite stream of K weighted Diracs, $x(t) = \sum_{k=0}^{K-1} a_k \delta(t - t_k)$, with the Gaussian kernel $h_\sigma(t) = e^{-t^2/2\sigma^2}$. Denote by y_n the samples of the noiseless signal and let $w_n = e^{n^2 T^2 / 2\sigma^2}$. We have shown that the weighted set of samples $u_n = y_n w_n$ can be expressed as a sum of real exponentials (3.4), that is,

$$u_n = \sum_{k=0}^{K-1} c_k e^{nt_k T / \sigma^2} = \sum_{k=0}^{K-1} c_k z_k^n,$$

where $z_k = e^{t_k T / \sigma^2}$ and $c_k = a_k w_k$. In practice, the samples u_n will be perturbed by noise, and the noisy measurements \tilde{u}_n can be expressed as

$$\tilde{u}_n = u_n + w_n \eta_n, \quad (3.19)$$

where η_n denote the samples of additive white Gaussian noise. Clearly, the problem in the presence of noise is exponential weighting of the samples (with terms n^2 in the exponent), and the Laplace domain formulation discussed in Section 3.2.1 does not provide a good alternative¹. We will thus present a similar approach to the one developed for periodic signals, which can be viewed as a generalization of the Laplace domain solution.

Consider again the subspace approach, where the following Hankel matrix is constructed:

$$\tilde{\mathbf{X}} = \begin{pmatrix} \tilde{u}_0 & \tilde{u}_1 & \dots & \tilde{u}_{N-1} \\ \tilde{u}_1 & \tilde{u}_2 & \dots & \tilde{u}_N \\ \vdots & \vdots & \ddots & \\ \tilde{u}_{M-1} & \tilde{u}_M & \dots & \tilde{u}_{M+N-2} \end{pmatrix}, \quad (3.20)$$

where $M, N \geq K$, and assume for simplicity that $M \geq N$. Denote by \mathbf{X} a matrix constructed from the noiseless samples u_n . Then we can write $\tilde{\mathbf{X}} = \mathbf{X} + \mathbf{W}$, where the matrix \mathbf{W} is made up of weighted samples of noise,

$$\mathbf{W} = \begin{pmatrix} w_0\eta_0 & w_1\eta_1 & \dots & w_{N-1}\eta_{N-1} \\ w_1\eta_1 & w_2\eta_2 & \dots & w_N\eta_N \\ \vdots & \vdots & \ddots & \\ w_{M-1}\eta_{M-1} & w_M\eta_M & \dots & w_{M+N-2}\eta_{M+N-2} \end{pmatrix}. \quad (3.21)$$

For medium to high values of SNR, the perturbation on the matrix \mathbf{X} has little effect on the principal singular vectors. In such a case, a rank K approximation of the noiseless data matrix \mathbf{X} can be obtained by computing the singular value decomposition of $\tilde{\mathbf{X}}$ and setting all but the K largest singular values to zero. However, in our case, due to the exponential weighting of noise samples, dominant singular values do not necessarily belong to the signal space, as they may also include those corresponding to noise. In the following, we propose a scaling technique that additionally multiplies the entries of the noisy matrix $\tilde{\mathbf{X}}$ in order to make the noise variance as uniform (and minimal) as possible. This will allow us to use the SVD for noise suppression.

The idea is to replace $\tilde{\mathbf{X}}$ with another matrix

$$\tilde{\mathbf{X}}_s = \mathbf{A}\tilde{\mathbf{X}}\mathbf{B} = \mathbf{A}\mathbf{X}\mathbf{B} + \mathbf{A}\mathbf{W}\mathbf{B}.$$

In general, \mathbf{A} and \mathbf{B} can be any invertible matrices, however, the goal is to choose those matrices such that the entries of $\mathbf{W}_s = \mathbf{A}\mathbf{W}\mathbf{B}$ have a uniform and minimum variance. One possible solution is to make both \mathbf{A} and \mathbf{B} to be diagonal matrices, since any linear combination of lines or columns of \mathbf{W} would increase the noise variance. In order to obtain a uniform variance, the elements of \mathbf{A} and \mathbf{B} can be chosen as:

$$\mathbf{A}[i, i] = \frac{1}{\frac{1}{N} \sum_{n=0}^{N-1} w_{n+i}}, \quad i = 0, \dots, M-1, \quad (3.22)$$

$$\mathbf{B}[j, j] = \frac{1}{\frac{1}{M} \sum_{m=0}^{M-1} \mathbf{A}[m, m] w_{m+j}}, \quad j = 0, \dots, N-1. \quad (3.23)$$

¹According to the Laplace domain solution, the samples are additionally weighted with exponentially decreasing terms, however, these terms must have n in the exponent in order to be able to express the weighted samples as a sum of (damped) exponentials.

As a result of such a transformation, one can think of the entries of \mathbf{W}_s as being the samples of additive white noise. Now we can use the singular value decomposition of the noisy matrix $\tilde{\mathbf{X}}_s$, i.e.

$$\tilde{\mathbf{X}}_s = \mathbf{U}_s \mathbf{S}_s \mathbf{V}_s^H + \mathbf{U}_n \mathbf{S}_n \mathbf{V}_n^H,$$

where the first term contains K principal components of $\tilde{\mathbf{X}}_s$. However, note that the above transformation destroys the Hankel structure of the original data matrix. Therefore, once the principal components of $\tilde{\mathbf{X}}_s$ have been computed, one can compensate for the effects of \mathbf{A} and \mathbf{B} by constructing a new, denoised data matrix \mathbf{X}_d as

$$\mathbf{X}_d = \mathbf{A}^{-1} \mathbf{U}_s \mathbf{S}_s \mathbf{V}_s^H \mathbf{B}^{-1}. \quad (3.24)$$

The above approach can further be simplified as follows. Suppose that we estimate the signal poles from right singular vectors of \mathbf{X}_d . In such a case, left multiplication of the matrix $\mathbf{U}_s \mathbf{S}_s \mathbf{V}_s^H$ by \mathbf{A}^{-1} is not required, since it does not change the right singular vectors.

3.3.2 Nonuniform splines

We will now extend the analysis to the more general class of finite-length signals with finite rate of innovation, such as non-uniform splines. A signal $x(t)$ is a nonuniform spline of degree R if and only if its $(R+1)$ -th derivative is a stream of weighted Diracs, that is,

$$x^{(R+1)}(t) = \sum_{k=0}^{K-1} c_k \delta(t - t_k). \quad (3.25)$$

Clearly, by sampling the signal $x^{(R+1)}(t)$ with the Gaussian kernel, we can reduce the problem of signal reconstruction to the one of estimating the parameters of superimposed weighted Diracs, which can be solved using the method from Section 2.3.1. However, since we have no access to the derivatives of the input signal, an equivalent approach would be to sample the input signal with an $(R+1)$ -th derivative Gaussian kernel. Such a kernel can be expressed as

$$h_\sigma^{(r+1)}(t) = \frac{d^r}{dt^r} \{e^{-t^2/2\sigma^2}\} = P_r(t) e^{-t^2/2\sigma^2}, \quad (3.26)$$

where $P_r(t)$ is a polynomial of degree r , given by the following recurrence relation:

$$P_0(t) = 1; \quad P_r(t) = P'_{r-1}(t) - \frac{t}{\sigma^2} P_{r-1}(t). \quad (3.27)$$

Note that in the case when $\sigma^2 = 1/2$, the polynomial $P_r(t)$ in (3.26)-(3.27) is a Hermite polynomial of degree r [17]. In Section 3.3.4, we will show how one can approximate such kernels with a linear combination of Gaussian functions. Such an approach will lead to a more practical version of the sampling scheme where the signal is sampled with the Gaussian kernel, while all further manipulations are carried out on a set of samples.

3.3.3 Piecewise polynomials

Similarly to the periodic case, a signal $x(t)$ is a piecewise polynomial with K pieces, each of maximum degree R , if and only if its $(R + 1)$ -th derivative is a stream of differentiated Diracs, that is,

$$x^{(R+1)}(t) = \sum_{k=0}^{K-1} \sum_{r=0}^R c_{k,r} \delta^{(r)}(t - t_k). \quad (3.28)$$

Thus, if the signal is sampled with a $(R + 1)$ -th derivative Gaussian kernel, the samples y_n are given by

$$y_n = \sum_{k=0}^{K-1} \sum_{r=0}^R c_{k,r} \left. \frac{d^r}{dt^r} \{e^{-(t-t_k)^2/2\sigma^2}\} \right|_{t=nT}. \quad (3.29)$$

As already discussed in Section 3.3.1, we can consider a new set of samples u_n , obtained by multiplying y_n with w_n . If we let $P_r(t)$ be an r -th order polynomial from (3.27) and $\tilde{c}_{k,r} = c_{k,r} e^{t_k^2/2\sigma^2}$, then the samples $u_n = y_n w_n$ can be expressed as:

$$u_n = \sum_{k=0}^{K-1} \sum_{r=0}^R \tilde{c}_{k,r} P_r(nT - t_k) e^{nt_k T/\sigma^2}. \quad (3.30)$$

Since in the above expression each exponential $e^{nt_k T/\sigma^2}$ is additionally multiplied by a polynomial in t_k , one can use the subspace approach discussed in Section 3.2.2 to solve for all the unknown parameters. Note that in this case one has to have access to the derivatives of the signal $x(t)$ as well, or alternatively, one should use the $(R + 1)$ -th derivative Gaussian kernel. However, such an approach is not desirable in practice, since one often cannot choose the sampling kernel arbitrarily. In the following, we present a method that allows the signal to be sampled with the Gaussian kernel, while the derivatives of the signal are then computed from a set of samples.

3.3.4 Practical realization of the Gaussian sampling schemes

Consider again the Gaussian kernel $h_\sigma(t) = e^{-t^2/2\sigma^2}$. The idea is to express the n -th derivative Gaussian kernel as a linear combination of the shifted versions of $h_\sigma(t)$. Let $h_\sigma^{(1)}(t) = h_\sigma(t - \sigma/m) - h_\sigma(t + \sigma/m)$, where σ/m is the corresponding shift. By choosing $m \geq 3$, the function $h_\sigma^{(1)}(t)$ becomes a very good approximation of the first derivative Gaussian function (up to a scaling factor). In order to show this, consider the Fourier transform of $h_\sigma^{(1)}(t)$, i.e.

$$H_\sigma^{(1)}(\omega) = H_\sigma(\omega) e^{j\omega\sigma/m} - H_\sigma(\omega) e^{-j\omega\sigma/m}, \quad (3.31)$$

where $H_\sigma(\omega)$ denotes the Fourier transform of $h_\sigma(t)$. Since $H_\sigma(\omega) = \sqrt{2\pi}\sigma e^{-\omega^2\sigma^2/2}$, we have

$$H_\sigma^{(1)}(\omega) = \sqrt{2\pi}\sigma e^{-\omega^2\sigma^2/2} \cdot (e^{j\omega\sigma/m} - e^{-j\omega\sigma/m}). \quad (3.32)$$

By using the Taylor series expansion of the second term in (3.32), we obtain

$$H_\sigma^{(1)}(\omega) = \sqrt{2\pi}\sigma e^{-\omega^2\sigma^2/2} \left(1 + j\omega\sigma/m + \frac{(j\omega\sigma/m)^2}{2!} + \frac{(j\omega\sigma/m)^3}{3!} + \dots \right)$$

$$\begin{aligned}
& - \sqrt{2\pi}\sigma e^{-\omega^2\sigma^2/2} \left(1 - j\omega\sigma/m + \frac{(j\omega\sigma/m)^2}{2!} - \frac{(j\omega\sigma/m)^3}{3!} + \dots\right) \\
& = \sqrt{2\pi}\sigma e^{-\omega^2\sigma^2/2} \left(2j\omega\sigma/m + 2\frac{(j\omega\sigma/m)^3}{3!} + 2\frac{(j\omega\sigma/m)^5}{5!} + \dots\right).
\end{aligned}$$

The key is to observe that $H_\sigma^{(1)}(\omega)$, which is given by a product of a polynomial in variable $\nu = \omega\sigma$, and an exponentially decaying function of ν^2 , contains only one dominant term, that is,

$$H_\sigma^{(1)}(\omega) \approx \sqrt{2\pi}\sigma e^{-\omega^2\sigma^2/2} \cdot 2j\omega \frac{\sigma}{m}. \quad (3.33)$$

This can be seen in Figure 3.1(a), where we plot the magnitude of the first three terms in the above sum for $m = 3$. Now one can compare the expression in (3.33) with an expression for the Fourier transform of the first-derivative Gaussian function, given by

$$\mathcal{F}\left\{\frac{d}{dt}h_\sigma(t)\right\} = \sqrt{2\pi}\sigma e^{-\omega^2\sigma^2/2} \cdot j\omega. \quad (3.34)$$

Note that there is only a scaling relation between the two expressions, therefore, the above approach gives a good approximation of the first derivative Gaussian function, which is illustrated in Figures 3.1(b)-(d).

The same idea can be used to approximate higher-order derivatives of the Gaussian kernel, using the following recurrence relation:

$$h_\sigma^{(n)}(t) = \frac{m}{2\sigma} (h_\sigma^{(n-1)}(t - \sigma/m) - h_\sigma^{(n-1)}(t + \sigma/m)), \quad n = 2, 3, 4, \dots \quad (3.35)$$

As in the previous case, the best way to see this is to note the following relation in the frequency domain:

$$e^{-\omega^2\sigma^2/2} (j\omega)^{n-1} (e^{j\omega\sigma/m} - e^{-j\omega\sigma/m}) \approx \frac{2\sigma}{m} e^{-\omega^2\sigma^2/2} (j\omega)^n. \quad (3.36)$$

Let us now return to the sampling problem for finite length signals. For example, consider a piecewise polynomial of maximum degree R . We have seen that in order to reconstruct the signal, one has to take samples with the $(R+1)$ -th derivative Gaussian kernel at locations kT . Following the procedure described above, these samples can be obtained from the set of samples taken with the Gaussian kernel at sampling instants $kT - r\sigma/2$, where $r = -R, -R+1, \dots, R$. This leads to a practical version of the developed algorithm, which we will illustrate in the next section.

3.4 Simulation Results

3.4.1 Periodic signals

In this section, we illustrate the performances of the developed schemes with simulation results. We first consider the case of a periodic nonuniform spline of period $T = 1000$ and degree $R = 1$, embedded in additive white Gaussian noise. The signal is filtered with a lowpass filter of bandwidth $B = [-50, 50]$ and a uniform set of 100 samples is taken from the lowpass version. In order

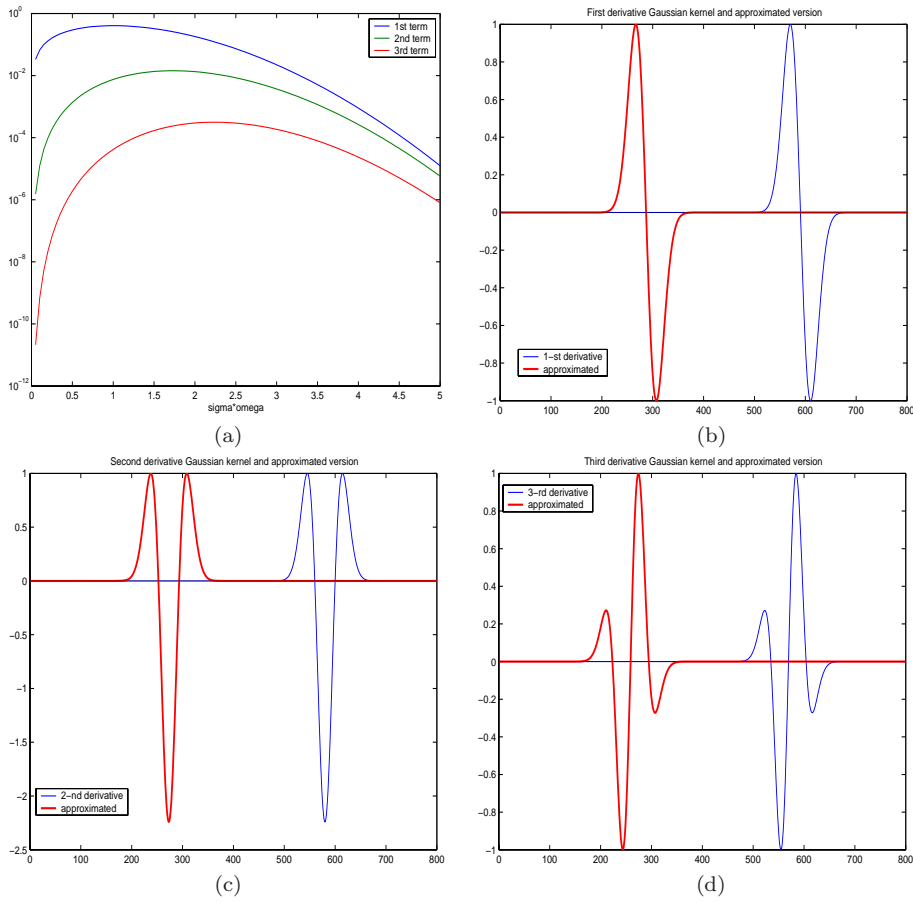


Figure 3.1: Approximation of the derivatives of a Gaussian kernel (a) Magnitude of the first three terms in the Taylor series expansion of $H_{\sigma}^{(1)}(\omega)$. (b) First derivative Gaussian kernel and its approximated version. (c) Second derivative Gaussian kernel and its approximation. (d) Third derivative Gaussian kernel and its approximation.

to reconstruct the signal from the set of samples, we used the approach from Section 3.2.1, where the scaling parameter s is chosen to be $s = 0.015$. In particular, we first estimated the locations of the transition points, and then found the least-squares (LS) linear fit between each two transitions based on a set of samples. In Figure 3.2, we show the noisy version (SNR=27dB) and the reconstructed signal, where the reconstruction error is MSE=0.0135. While in this case we have obtained a good reconstruction of the original signal, in general, for $R > 1$, the method becomes more sensitive to noise, as already discussed in Section 3.2.1.

In the following example, we consider a noisy piecewise linear signal of length 1000 (SNR=15dB), made up of 7 pieces. The signal is passed through a low-pass filter of bandwidth $B = [-100, 100]$, and a set of 200 uniform samples is taken from the lowpass version. We used the approach from Section 3.2.2 to reconstruct the signal, with the scaling parameter $s = 0.01$. As in the previous case, we first extracted the locations and weights of the discontinuities,

and then computed the best (LS) linear fit between each two adjacent discontinuities. In Figure 3.2(b), we show the noisy version and the reconstructed signal. The reconstruction error is $MSE=0.015$, however, we should note that as SNR decreases, the method is less sensitive to noise than it was the case with nonuniform splines.

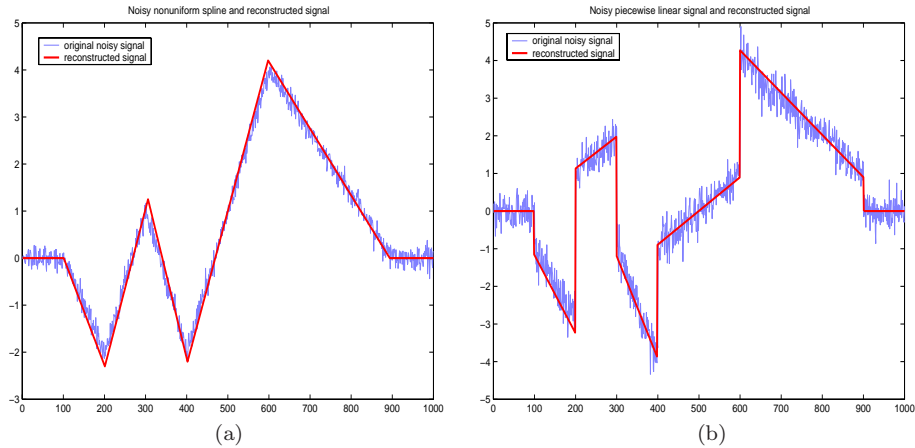


Figure 3.2: Periodic nonuniform splines and piecewise polynomials (a) *Noisy nonuniform spline (SNR=27dB) of degree $R = 1$ and reconstructed signal. The signal is reconstructed with an error of $MSE=0.0135$. The error is defined as $MSE = E\{(x_{est} - x)^2\}/E\{x^2\}$, where x_{est} and x denote respectively, the estimated signal and the original signal in one period.* (b) *Noisy piecewise linear signal (SNR=15dB) and reconstructed signal. MSE of reconstruction is $MSE=0.015$.*

3.4.2 Finite length signals

In this set of simulations, we consider finite length signals and evaluate the performance of the schemes based on a Gaussian sampling kernel. We first analyze the case of a length 1000 signal, made up of K weighted Diracs, where K takes on values between $K = 2$ and $K = 12$. We assume that the spacing between the Diracs is a Gaussian random variable with mean $t_s = 60$ and standard deviation $d = 3$. The signal is filtered with a Gaussian kernel $h_\sigma(t) = e^{-t^2/2\sigma^2}$. In Figure 3.3(a), we show the MSE (normalized to the length of the signal) of position estimates obtained using the method from Section 3.3.1, in the case when $K = 6$ and $\sigma = 35$. The results are compared to the error obtained using the original method (i.e. no weighting of the data matrix). Note that by using the original method, it is not possible to reconstruct the signal for values of SNR lower than 25dB, whereas preconditioning of the data matrix \mathbf{X} (3.20) allows for significantly better estimation performance. Yet, in order to ensure a good performance of the algorithm, the width of the Gaussian kernel σ must be chosen carefully. This can be seen in Figures 3.3(b)-(c), where we plot the reconstruction error as a function of the parameter σ/t_s , where t_s denotes the average spacing between the components. The error is plotted for different values of SNR (Figure 3.3(b)), as well as different number of Diracs K (Figure 3.3(c)). The results indicate strong sensitivity to the choice of the parameter σ , specifically as K increases. In Figure 3.3(d), we show the reconstruction error

versus the number of Diracs K , while the parameter σ is chosen such that the MSE of reconstruction is minimized. Note that for all considered values of SNR, the method yields good performance for $K < 10$, however, when the number of Diracs further increases, the performance degrades significantly. The main reason for such a behavior is the following: as the number of components K increases, the time window where the signal must be sampled increases as well, and its duration is approximately given by Kt_s . Yet, the optimum width σ_{opt} of the sampling kernel is only a fraction of the average spacing t_s , for example, when $K = 8$, $\sigma_{opt} \approx 0.7t_s$ (see Figure 3.3(c)). Given the exponential decay of the Gaussian kernel, for large values of K , at each sampling instant we will obtain the information only about a limited number ($K_1 < K$) of Diracs, which results in bad conditioning of the system. This makes the Gaussian scheme suitable mainly for local reconstruction, where the overall sampling window is adapted to the width of the kernel. This is illustrated in Figure 3.3(d) as well, where we plot the MSE for $K \geq 9$, in the case when we sample the signal over two distinct time windows (of approximately equal duration), and in each window we perform local reconstruction. Such an approach clearly improves the performance of the original method.

In Figure 3.4(a), we illustrate a noisy piecewise constant signal (SNR=25dB) of length 1000, made up of 7 pieces. The signal is filtered with a Gaussian kernel with $\sigma = 75$, as shown in Figure 3.4(b), and a set of 160 samples is taken from the filtered version shown in Figure 3.4(c). The first derivative of the signal is computed according to (3.35), and the method from Section 3.3.1 is used for reconstruction. A reconstructed signal is illustrated in Figure 3.4(d), where the reconstruction error is $\text{MSE} = 6 \cdot 10^{-3}$. In Figure 3.4(e), we show the MSE of reconstruction versus SNR, for several different values of the number of samples N . The results indicate that the performance of the method improves as the number of samples increases. In this case, a very good reconstruction can be already obtained for $N = 120$, and by further increasing the number of samples, the performance does not significantly improve.

3.4.3 Model mismatch

In Figures 3.5 and 3.6, we illustrate robustness of our schemes to model mismatch. We first consider a noisy signal made up of $K = 15$ weighted Diracs, where the locations are randomly chosen according to a uniform distribution over the interval $[1, 1000]$, while the weights are i.i.d. zero mean Gaussian random variables with unit variance. The signal is filtered with a lowpass filter of bandwidth $[-100, 100]$ and 200 uniform samples are taken from the lowpass version. We used the subspace method from Section 2.3.1, where no prior knowledge of the model order is assumed. That is, the number of components is estimated as the number of dominant singular vectors of the corresponding data matrix. In Figure 3.5(b), we show the reconstructed stream of pulses, and obviously, only the dominant pulses have been extracted.

We next consider the case of a periodic piecewise polynomial signal of degree $R = 3$ embedded in noise, where the signal model is not known in advance. The signal is lowpass filtered and a uniform set of 40 samples is taken from the lowpass version. Since we made no assumption on the model, we approximated the signal with a piecewise constant function with $M = 16$ pieces, as illustrated in Figure 3.6(a). In Figure 3.6(b), we show the noiseless signal and

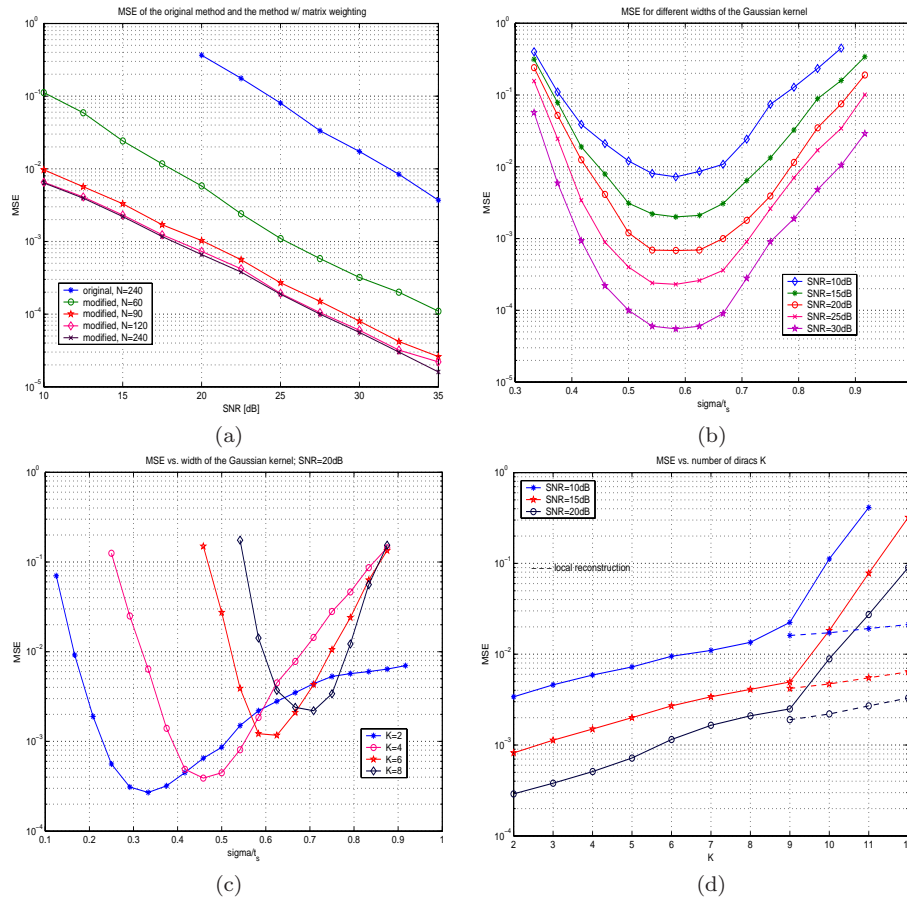


Figure 3.3: Aperiodic stream of Diracs: We consider a signal of length 1000, made up of K weighted Diracs (K is varied between 2 and 12), and sampled with the Gaussian kernel $e^{-t^2/2\sigma^2}$. Average spacing between the components is assumed to be $t_s = 60$. (a) MSE of position estimates vs. SNR, for $K = 6$, $\sigma = 35$. The MSE of the original method (i.e. with no weighting of the data matrix) is compared to the MSE obtained by the method from Section 3.3.1. (b) MSE of reconstruction vs. the width of the Gaussian kernel. The error is plotted as a function of the parameter σ/t_s (and is shown for different values of SNR), indicating a sensitivity of the method to the choice of the width σ . (c) MSE vs. σ/t_s , for different values of K . (d) MSE vs. number of Diracs K . For each value of K , we chose the optimal value of the kernel width σ , that is, the one which minimizes a reconstruction error. Dashed lines correspond to the MSE obtained by sampling the signal over two smaller time windows and finding local reconstruction in each window.

the reconstructed lowpass version using Shannon's interpolation formula, where the frequency band used for reconstruction is the same as in the previous case. Obviously, our approach yields a better representation of discontinuities, which points to some robustness of our scheme to model mismatch.

3.5 Conclusion

In this chapter, we have considered the sampling problem for signals of finite rate of innovation in the presence of noise. We have revisited some of the results for deterministic, noiseless signals [85], and developed more robust methods that improve conditioning of the original schemes and allow for much better numerical performance. For classes of periodic signals, such as piecewise polynomials and nonuniform splines, we proposed novel algebraic solutions that use proper windowing and solve the problem in the Laplace domain. While some of the tools we used were borrowed from spectral analysis [74], our framework extends classic spectral estimation techniques and allows for solving more general classes of nonlinear estimation problems. We have also considered finite-length signals, and proposed improved schemes based on a Gaussian sampling kernel and weighting of the data matrix. Both the numerical analysis and simulation results indicate desirable properties of the proposed methods, particularly for classes of signals that contain discontinuities.

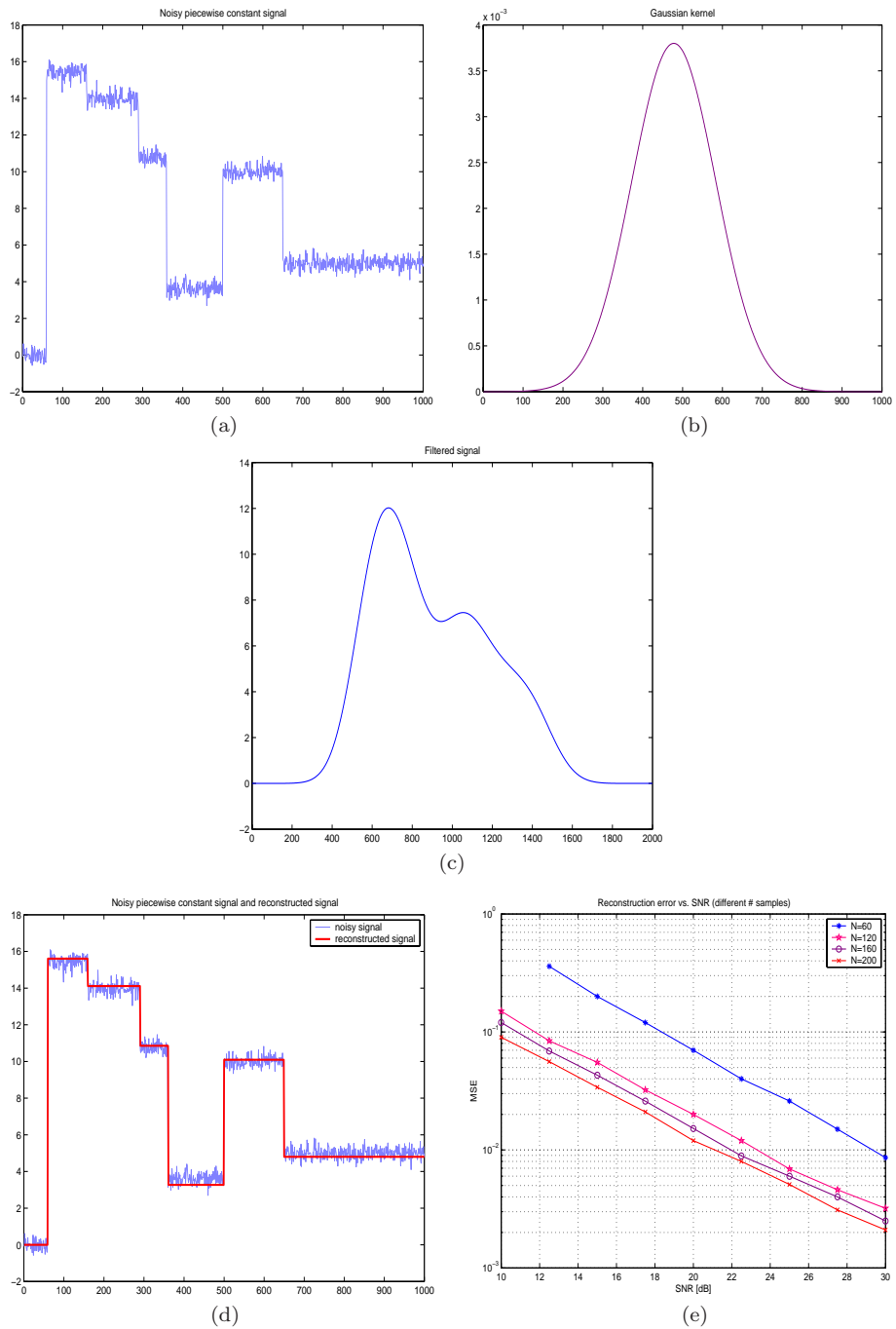


Figure 3.4: Aperiodic piecewise constant signal (a) *Noisy piecewise constant signal* ($SNR=25dB$). (b) *Gaussian kernel*. (c) *Filtered signal*. (d) *Noisy signal and reconstructed piecewise constant signal*. The signal is reconstructed from $N = 160$ samples, with an error of $MSE = 6 \cdot 10^{-3}$. (e) *Reconstruction error vs. SNR for different number of samples*. The error is defined as $MSE = E\{(x_{est} - x)^2\}/E\{x^2\}$.

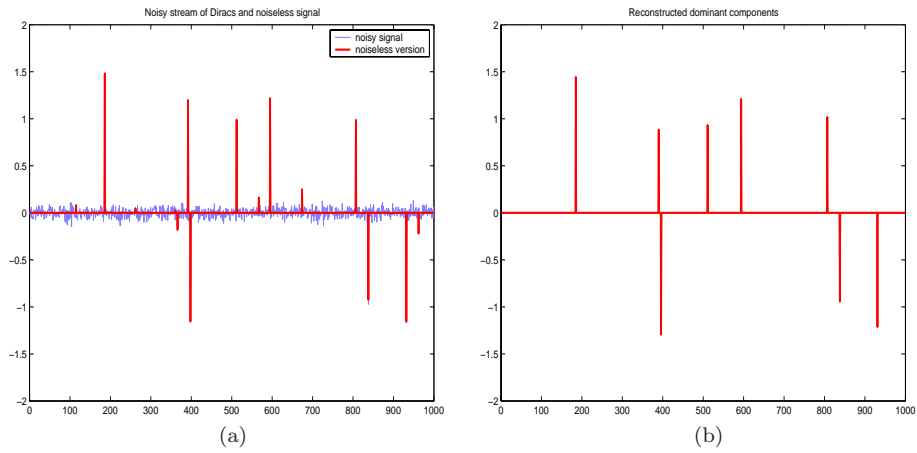


Figure 3.5: Model mismatch: unknown model order (a) *The periodic signal made up of 15 weighted Dirac pulses, with 8 pulses being dominant.* (b) *Reconstructed dominant components.*

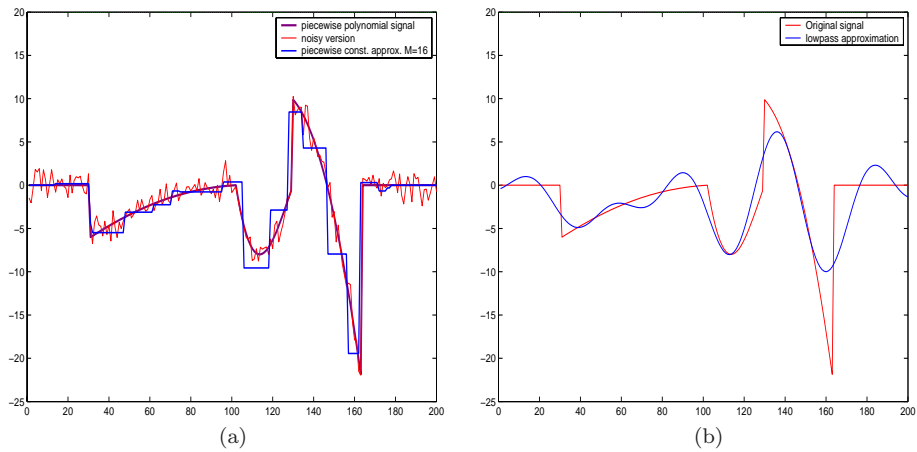


Figure 3.6: Model mismatch: unknown signal model (a) *Piecewise polynomial signal, noisy signal and the piecewise constant approximation.* (b) *Original signal and reconstructed lowpass version using Shannon's interpolation formula.*

Chapter 4

High-Resolution Synchronization and Channel Estimation in Ultra-Wideband Systems

Ultra-wideband (UWB) technology has recently received much attention due to the benefits of an extremely wide transmission bandwidth, such as very fine time resolution for accurate ranging and positioning as well as multipath fading mitigation in indoor wireless networks [16] [25] [92] [93] [94]. Although techniques for UWB signaling have been investigated for at least two decades, primarily for radar and remote sensing applications, there are many open problems that need to be solved before this technology becomes pervasive. Some of the remaining issues include low-power and low-cost designs and efficient algorithmic solutions suitable for digital implementation.

The wideband nature of UWB brings new research challenges both in the analysis and practice of reliable systems. One of the main challenges in the design of digital UWB receivers is rapid acquisition and synchronization. While several high-performance methods for analog UWB systems already exist [24] [25], no comparable techniques have emerged yet for digital solutions, mainly due to prohibitively high computational requirements [22] [89]. Furthermore, implementation of standard synchronization techniques in digital UWB receivers would require very fast A/D converters, operating in the gigahertz range, and thus high power consumption. Another challenge arises from the fact that the design of an optimal UWB receiver must take into account certain frequency-dependent effects on the received waveform. That is, due to the broadband nature of UWB signals, the components propagating along different paths typically undergo different frequency-selective distortions [13] [16]. As a result, a received signal is made up of pulses with different pulse shapes, which makes the problem of optimal receiver design a much more delicate task than in other wideband systems.

In this chapter, we present a new approach to channel estimation and timing in digital UWB receivers, which allows for sub-Nyquist sampling rates and

reduced receiver complexity, while retaining a good performance. We develop a frequency domain framework which yields high-resolution estimates of channel parameters by sampling a low-dimensional subspace of the received signal. Our approach allows for lower sampling rates and reduced complexity and power consumption compared to other digital techniques [22] [30] [89]. It is particularly suitable in applications such as precise position location or ranging, synchronization in wideband systems, but can also be used for characterization of general wideband channels [16] without requiring additional hardware support.

The outline of this chapter is as follows. In Section 4.1, we introduce a model of a multipath fading channel and present the frequency domain framework that allows for high-resolution channel estimation from a subsampled version of the received signal. In Section 4.2, the case of more realistic UWB channel models is studied, where we extend our framework to the problem of joint estimation of pulse shapes and time delays along different propagation paths. In Section 4.3, we discuss possible generalizations of our results to the problem of estimating channel parameters from multiple (not necessarily adjacent) frequency bands. In particular, we develop a more general framework that incorporates a filter bank at the receiver and allows for the estimation of the channel from several bands with highest signal-to-noise ratio¹. In Section 4.4, we discuss numerical performances and computational complexity of the proposed algorithms and present alternative methods with lower computational requirements, which can be used to estimate the parameters of a few dominant paths. One possible application of our results to low-complexity synchronization in UWB systems for precise position location is presented in Section 4.5. We specifically discuss a multiresolution or two-step approach to acquisition in such systems, which provides unique advantages over existing techniques in terms of acquisition speed as well as computational and power requirements. In Section 4.6, we present some simulation results that indicate the effectiveness of our schemes, showing performances that exceed those of conventional methods. In Section 4.7, we briefly describe the application of our method to low-complexity synchronization in wideband CDMA systems, and to the problem of joint angle and delay estimation. Finally, in Section 4.8, we conclude with a summary of our results.

4.1 Channel Estimation at Low Sampling Rate

4.1.1 Problem statement

A number of propagation studies for ultra-wideband signals have been done, taking into account temporal properties of a channel or characterizing a spatio-temporal channel response [16]. A typical model for the impulse response of a multipath fading channel is given by

$$h(t) = \sum_{l=1}^L a_l \delta(t - t_l) \quad (4.1)$$

where t_l denotes a signal delay along the l -th path while a_l is a propagation coefficient along the l -th path. Although this model does not adequately reflect

¹This has the notion of prescribing which signal samples to include in order to maximize the performance, given the total number of samples allowed in the system.

specific frequency-dependent effects, it is commonly used for diversity reception schemes in conventional wideband receivers (e.g. RAKE receivers) [61]. Equation (4.1) can be interpreted as saying that a received signal $y(t)$ is made up of a weighted sum of attenuated and delayed replicas of the transmitted signal $s(t)$, i.e.

$$y(t) = \sum_{l=1}^L a_l s(t - t_l) + \eta(t) \quad (4.2)$$

where $\eta(t)$ denotes receiver noise. Note that the received signal $y(t)$ has only $2L$ degrees of freedom, that is, time delays t_l and propagation coefficients a_l . Therefore, when $s(t)$ is known a priori and there is no noise, it would be possible to perfectly reconstruct the signal by taking only $2L$ samples of $y(t)$. While all the unknown parameters can be estimated using the time domain model (4.2), an efficient, closed-form solution is possible if we consider the problem in the frequency domain.

Let $Y(\omega)$ denote the Fourier transform of the received signal

$$Y(\omega) = \sum_{l=1}^L a_l S(\omega) e^{-j\omega t_l} + \mathcal{N}(\omega) \quad (4.3)$$

where $S(\omega)$ and $\mathcal{N}(\omega)$ are the Fourier transforms of $s(t)$ and $\eta(t)$ respectively. Clearly, spectral components are given by a sum of complex exponentials, where the unknown time delays appear as complex frequencies while propagation coefficients appear as unknown weights. Therefore, by considering the frequency domain representation of the signal, we have converted the problem of estimating the unknown channel parameters $\{t_l\}_{l=0}^{L-1}$ and $\{a_l\}_{l=0}^{L-1}$ into the problem equivalent to the one discussed in Chapter 2. However, rather than estimating the channel parameters from a lowpass version of the signal, we will estimate it from a bandpass version. The reason for using the bandpass approximation is that the power spectral density (PSD) of the signal at low frequencies is often very low, and the idea is to estimate the channel parameters from a frequency band where the PSD of the signal is highest.

In the following, we will show that it is possible to obtain high-resolution estimates of all the relevant parameters by sampling the received signal below the traditional Nyquist rate. The general setup we will be considering is shown in Figure 4.1.

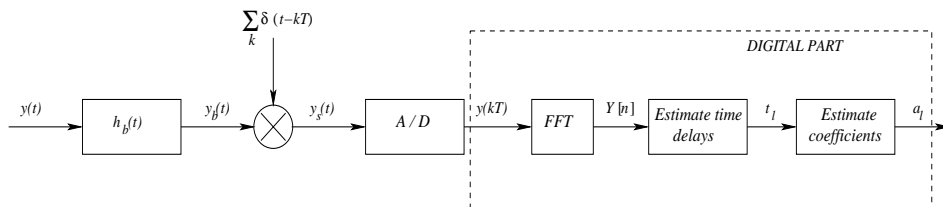


Figure 4.1: Receiver block diagram

4.1.2 Bandpass sampling scheme

Suppose that the received signal $y(t)$ is filtered with an ideal bandpass filter $H_b = \text{rect}(\omega_L, \omega_U)$ of bandwidth $B = \omega_U - \omega_L$, and assume for simplicity that $\omega_L = kB$, where k is a non-negative integer number. Let $\{y_n\}_{n=0}^{N-1}$ denote a uniform set of samples taken from the filtered version,

$$y_n = \langle h_b(t - nT), y(t) \rangle, \quad n = 0, \dots, N - 1. \quad (4.4)$$

where T is the sampling period, while $h_b(t)$ is the time domain representation of the filter H_b . Note that the above assumption on the position of the filter passband allows one to sample the signal at a rate determined by the bandwidth of the filter $R_s \geq 2\frac{B}{2\pi}$, which is commonly referred to as bandpass sampling [82]. Otherwise, one can use a more traditional approach of downconverting the filtered version prior to sampling, which also allows for sub-Nyquist sampling rates, but requires additional hardware stages in the analog front end. From the set of samples $\{y_n\}_{n=0}^{N-1}$, one can compute N uniformly spaced samples of the Fourier transform $Y(\omega)$ [85],

$$Y[m] = Y(m\omega_0), \quad \text{where } \omega_0 = \frac{B}{N-1}, \quad m = M_1, \dots, M_2. \quad (4.5)$$

Denote by $Y_s[m] = Y[m]/S[m]$, and $N_s[m] = N[m]/S[m]$, where $S[m]$ are the samples of the Fourier transform $S(\omega)$ of the transmitted UWB pulse. Assuming that in the considered frequency band the above division is not ill-conditioned, the samples $Y_s[m]$ can be expressed as a sum of complex exponentials (4.3),

$$Y_s[m] = \sum_{l=1}^L a_l e^{-j(m\omega_0)t_l} + N_s[m] \quad (4.6)$$

In practice, the discrete Fourier transform (DFT) will be used to determine $Y[m]$ and $S[m]$, therefore, in general, (4.6) will not hold exactly. However, it will be asymptotically accurate, since the error introduced by DFT is on the order of $\mathcal{O}(1/N)$ (recall that N corresponds to the number of samples). When $y(t)$ is a periodic signal (e.g. as in the case discussed in Section 4.5), the DFT coefficients will exactly satisfy (4.6).

As already discussed in Chapter 2, one possible approach to estimating the channel parameters from the coefficients $Y_s[m]$ is to use the annihilating filter method. That is, one can consider an L -th order FIR filter $H(z) = \sum_{m=0}^L H[m]z^{-m}$, having L zeros at $z_l = e^{-j\omega_0 t_l}$,

$$H(z) = \prod_{l=1}^L (1 - e^{-j\omega_0 t_l} z^{-1}) \quad (4.7)$$

Since each of the exponentials in $Y_s[m]$ will be annihilated by one of the roots of $H(z)$, we have

$$(H * Y_s)[n] = \sum_{k=0}^L H[k]Y_s[n-k] = 0, \quad \text{for } n = L, \dots, N-1. \quad (4.8)$$

Therefore, the information about the time delays t_l can be extracted from the roots of the filter $H(z)$. The corresponding propagation coefficients a_l are then estimated by solving the system of linear equations (4.6).

4.1.3 Subspace-based approach to channel estimation

Given the set of coefficients $Y_s[m]$ (4.6), construct a Hankel data matrix \mathbf{Y}_s of size $P \times Q$, where $P, Q > L$,

$$\mathbf{Y}_s = \begin{pmatrix} Y_s[M_1] & Y_s[M_1 + 1] & \dots & Y_s[M_1 + Q - 1] \\ Y_s[M_1 + 1] & Y_s[M_1 + 2] & \dots & Y_s[M_1 + Q] \\ \vdots & \vdots & \ddots & \vdots \\ Y_s[M_1 + P - 1] & Y_s[M_1 + P] & \dots & Y_s[M_1 + P + Q - 2] \end{pmatrix} \quad (4.9)$$

For simplicity, we have constructed \mathbf{Y}_s using only the coefficients with positive indices, while the method can be extended to include the coefficients with negative indices as well, similarly to the approach from Section 2.5.2. In the absence of noise, the elements of the matrix \mathbf{Y}_s are given by

$$\mathbf{Y}_s[p, q] = \sum_{l=1}^L a_l z_l^{M_1} z_l^{p+q} = \tilde{a}_l z_l^{p+q}, \quad 0 \leq p \leq P - 1, \quad 0 \leq q \leq Q - 1. \quad (4.10)$$

where $z_l = e^{-j\omega_0 t_l}$ are the signal poles and $\tilde{a}_l = a_l z_l^{M_1}$. Therefore, as already discussed in Chapter 2, one possible decomposition of the matrix \mathbf{Y}_s is given by $\mathbf{Y}_s = \mathbf{U}\mathbf{S}\mathbf{V}^H$, with the following matrices \mathbf{U} , \mathbf{S} and \mathbf{V} ,

$$\mathbf{U} = \begin{pmatrix} 1 & 1 & 1 & \dots & 1 \\ z_1 & z_2 & z_3 & \dots & z_L \\ \vdots & \vdots & \vdots & \ddots & \vdots \\ z_1^{P-1} & z_2^{P-1} & z_3^{P-1} & \dots & z_L^{P-1} \end{pmatrix}, \quad (4.11)$$

$$\mathbf{S} = \text{diag}(\tilde{a}_1 \quad \tilde{a}_2 \quad \tilde{a}_3 \quad \dots \quad \tilde{a}_L), \quad (4.12)$$

$$\mathbf{V} = \begin{pmatrix} 1 & 1 & 1 & \dots & 1 \\ z_1^* & z_2^* & z_3^* & \dots & z_L^* \\ \vdots & \vdots & \vdots & \ddots & \vdots \\ z_1^{*Q-1} & z_2^{*Q-1} & z_3^{*Q-1} & \dots & z_L^{*Q-1} \end{pmatrix}. \quad (4.13)$$

Clearly, \mathbf{U} , \mathbf{S} and \mathbf{V} have the same structure as in Section 2.3.1, except that the diagonal elements of \mathbf{S} are now given by $\tilde{a}_l = a_l z_l^{M_1}$. Therefore, in order to extract the unknown signal poles, we can exploit the following shift-invariant subspace property

$$\overline{\mathbf{U}} = \underline{\mathbf{U}} \cdot \Phi \quad \text{or} \quad \overline{\mathbf{V}} = \underline{\mathbf{V}} \cdot \Phi^H \quad (4.14)$$

where Φ is a diagonal matrix having z_l 's along the main diagonal. Once the signal poles have been estimated, the coefficients a_l can be found as a least-squares solution to (4.6).

Following the discussion from Chapter 2, when \mathbf{Y}_s is decomposed using the SVD, that is,

$$\mathbf{Y}_s = \mathbf{U}_s \mathbf{S}_s \mathbf{V}_s^H + \mathbf{U}_n \mathbf{S}_n \mathbf{V}_n^H, \quad (4.15)$$

one will not obtain the same matrices \mathbf{U} , \mathbf{S} and \mathbf{V} as in (4.11)-(4.13). However, the shift-invariance property will hold as well, whereas the only difference is that the signal poles should be now estimated as the eigenvalues of the operator that maps $\underline{\mathbf{U}}_s$ onto $\overline{\mathbf{U}}_s$ (or $\underline{\mathbf{V}}_s$ onto $\overline{\mathbf{V}}_s$). In order to keep this chapter self-contained, in the following, we briefly summarize the subspace algorithm.

Algorithm outline

1. Given the set of the coefficients $Y_s[n]$, construct a $P \times Q$ matrix \mathbf{Y}_s as in (4.9), where $P, Q \geq L$.
2. Compute the singular value decomposition of \mathbf{Y}_s as in (5.45), and approximate the noiseless data matrix with a rank L matrix, using only L principal components, that is,

$$\mathbf{Y}_s \approx \mathbf{U}_s \mathbf{S}_s \mathbf{V}_s^H. \quad (4.16)$$

3. Estimate the signal poles $z_l = e^{-j\omega_0 t_l}$ by computing the eigenvalues of a matrix \mathbf{Z} , defined as

$$\mathbf{Z} = \underline{\mathbf{U}}_s^+ \cdot \overline{\mathbf{U}}_s \quad (4.17)$$

Alternatively, if \mathbf{V}_s is used in (4.17) instead of \mathbf{U}_s , one would estimate complex conjugates of z_l 's.

4. Find the coefficients a_l as a least-squares solution to (4.6).

Clearly, by considering the frequency domain representation of the signal, we have converted the nonlinear estimation problem into the simpler problem of estimating the parameters of a linear model. Nonlinearity is postponed for the step where the information about the time delays is extracted from the estimated signal poles [65]. However, we have avoided the estimation of the covariance matrix in the first place, which generally requires a larger data set and represents a computationally demanding part in other methods [4] [58]. By avoiding this step, we can allow for reduced sampling rates and lower computational requirements and yet obtain the same estimation performance.

Finally, we should note that since we are estimating the signal parameters from the coefficients $Y_s[n] = Y[n]/S[n]$ (where $S[n]$ are the DFT coefficients of the transmitted pulse), in general, noise will no longer be white. However, since we are using only a portion of the signal bandwidth, we can estimate the parameters from the frequency band where the power spectral density of the transmitted signal is nearly flat², thus having the assumption on white noise still valid. Otherwise, one can use the weighting technique developed in Section 3.3.1, as one possible method of "noise whitening" prior to estimation. In particular, instead of considering the original data matrix \mathbf{Y}_s , one can consider another, weighted matrix $\mathbf{A}\mathbf{Y}_s\mathbf{B}$, where the matrices \mathbf{A} and \mathbf{B} are chosen such that the entries of the new data matrix have a uniform and minimum variance. As already discussed in Section 3.3.1, one possible choice for \mathbf{A} and \mathbf{B} is given by,

$$\mathbf{A}[i, i] = \frac{1}{\frac{1}{Q} \sum_{q=0}^{Q-1} S[q+i]^{-1}}, \quad i = 0, \dots, P-1, \quad (4.18)$$

$$\mathbf{B}[j, j] = \frac{1}{\frac{1}{P} \sum_{p=0}^{P-1} \mathbf{A}[p, p] S[p+j]^{-1}}, \quad j = 0, \dots, Q-1. \quad (4.19)$$

We can next use the singular value decomposition of the new data matrix, and reduce the effect of noise by extracting L principal components $\mathbf{U}_s \mathbf{S}_s \mathbf{V}_s^H$.

²In systems that are properly designed, this is always the case.

Once the principal components have been computed, one can compensate for the effects of \mathbf{A} and \mathbf{B} by constructing a new, denoised data matrix \mathbf{Y}_{sd} as $\mathbf{Y}_{sd} = \mathbf{A}^{-1} \mathbf{U}_s \mathbf{S}_s \mathbf{V}_s^H \mathbf{B}^{-1}$, from which the signal poles should be estimated.

As already discussed in Chapter 2, in the case when the signal contains closely spaced components, one can improve the resolution performance of the subspace method (without increasing the computational complexity), by exploiting the shift-invariance property in a different way, specifically,

$$\overline{\mathbf{U}}_s^d = \underline{\mathbf{U}}_{s,d} \cdot \Phi^d \quad \text{and} \quad \overline{\mathbf{V}}_s^d = \underline{\mathbf{V}}_{s,d} \cdot \Phi^{Hd} \quad (4.20)$$

where $\overline{(\cdot)}^d$ and $\underline{(\cdot)}_d$ denote the operations of omitting the first d rows and last d rows of (\cdot) respectively. In this case, the matrix Φ^d has elements $z_l^d = e^{-j\omega_0 dt_l}$ on its main diagonal, meaning that the effective separation among the estimated time delays is increased d times. Another way for improving the resolution capabilities would be to construct the data matrix in a different way, by interleaving the rows (or columns) of the original data matrix \mathbf{Y}_s . Both methods are described in more detail in Section 2.5.1.

In Section 4.3, we will discuss further modifications of the framework, which can result in improved numerical performance by estimating the channel from multiple bands.

4.2 Estimating More Realistic Channel Models

4.2.1 Theory

We will now extend our analysis to the more complex case of a channel that takes into account certain bandwidth-dependent properties. Namely, as a result of the very large bandwidth of UWB signals, components propagating along different propagation paths undergo different frequency selective distortion and a more realistic channel model for UWB systems is of the form [16]

$$h(t) = \sum_{l=1}^L a_l p_l(t - t_l) \quad (4.21)$$

where $p_l(t)$ are different (normalized) pulse shapes that correspond to different propagation paths. In this case, the DFT coefficients computed from a bandpass version of the received signal can be expressed as

$$Y[n] = S[n] \sum_{l=1}^L P_l[n] \tilde{a}_l e^{-jn\omega_0 t_l} + N[n] \quad (4.22)$$

where $P_l[n]$ are now unknown coefficients. Recall that $\omega_0 = \frac{B}{N-1}$ and $\tilde{a}_l = a_l e^{-jM_1 \omega_0 t_l}$. Clearly, in order to completely characterize the channel, we need to estimate the a_l 's and t_l 's as well as all the coefficients $P_l[n]$, which, in general, requires a non-linear estimation procedure. However, one possible way to obtain a closed form solution is to approximate the coefficients $P_l[n]$ with polynomials of degree $D \leq R - 1$, that is,

$$P_l[n] = \sum_{r=0}^{R-1} p_{l,r} n^r \quad (4.23)$$

Equation (4.22) now becomes

$$Y[n] = S[n] \sum_{l=1}^L \tilde{a}_l \sum_{r=0}^{R-1} p_{l,r} n^r e^{-jn\omega_0 t_l} + N[n] \quad (4.24)$$

By denoting $c_{l,r} = \tilde{a}_l p_{l,r}$, $Y_s[n] = Y[n]/S[n]$ and $N_s[n] = N[n]/S[n]$, we obtain

$$Y_s[n] = \sum_{l=1}^L \sum_{r=0}^{R-1} c_{l,r} n^r e^{-jn\omega_0 t_l} + N_s[n] \quad (4.25)$$

The problem of estimating the parameters $c_{l,r}$ and t_l from $Y_s[n]$ is now equivalent to the one we considered in the previous chapter (Section 3.2.2), that is, the problem of estimating the parameters of piecewise polynomials. In order to derive a closed-form subspace solution to this problem, we have first considered the annihilating filter approach, in particular, we have seen that the annihilating filter for $Y_s[n]$ will have multiple roots at $z_l = e^{-j\omega_0 t_l}$,

$$H(z) = \prod_{l=1}^L (1 - e^{-j\omega_0 t_l} z^{-1})^R = \sum_{k=0}^{RL} H[k] z^{-k}. \quad (4.26)$$

Using the result on equivalence between the subspace and annihilating filter solutions, stated in Proposition 1 (Section 2.3.2), one can develop a subspace-based estimator, which we briefly summarize in the following.

4.2.2 Algorithm outline

1. Given a set of coefficients $Y_s[m]$, construct an $M \times N$ matrix data \mathbf{X} as in (2.19), where $M, N \geq RL$.
2. Compute the singular value decomposition of \mathbf{X} , that is, $\mathbf{Y}_s = \mathbf{U}\mathbf{S}\mathbf{V}^H$. Find RL principal left and right singular vectors, \mathbf{U}_s and \mathbf{V}_s , as the singular vectors corresponding to the K largest singular values of \mathbf{Y}_s .
3. Estimate the signal poles $z_l = e^{-j\omega_0 t_l}$ by computing the eigenvalues of a matrix \mathbf{H} , defined as

$$\mathbf{H} = \underline{\mathbf{U}}_s^+ \cdot \overline{\mathbf{U}}_s. \quad (4.27)$$

Alternatively, if \mathbf{V}_s is used in (4.27), one would estimate complex conjugates of z_k 's. While in the noiseless case one should find RL eigenvalues, each of multiplicity L , in the presence of noise, it is more desirable to approximate the signal poles with the eigenvalues of \mathbf{H} that are closest to the unit circle.

4. Find the coefficients c_k as a least-squares solution to the Vandermonde system (2.7), that is,

$$Y_s[n] = \sum_{l=1}^L \sum_{r=0}^{R-1} c_{l,r} n^r e^{-jn\omega_0 t_l} + N_s[n].$$

At this point, it is important to note that the reconstruction of the pulse shapes from the set of estimated coefficient $c_{l,r}$ must be done carefully. In [50], the pulse shapes are reconstructed from the estimated lowpass version of the signal, using the polynomial approximation (4.23). This can create ripples in the reconstructed signal due to the Gibbs phenomenon. Similarly, reconstructing the signal from a larger set of DFT coefficients, obtained by spectral extrapolation from (4.23), is often numerically unstable. A conventional way to treat this problem is to use a less abrupt truncation of the DFT coefficients by appropriate windowing [57]. One possible solution is to do weighting of the extrapolated DFT coefficients with an exponentially decaying function. This can significantly improve the accuracy of reconstruction, as we will show in Section 4.6.

4.3 Improvements of the Subspace Method

4.3.1 Filter bank approach

So far we have considered only a low-dimensional subspace of the received signal and all the methods were developed under the assumption that we have access to consecutive DFT coefficients of the signal. While in the noiseless case it is possible to estimate the parameters from any subspace of appropriate dimension, in the presence of noise the best performance of our algorithm is expected when the channel is estimated from a frequency band with highest signal-to-noise ratio. An alternative approach would be to estimate the channel from a larger subspace, using a filter bank at the receiver, where each subband is sampled at a rate determined by the filter bandwidth. The set of coefficients $Y_s[n]$ is then computed separately for each subband and combined to form the matrix \mathbf{Y}_s in (4.9), or to compute the annihilating filter coefficients in (2.14). An obvious advantage of this approach is that a larger data set is used for estimation, which results in improved numerical performance, yet at the expense of increased computational and power requirements.

In the case when the channel parameters are estimated from adjacent subbands, the algorithm presented in Section 2.3.1 remains essentially the same, since we have access to consecutive coefficients $Y_s[n]$. A more interesting case, and potentially more important in practice, is when the parameters are estimated from bands that are not necessarily adjacent. For example, if the noise level in certain bands is relatively high, or if some bands are subject to strong interference, it is desirable to estimate the channel by sampling only those bands where SNIR (signal-to-noise-plus-interference ratio) is sufficiently high. We will show that our developed algorithms can be adapted rather simply to handle this case.

4.3.2 Estimation from non-adjacent bands

Consider first the channel model given by (4.1). For simplicity, we will analyze the case when the channel parameters are estimated by sampling only two non-adjacent bands $B_1 = (M_1\omega_0, N_1\omega_0)$ and $B_2 = (M_2\omega_0, N_2\omega_0)$, while the same approach can be generalized to the case with multiple frequency bands. Let $Y[n]$ be the DFT coefficients of the received signal corresponding to the bands B_1 and B_2 , and let $Y_s[n] = Y[n]/S[n]$ (assuming again that this division is

well-conditioned). Under the above assumptions, the noiseless coefficients $Y_s[n]$ are given by $Y_s[n] = \sum_{l=1}^L a_l z_l^n$, where $n \in [M_1, N_1] \cup [M_2, N_2]$. Next define a block-Hankel data matrix \mathbf{Y}_s as

$$\mathbf{Y}_s = \begin{pmatrix} Y_s[M_1] & Y_s[M_1 + 1] & \dots & Y_s[M_1 + Q - 1] \\ \vdots & \vdots & \vdots & \vdots \\ Y_s[M_1 + P_1 - 1] & Y_s[M_1 + P_1] & \dots & Y_s[M_1 + P_1 + Q - 2] \\ Y_s[M_2] & Y_s[M_2 + 1] & \dots & Y_s[M_2 + Q - 1] \\ \vdots & \vdots & \vdots & \vdots \\ Y_s[M_2 + P_2 - 1] & Y_s[M_2 + P_2] & \dots & Y_s[M_2 + P_2 + Q - 2] \end{pmatrix}. \quad (4.28)$$

In the noiseless case, the matrix \mathbf{Y}_s can be written as $\mathbf{Y}_s = \mathbf{U}\mathbf{S}\mathbf{V}^H$, where \mathbf{U} , \mathbf{S} , and \mathbf{V} are now given by

$$\mathbf{U} = \begin{pmatrix} z_1^{M_1} & z_2^{M_1} & z_3^{M_1} & \dots & z_L^{M_1} \\ \vdots & \vdots & \vdots & \vdots & \vdots \\ z_1^{M_1+P_1-1} & z_2^{M_1+P_1-1} & z_3^{M_1+P_1-1} & \dots & z_L^{M_1+P_1-1} \\ z_1^{M_2} & z_2^{M_2} & z_3^{M_2} & \dots & z_L^{M_2} \\ \vdots & \vdots & \vdots & \vdots & \vdots \\ z_1^{M_2+P_2-1} & z_2^{M_2+P_2-1} & z_3^{M_2+P_2-1} & \dots & z_L^{M_2+P_2-1} \end{pmatrix}, \quad (4.29)$$

$$\mathbf{S} = \text{diag}(a_1 \ a_2 \ a_3 \ \dots \ a_L), \quad (4.30)$$

$$\mathbf{V} = \begin{pmatrix} 1 & 1 & 1 & \dots & 1 \\ z_1^* & z_2^* & z_3^* & \dots & z_L^* \\ \vdots & \vdots & \vdots & \vdots & \vdots \\ z_1^{*Q-1} & z_2^{*Q-1} & z_3^{*Q-1} & \dots & z_L^{*Q-1} \end{pmatrix}. \quad (4.31)$$

Clearly, the matrix \mathbf{V} has the same Vandermonde structure as in (2.21), meaning that the shift-invariance property (2.25) holds in this case as well, that is, $\overline{\mathbf{V}} = \underline{\mathbf{V}} \cdot \Phi$, where Φ is the diagonal matrix having z_l 's along the main diagonal. Therefore, one can use the algorithm described in Section 2.3.1 to estimate the signal poles z_l 's from \mathbf{V} , or alternatively, from the right singular vectors of \mathbf{Y}_s . However, a similar approach can also be used to estimate the poles from the left singular vectors. This is the case of interest when the number of rows in the data matrix \mathbf{Y}_s is larger than the number of columns, which may come about as a result of sampling multiple frequency bands that are relatively narrow compared to the signal bandwidth. Namely, the key is to observe the following property of the matrix \mathbf{U}

$$\overline{\overline{\mathbf{U}}} = \underline{\underline{\mathbf{U}}} \cdot \Phi \quad (4.32)$$

where $\overline{(\cdot)}$ stands for the operation of omitting the rows 1 and $P_1 + 1$ of (\cdot) , and similarly, $\underline{(\cdot)}$ denotes the operation of omitting the rows P_1 and $P_1 + P_2$ of (\cdot) . That is, the shift-invariance property can be exploited in this case as well, while the only modification in the developed algorithm is that the matrices $\overline{\overline{\mathbf{U}}}$ and $\underline{\underline{\mathbf{U}}}$ are constructed by removing the first and the last row respectively from each block of \mathbf{U} .

Therefore, we can state the following proposition:

Proposition 4.1 Consider a set of coefficients $Y_s[n]$ given by $Y_s[n] = \sum_{l=1}^L a_l z_l^n$, where $n \in [M_1, N_1] \cup [M_2, N_2]$. Define a block-Hankel data matrix \mathbf{Y}_s as in (4.28), and let $\mathbf{Y}_s = \mathbf{U}\mathbf{S}\mathbf{V}^H$ denote one possible decomposition of \mathbf{Y}_s , with \mathbf{S} being an $L \times L$ matrix. Then the following holds:

1. Eigenvalues of the matrix $\mathbf{Z} = \underline{\underline{\mathbf{U}}}^+ \cdot \overline{\overline{\mathbf{U}}}$ are identical to the signal poles $\{z_l\}_{l=1}^L$.
2. Eigenvalues of the matrix $\mathbf{Z}_1 = \underline{\underline{\mathbf{V}}}^+ \cdot \overline{\overline{\mathbf{V}}}$ are identical to the complex conjugates of the signal poles, that is, $\{z_l^*\}_{l=1}^L$.

When there is additive noise, one should first extract the principal components by computing the singular value decomposition of \mathbf{Y}_s (5.45), and then estimate the signal poles $z_l = e^{-j\omega_0 t_l}$ as eigenvalues of a matrix \mathbf{Z} , defined as

$$\mathbf{Z} = \underline{\underline{\mathbf{U}_s}}^+ \cdot \overline{\overline{\mathbf{U}_s}} \quad (4.33)$$

Alternatively, we could define \mathbf{Z}_c as

$$\mathbf{Z}_c = \underline{\underline{\mathbf{V}_s}}^+ \cdot \overline{\overline{\mathbf{V}_s}} \quad (4.34)$$

in which case the eigenvalues of \mathbf{Z}_c are complex conjugates of z_l 's.

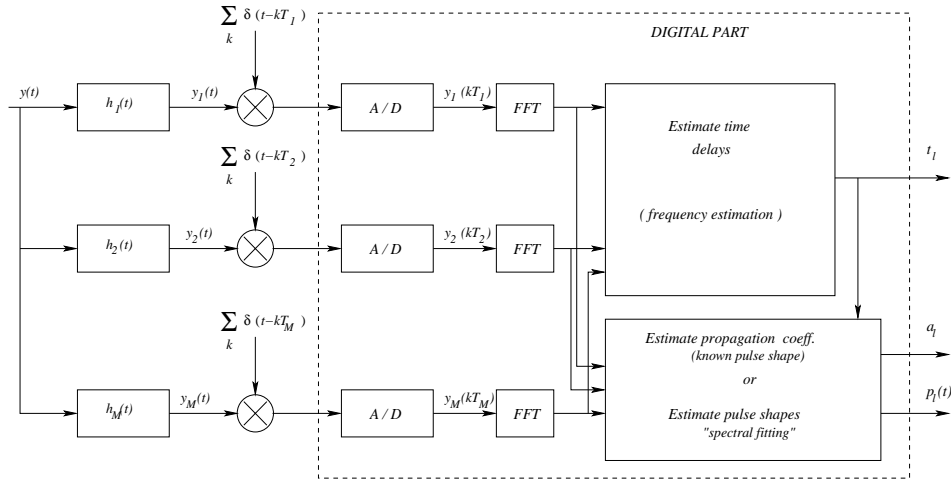


Figure 4.2: Estimation from multiple bands: receiver block diagram

A block diagram of the estimator where multiple bands are used for estimation is illustrated in Figure 4.2.

4.4 Numerical Performance and Complexity

4.4.1 Analysis of noise sensitivity

Part of the analysis on numerical performance of the subspace approach has been already presented in Chapter 2 (Section 2.4). In this section, we give

exact expressions for the MSE of the frequency estimate in the case of a single exponential (with amplitude a_1), which, in our framework, corresponds to the estimate of the time delay t_1 of the dominant path.

Consider first the subspace-based approach from Section 2.3.1. Let the data matrix \mathbf{Y}_s be of size $P \times Q$, and let $N = P + Q - 1$ be the total number of DFT coefficients $Y_s[n]$ used for estimation. Recall that the coefficients $Y_s[n]$ are obtained from the bandpass version of the received signal $y(t)$, that is, $Y_s[n] = Y[n]/S[n]$, $n \in [N_1, N_1 + N - 1]$ (2.7). If we define $\omega_1 = \omega_0 t_1$, and assuming that the signal and noise are uncorrelated, the MSE of the state space approach can be expressed as [32]

$$E\{\Delta\omega_1^2\} \approx \begin{cases} \frac{1}{Q(N-Q)^2} \frac{\sigma_n^2}{|a_1|^2} \frac{N}{\sum_n |S[n]|^2}, & \text{for } Q \leq N/2 \\ \frac{1}{Q^2(N-Q)} \frac{\sigma_n^2}{|a_1|^2} \frac{N}{\sum_n |S[n]|^2}, & \text{for } Q > N/2 \end{cases} \quad (4.35)$$

where σ_n^2 is noise variance. Note that the error is inversely proportional to the SNR at the output of the bandpass filter, defined as

$$\text{SNR} = \frac{|a_1|^2 \sum_n |S[n]|^2}{\sigma_n^2 N}. \quad (4.36)$$

Therefore, for a given bandwidth of the filter, it is desirable to estimate the channel from a frequency band where the SNR is highest. The optimum performance is then achieved when $Q = N/3$ or $Q = 2N/3$, resulting in the MSE of time delay estimation

$$E\{\Delta t_1^2\} \approx \frac{1}{\omega_0^2} \frac{27}{4N^3} \frac{1}{\text{SNR}} \quad (4.37)$$

This is very close to the Cramer-Rao bound (CRB) [77], given by

$$\text{CRB} = \frac{1}{\omega_0^2} \frac{6}{N^3} \frac{1}{\text{SNR}} \quad (4.38)$$

which indicates desirable numerical performances of the state space approach. Similar performance can be achieved with the annihilating filter method [32], with an MSE of the form

$$E\{\Delta\omega_1^2\} \approx \begin{cases} \frac{2(2Q+1)}{3(N-Q)^2 Q(Q+1)} \frac{1}{\text{SNR}}, & \text{for } Q \leq N/2 \\ \frac{2(-(N-Q)^2 + 3Q^2 + 3Q + 1)}{3(N-Q)Q^2(Q+1)^2} \frac{1}{\text{SNR}}, & \text{for } Q > N/2 \end{cases} \quad (4.39)$$

where in this case, Q represents the polynomial degree. As already mentioned in Chapter ??, a choice of the polynomial degree directly affects the estimation performance, and the minimum MSE is achieved for $Q = N/3$ or $Q = 2N/3$, leading to

$$E\{\Delta t_1^2\} \approx \frac{1}{\omega_0^2} \frac{9}{N^3} \frac{1}{\text{SNR}}. \quad (4.40)$$

At this point, it is worth noting that expressions for performance bounds (4.37), (4.38) and (4.40), are obtained using the first order perturbation analysis and are generally valid only for medium to high signal-to-noise ratios. Still, these results give us a good indication as to the performance of the proposed methods at different sampling rates. That is, since the root mean square error (RMSE)

for the time delay estimation is on the order of $\mathcal{O}(1/N^{3/2})$, by decreasing the sampling rate K times, RMSE increases by a factor of (approximately) $K^{3/2}$. Specifically, the following general relation between the RMSE of a subsampled estimator (RMSE_{ss}) and the RMSE of a Nyquist-sampled estimator (RMSE_{nq}) holds for all the considered methods,

$$\text{RMSE}_{ss} \sim \text{RMSE}_{nq} K^{3/2} \left(\frac{\text{SNR}_{nq}}{\text{SNR}_{ss}} \right)^{1/2} \quad (4.41)$$

where SNR_{nq} denotes the overall signal-to-noise ratio, while SNR_{ss} is the signal-to-noise ratio at the output of the corresponding bandpass filter. Clearly, even though the SNR after filtering may increase, the performance of a subsampled estimator is expected to degrade, due to a smaller data set used for estimation. However, in Section 4.6, we will show that in problems encountered in practice, it is possible to obtain high-resolution estimates with sub-Nyquist sampling rates. Finally, note that equation (4.41) implies that the performance bounds of subsampled state space or annihilating filter methods are again very close to the CRB of a subsampled ML estimator.

4.4.2 Computational complexity and alternative solutions

A major computational requirement for all the developed algorithms is associated with the singular value decomposition step, which is an iterative algorithm with computational order of $\mathcal{O}(N^3)$ per iteration. Often, however, we are interested in estimating the parameters of only a few strongest paths, therefore, computing the full SVD of the data matrix \mathbf{Y}_s is not necessary. Alternatively, we can use some simpler methods to find principal singular vectors, which have lower computational requirements and converge very fast to the desired solution [19] [27]. We first give an outline of the *Power method* [27], that can be used to compute only one dominant right (or left) singular vector of \mathbf{Y}_s . This can be of interest for initial synchronization or in applications such as ranging or positioning. Later, we present its extended version applicable to the general case of estimating $M_d > 1$ principal singular vectors.

Power Method

Consider a matrix $\mathbf{F} = \mathbf{Y}_s \mathbf{Y}_s^H$ of size $P \times P$, and suppose that \mathbf{F} is diagonalizable, that is, $\mathbf{\Lambda}^{-1} \mathbf{F} \mathbf{\Lambda} = \text{diag}(\lambda_1, \dots, \lambda_P)$ with $\mathbf{\Lambda} = [\mathbf{y}_1, \dots, \mathbf{y}_P]$ and $|\lambda_1| > |\lambda_2| \geq \dots \geq |\lambda_P|$. Given $\mathbf{y}^{(0)}$, the Power method produces a sequence of vectors $\mathbf{y}^{(k)}$ in the following way:

$$\begin{aligned} \mathbf{z}^{(k)} &= \mathbf{F} \mathbf{y}^{(k-1)} \\ \mathbf{y}^{(k)} &= \mathbf{z}^{(k)} / \|\mathbf{z}^{(k)}\|_2 \end{aligned} \quad (4.42)$$

The method converges if λ_1 is dominant and if $\mathbf{y}^{(0)}$ has a component in the direction of the corresponding dominant eigenvector \mathbf{y}_1 . It is easily verified that $\mathbf{y}_1, \dots, \mathbf{y}_P$ are the left singular vectors of \mathbf{Y}_s , therefore, once the principal singular vector \mathbf{y}_1 has been estimated, the signal pole z_1 corresponding to the strongest signal component is given by $z_1 = \underline{\mathbf{y}}_1^+ \overline{\mathbf{y}}_1$. A potential problem with this method is that its convergence rate depends on $|\lambda_2/\lambda_1|$, a quantity which may be close to 1 and thus cause slow convergence. Improved versions of the

algorithm which overcome this problem are discussed in [19]. Note that the power method involves only simple matrix multiplications and has a computational order of $\mathcal{O}(P^2)$ per iteration.

Orthogonal Iteration

A straightforward generalization of the power method can be used to compute higher-dimensional invariant subspaces, that is, to find $M_d > 1$ dominant singular vectors. The method is typically referred to as *Orthogonal iteration* or *Subspace iteration* and can be summarized as follows.

Given a $P \times M_d$ matrix $\mathbf{W}^{(0)}$, the method generates a sequence of matrices $\mathbf{W}^{(k)}$ through the iteration

$$\mathbf{Z}^{(k)} = \mathbf{F}\mathbf{W}^{(k-1)} \quad (4.43)$$

$$\mathbf{W}^{(k)}\mathbf{R}^{(k)} = \mathbf{Z}^{(k)} \quad (Q - R \text{ factorization}) \quad (4.44)$$

The computational complexity of the method is on the order of $\mathcal{O}(P^2M_d)$ per iteration, and clearly, when $M_d = 1$ the algorithm is equivalent to the power method. In practice, \mathbf{F} is first reduced to upper Hessenberg form (that is, \mathbf{F} is zero below the first subdiagonal) and the method is implemented in a simpler way, avoiding explicit $Q - R$ factorization in each iteration. A more detailed discussion on this topic can be found in [19].

4.5 Low-Complexity Rapid Acquisition in UWB Localizers

4.5.1 System model

One of the most interesting applications of our framework can be found in ultra-wideband transceivers intended for low-rate, low-power indoor wireless systems, for example, in systems used for precise position location. Such UWB transceivers, called localizers, have already been developed [25] and they use low duty-cycle periodic transmission of a coded sequence of impulses to ensure low-power operation and good performance in a multipath environment. Yet, rapid synchronization still presents the most challenging part in the transceiver design. Current solutions are still analog and use a cascade of correlators to perform exhaustive search through all possible code positions, which is inherently time consuming. A similar architecture, based on a “mostly digital” conception, is proposed in [22], where sampling is achieved using an A/D converter designed to run at 2GHz. In addition to the high sampling rates, implementation of the cascade of correlators can take up to 30% of the circuit area and tends to consume a major amount of the total power. Therefore, developing alternative methods that would allow for faster acquisition and lower power consumption is still an open problem.

Our previous results can be directly applied to the problem of timing synchronization in such systems, by modeling the received noiseless signal $y(t)$ as a convolution of L delayed, possibly different, impulses with a known coding

sequence $g(t)$, that is,

$$y(t) = \sum_{l=1}^L a_l p_l(t - t_l) * g(t) \quad (4.45)$$

As $y(t)$ is a periodic signal, its spectral coefficients are exactly given by

$$Y[n] = \sum_{l=1}^L a_l P_l[n] G[n] e^{-jn\omega_c t_l} \quad (4.46)$$

where $\omega_c = 2\pi/T_c$, while T_c denotes a cycle time. If we use the polynomial approximation (4.23) of the spectral coefficients $P_l[n]$, the total number of degrees of freedom per cycle is $2RL$. Therefore, the signal parameters can be estimated by sampling the signal uniformly at a sub-Nyquist rate, using the method presented in Section 4.2. Note that unlike the conventional techniques [22] [25], our approach does not require prior knowledge of the transmitted or received pulse shape.

4.5.2 Two-step estimation

Another advantage of our framework in ranging/positioning applications is that it allows for a “multiresolution” approach, that is, one can first obtain a rough estimate of the sequence timing, by taking uniform samples at a low rate over the entire cycle. Later, precise delay estimation can be carried out by increasing the sampling rate, yet sampling the received signal only within a narrow time window where the signal is present. The rationale for using the two-step approach is that in such systems a sequence duration T_s typically spans a small fraction of the cycle time T_c (e.g. less than 20%). As a result, all search-based methods [22] [25] [30], require a very long acquisition time and apparently “waste” power in sampling and processing time slots where the signal is not present.

A natural question arising from our discussion is how much one can reduce computational and power requirements using the two-step approach. In order to answer this question, consider the following scenario. Assume that the signal is first sampled at a low rate N_l over the entire cycle, and the Power method is used to achieve coarse synchronization. Assume next that the signal is sampled at a higher rate N_h (N_h is still below the Nyquist rate N_n) over a narrow time window of duration (roughly) T_s , and that M_d dominant signal components are estimated using the method of Orthogonal iteration. Since we are mostly interested in the low SNR regime ($\text{SNR} < 0\text{dB}$), a typical range for N_l is between $N_n/40$ and $N_n/20$, while N_h takes on values between $N_n/10$ and $N_n/2$.

Table 4.1: Comparison of different acquisition algorithms: computational complexity, power consumption and the number of sampling cycles

Method	Two-step approach		Subspace method	Matched filter
	coarse synch.	fine synch.		
Complexity	$\mathcal{O}((N_l T_c)^2)$	$\mathcal{O}(M_d (N_h T_s)^2)$	$\mathcal{O}(M_d (N_h T_c)^2)$	$\mathcal{O}((N_n T_c)^2)$
Power cons.	$\sim N_l T_c$	$\sim N_h T_s$	$\sim N_h T_c$	$\sim N_n T_c$
# cycles	$N_c = 2$		$N_c = 1$	$N_c \sim N_n T_c / K_{corr}$

In Table 4.1, we list the computational complexity, power consumption of A/D converters and the number of sampling cycles required to acquire the signal, for the following methods: the two-step algorithm, the subspace-based approach from Section 4.1.3, assuming uniform sampling at the rate N_h during the entire cycle, and the matched filter approach [22], with a cascade of K_{corr} correlators working at the Nyquist sampling rate N_n . Note that we have considered only the power consumption associated with A/D conversion, assuming a linear dependence on the sampling frequency [15], while a more precise analysis should also take into account the power consumption due to processing.

The benefits of the two-step approach are obvious: as the ratio T_c/T_s increases, the computational and power requirements can be reduced significantly. For example, when $N_l = N_n/40$, $N_h = N_n/4$, $M_d = 1$ and $T_c/T_s = 10$, the two-step approach reduces complexity of the original subspace method approximately by a factor of 50, while power consumption is reduced by a factor of 5. Similarly, as N_h decreases, the advantages of the subspace method over the matched filter approach become more evident. Also note that due to the search-based nature of the matched filter method, it requires a much longer acquisition time compared to the other two approaches, where it suffices to sample at most two signal cycles. In practice, in the low SNR regime, it is desirable to average the samples from multiple cycles in order to increase the effective SNR and, therefore, improve the numerical performance. While this does not have a major effect on the computational requirements, power consumption increases linearly with the number of averaging cycles. Thus, a good choice of the number of cycles depends on power constraints, a desirable estimation precision and acquisition time. Note that for the two-step approach, the overall performance improves by averaging the samples during the second phase only, when the fine synchronization takes place. During the first phase, it is useful to average the samples only if the processing gain is not sufficiently high to allow for coarse acquisition from a subsampled signal, while it does not affect the overall performance, as we will show in the sequel.

4.6 Simulation Results

In this section, we show some simulation results that illustrate the performances of the proposed algorithms. All results are based on averages over 500 trials, each with a different realization of additive white Gaussian noise. We consider an UWB system where a coded sequence of UWB impulses is periodically transmitted, while coding is achieved with a PN sequence of length 127. That is, the n -th transmitted pulse is multiplied by $+1$ or -1 , according to the n -th chip in the PN sequence. Since we will be considering discrete time signals, time will be expressed in terms of samples, where one sample corresponds to the period of Nyquist-rate sampling. The relative time delay between the transmitted pulses (i.e. the chips in the sequence) is assumed to be 20 samples, while the sequence duration T_s spans approximately 20% of the cycle time T_c .

4.6.1 Timing performance

We first consider the case of a channel model given by (4.1), assuming six propagation paths with one dominant path (containing 70% of the total power),

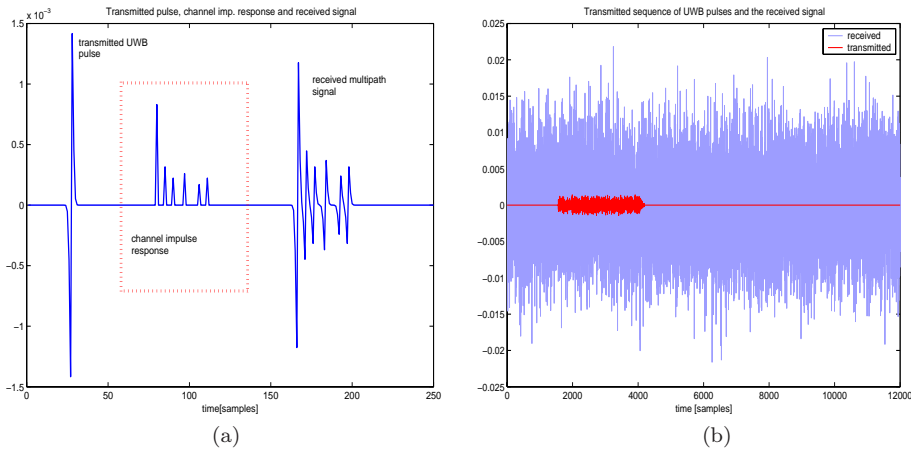
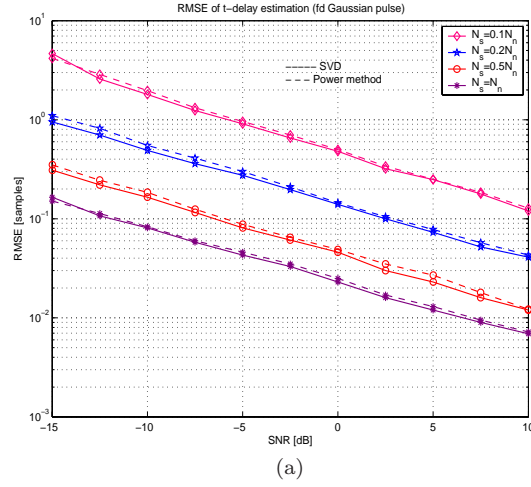


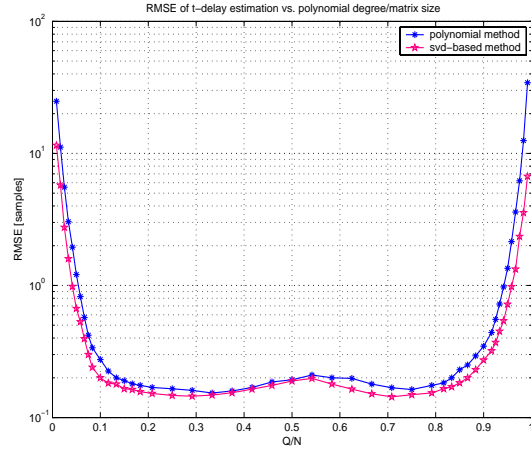
Figure 4.3: System model (a) The transmitted (single) UWB pulse is assumed to have an ideal first-derivative Gaussian shape. We considered the channel model (4.1), with six propagation paths and one dominant path (containing 70% of the total power). The received pulse is made up of six attenuated and delayed replicas of the transmitted pulse. (b) A coded sequence of 127 UWB impulses (red) is periodically transmitted over multiple cycles, while the sequence duration spans approximately 20% of the cycle time T_c . Coding is achieved with a PN sequence of length 127, and the relative delay between the transmitted pulses is 20 samples. The received signal (blue) is dominated by noise. In this case, the received signal-to-noise ratio is $\text{SNR}=-15\text{dB}$.

as illustrated in Figure 4.3(a). The transmitted UWB pulse is an ideal first-derivative Gaussian impulse, while the duration of the impulse is approximately $T_p = 5$ samples. The received noiseless sequence and a received noisy signal within one cycle are shown in Figure 4.3(b). We first analyze the timing estimation performance of the subspace method developed in Section 4.1.3, and this for different sampling rates as well as for various values of the received SNR (defined here as the ratio between the energy of the sequence in one cycle and a power spectral density of noise). The root-mean square errors (RMSE) of time delay estimation for the dominant component are shown in Figure 4.4(a). The results indicate that the method yields highly accurate estimates (that is, with a sub-chip precision) for a wide range of SNR's, and this with sub-Nyquist sampling rates. For example, with the sampling rate of one fifth the Nyquist rate ($N_s = N_n/5$) and $\text{SNR}=-10\text{dB}$, the time delay along the dominant path can be estimated with an RMSE of approximately 0.5 samples. The timing performance of the SVD-based algorithm is compared with the results obtained using a simpler approach based on the Power method. The two considered methods yield essentially the same RMSE, and obviously, the performance of the algorithms improves as the sampling rate increases.

In Figure 4.4(b), we compare the performances of the annihilating filter method and the subspace-based method. We assume that the sampling rate is $N_s = 0.2N_n$ and plot the RMSE for different values of a parameter Q , which denotes the polynomial degree (annihilating filter method), or alternatively, the number of columns in the data matrix \mathbf{Y}_s (subspace method). The two methods have very similar performances, and in general, the good choice for Q is $N/10 < Q < 9N/10$. However, the choice of Q directly affects the complexity of the polynomial method, as it requires computing Q zeros in order to extract only one



(a)

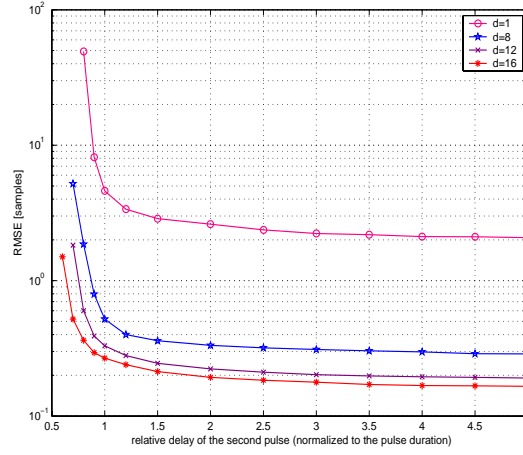


(b)

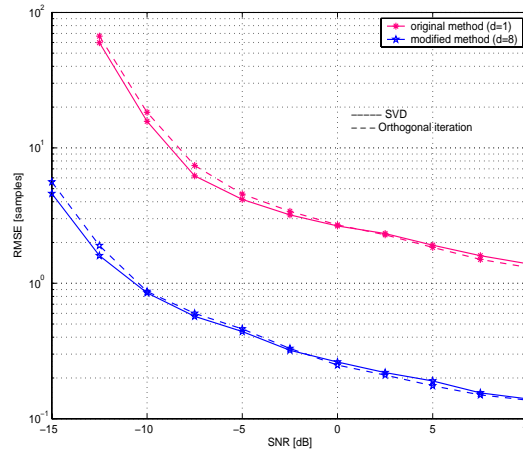
Figure 4.4: Timing recovery in UWB systems (a) Root-mean square error (RMSE) of delay estimation (in terms of number of samples) vs. SNR, for the case with one dominant path. We compare performances of the SVD-based algorithm and the Power method for several values of the sampling rate N_s . N_n denotes the Nyquist rate. (b) RMSE of t -delay estimation (SNR=0dB) for the annihilating filter and the SVD-based method, and this for different values of Q , which denotes the polynomial degree (annihilating filter method) or the number of columns in the data matrix \mathbf{Y}_s (SVD-based method). N is the total number of samples used for estimation.

signal pole. As already discussed in Section 4.1.3, the subspace-based approach avoids the problem of overmodeling and is computationally more efficient.

We next consider the same channel model (4.1), yet with two dominant components, each containing 40% of the total power. RMSE of time delay estimation over the dominant paths versus the relative delay between the two components is shown in Figure 4.5(a), for the case when SNR=-5dB and the sampling rate is $N_s = N_n/5$. We compare the results obtained with the original SVD-based algorithm and its modified version from Section 4.1.3, equation (4.20), referred to as subspace-shifting method (see Chapter 2, Section 2.5.1). The results are shown



(a)



(b)

Figure 4.5: Timing recovery: the case with two dominant paths (a) RMSE of delay estimation of the two dominant components vs. relative time delay (i.e. peak-to-peak delay) between the pulses. We show the performance of the original subspace algorithm ($d = 1$) and the modified (subspace-shifting) algorithm from Section 4.1.3 ($d = 8, 12, 16$), assuming that $N_s = N_n/5$ and $SNR = -5dB$. (b) RMSE of delay estimation vs. received SNR, and this for the original algorithm ($d = 1$) and the subspace-shifting method ($d = 8$). The sampling rate is $N_s = N_n/5$, while the relative delay between the dominant components equals the pulse duration. In both cases, we plot the RMSE obtained with the SVD-based method and the method of Orthogonal iteration.

for different values of the parameter d , which determines the effective separation between the estimated time delays. Obviously, the modified method yields by an order of magnitude better resolution performance. Furthermore, as the time delay of the second component relative to the first decreases below the pulse duration, the performance of the original method degrades rapidly, while the modified algorithm can alleviate this problem by increasing the value of d . For example, when $d = 12$, it is possible to resolve the two components even when the relative (peak-to-peak) time delay between the pulses is a fraction of the

pulse duration T_p . In Figure 4.5(b), we show the delay estimation performance of the two considered methods versus received SNR, assuming that the relative delay between the dominant components is fixed (*i.e.* the peak-to-peak spacing equals the pulse duration). Similarly to the previous case, the performance improvement achievable with the modified algorithm is significant, specifically for very low SNR's. It is also interesting to note that the results obtained using the SVD-based approach and its simplified version using Orthogonal iteration are almost identical, which makes the latter solution an attractive option in practice.

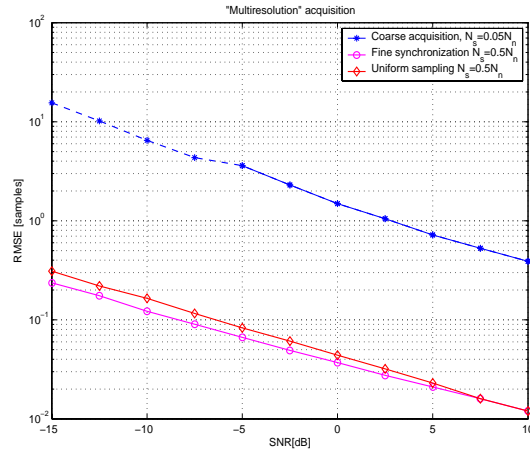
4.6.2 Two-step estimation

In Figure 4.6, we show the performance of the multiresolution or two-step delay estimation. That is, the first step is coarse synchronization, when the signal is sampled uniformly over the entire cycle at a low rate N_l to obtain a rough estimate of the sequence timing. The second step is fine synchronization, where the signal is sampled only within a narrow time window where the signal is assumed to be present, yet at a higher rate N_h . RMSE of the two-step approach for $N_l = 0.05N_n$ and $N_h = 0.5N_n$ is shown in Figure 4.6(a). As the subsampling factor during the first phase is 20, for low values of SNR (that is, less than -5dB), the samples are averaged over multiple cycles in order to increase the effective SNR. The error is compared to the RMSE obtained when the signal is sampled uniformly at a rate $N_h = 0.5N_n$ over the entire cycle. The results indicate that the two methods yield a very similar performance, however, in this case, the two-step approach reduces the computational requirements by a factor of 20, and the power consumption by a factor of 3.3.

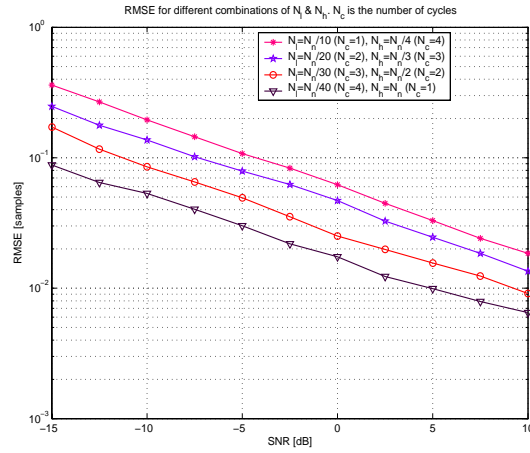
In Figure 4.6(b), we plot the RMSE of delay estimation for different combinations of N_l and N_h , assuming that the total number of averaging cycles is 5. The number of cycles during each phase is chosen such that the overall power consumption remains constant. As already discussed in Section 4.5, the best performance can be expected when the sampling rate N_h during the second phase is highest. Namely, by increasing N_h , the number of samples used for fine synchronization increases, while the effective SNR remains the same, given the above assumption on the number of averaging cycles. This results in an improved performance (see (4.37)), yet at the expense of increased computational complexity.

4.6.3 Estimation from non-adjacent bands

We next consider the case of timing estimation from non-adjacent bands. The received signal is sampled at one one fifth the Nyquist rate, where the frequency bands B_1 , B_2 and B_3 used for estimation are shown in Figure 4.7(a). We assumed the same noise level in all bands and considered two cases: (a) the channel is estimated by sampling B_1 and B_2 . (b) The band B_2 is subject to a strong wideband interference, thus the channel is estimated from bands B_1 and B_3 , using the method described in Section 4.3. The RMSE of delay estimation for the dominant path vs. received SNR is presented in Figure 4.7(b). The results obtained for the two analyzed cases are very similar, which suggests that excluding a few bands does not considerably affect the performance of the



(a)



(b)

Figure 4.6: Two-step delay estimation (a) Coarse synchronization is obtained by sampling the received signal uniformly (over the entire cycle) at a low rate $N_i = N_n/20$. For low SNR's (less than -5dB) the samples are averaged over multiple cycles (dashed line). Once a rough estimate of the sequence timing is obtained, fine synchronization follows: the signal is sampled only within a narrow window, yet at a higher rate $N_h = N_n/2$. RMSE of time delay estimation is compared to the RMSE obtained with high-rate uniform sampling over the entire cycle. (b) RMSE of delay estimation for different combinations of N_i (the sampling rate for coarse synchronization) and N_h (the sampling rate for fine synchronization). N_c denotes the number of averaging cycles during each phase, chosen such that the total power consumption remains constant.

method, provided that the overall size of the frequency band used for estimation is approximately the same.

4.6.4 Timing in the case of a non-ideal channel

In Figure 4.8, we show the delay estimation performance for the dominant component in the case when received pulses are distorted versions of a transmitted

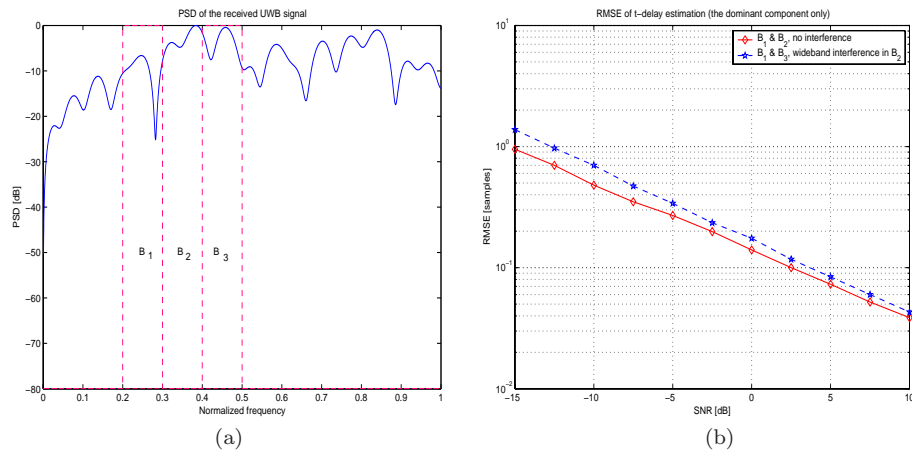


Figure 4.7: Estimation from non-adjacent bands (a) Normalized power spectral density (PSD) of the received pulse and frequency bands used for estimation. (b) The channel is estimated from bands B_1 and B_2 (no interference) and the delay estimation performance is compared to the case when B_1 and B_3 are sampled (strong interference in B_2).

impulse. As in the previous experiments, we assumed that a sequence of 127 coded impulses is periodically transmitted, where a transmitted impulse and a measured received waveform³ are illustrated in Figure 4.8(a). The normalized power spectral density and the bands used for estimation are shown in Figure 4.8(b). We used the Power method to estimate the time delay of the dominant component, and this for three different values of the sampling rate: $N_s = 0.1N_n$, $N_s = 0.2N_n$ and $N_s = 0.3N_n$. The results are compared with those obtained using the matched filter approach (at Nyquist rate sampling N_n) [22], indicating that our method is more robust to waveform mismatch. For example, with the sampling rate of $N_s = 0.2N_n$, the timing performance is very similar to that of the matched filter, while for $N_s = 0.3N_n$, our scheme clearly yields much better performance.

4.6.5 Higher-rank channel models

We next consider the case of the channel model given by (4.1), assuming $L = 70$ propagation paths with eight dominant paths (containing 85% of the total power), as illustrated in Figure 4.9(a). We assumed that the average (peak-to-peak) time delay between the received dominant components is equal to $2T_p$. In Figure 4.9(b), we show RMSE of delay estimation for the dominant components vs. SNR. We used the approach presented in Section 4.1.3 (4.20), where the parameter d is chosen to be $d = 30$. The method yields highly accurate estimates in this case as well, and this for a wide range of SNR's. For example, when $N_s = N_n/4$ and $SNR = -5dB$, the delay of the dominant components can be estimated with an RMSE of approximately 1 sample.

The effects of quantization on the estimation performance are shown in Figure 4.9(c). In particular, we considered 4-7 bit architectures and for each case we plot the RMSE versus received SNR. The results are also compared to the

³The propagation experiment was performed at the Berkeley Wireless Research Center [12]

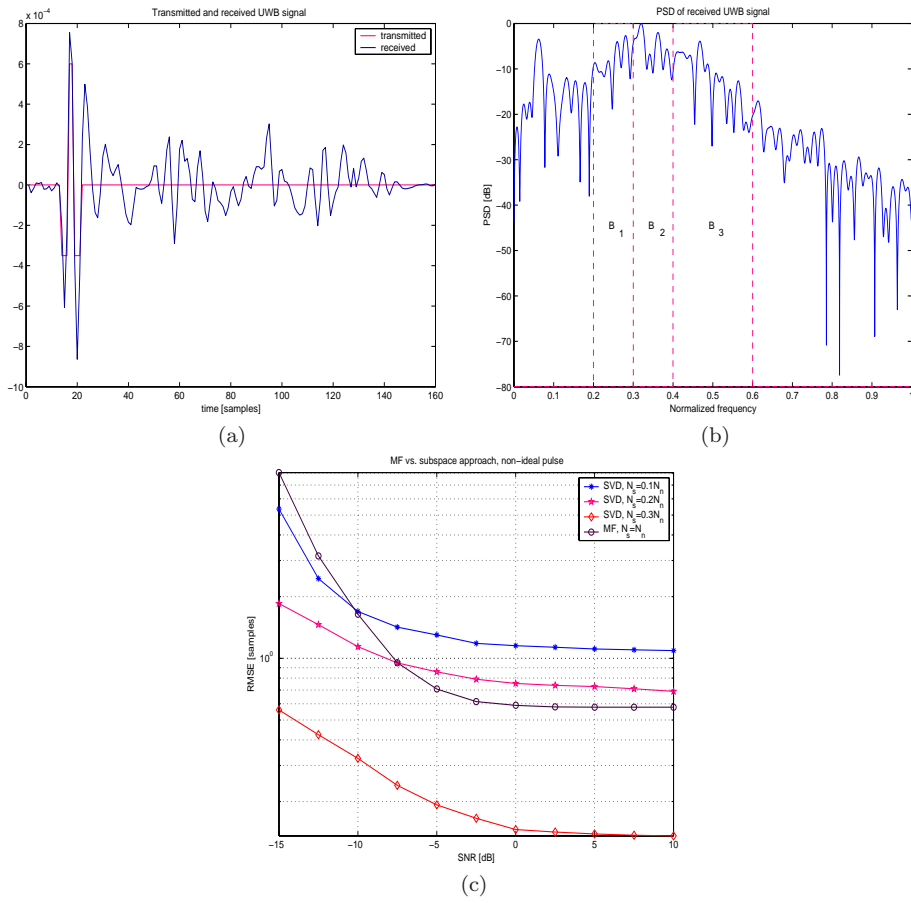


Figure 4.8: Timing recovery in non-ideal channels (a) Received waveform (single pulse, including multipaths) and transmitted pulse. (b) Normalized power spectral density (PSD) of the received pulse and frequency bands used for estimation. (c) Timing estimation performances of the SVD-based method and the matched filter approach. The sampling rate for the SVD approach is $N_s = 0.1N_n$ (the band B_1 is sampled), $N_s = 0.2N_n$ (B_1 and B_2 are sampled) and $N_s = 0.3N_n$ (B_2 and B_3 are sampled), while for the matched filter $N_s = N_n$.

“ideal” case when $n_b = 32$ bits are used for quantization. Clearly, as the number of bits increases, the overall performance improves. Generally, the 5-bit architecture already yields a very good performance. Also note that when $n_b \geq 5$ and the value of SNR is low (e.g. $SNR < 0dB$), quantization has almost no impact on the estimation performance. However, as the value of SNR increases, quantization noise becomes dominant and determines the overall numerical performance.

4.6.6 Joint pulse shape and delay estimation

We next consider the case of the channel model given by (4.21). Specifically, we assume that a coded sequence of first-derivative Gaussian impulses is periodically transmitted over a channel with three propagation paths, where a received

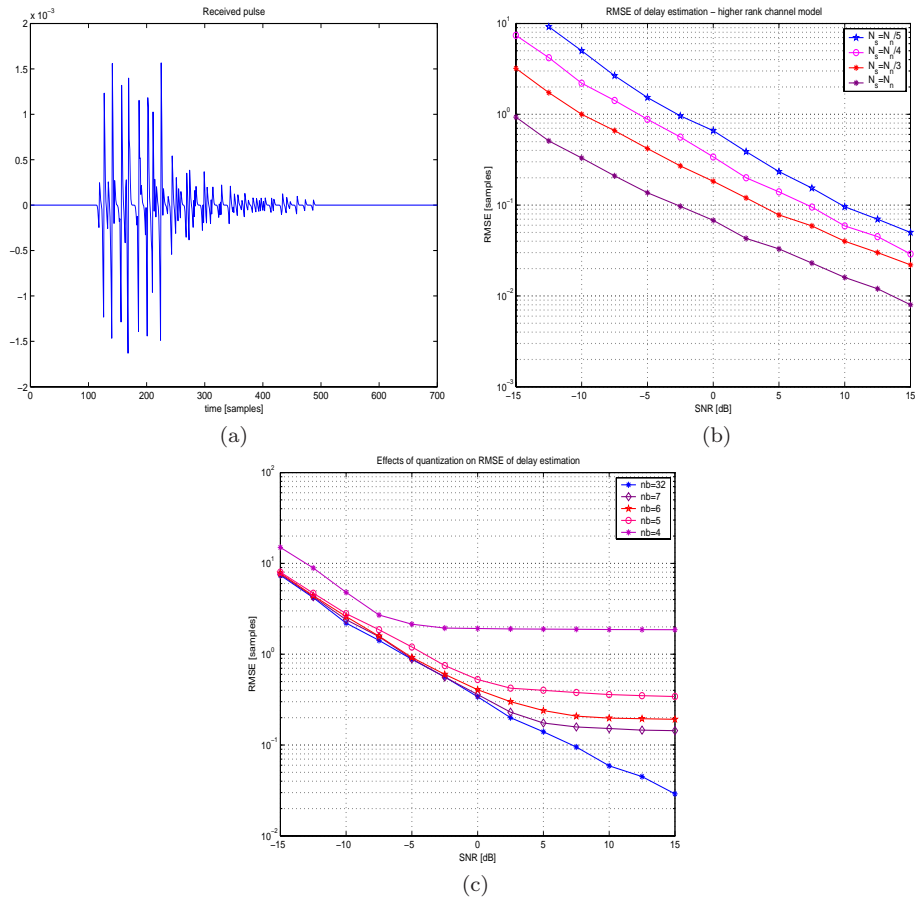


Figure 4.9: Higher-rank channel models (a) Received UWB signal made up of 70 pulses, with 8 components being dominant (containing approximately 85% of the total power). (b) RMSE of delay estimation of the dominant components vs. SNR. (c) Effects of quantization on the RMSE of delay estimation for 4-7 bit receiver architectures. The results are compared to the case when the number of bits is $n_b = 32$. The sampling rate is one fourth the Nyquist rate ($N_s = N_n/4$).

(single) UWB signal is made up of three pulses having different shapes. This is illustrated in Figure 4.10(a), where the received noiseless and noisy UWB signals for SNR=0dB are shown. The received signal is sampled uniformly over the entire cycle at one fifth the Nyquist rate and the samples are averaged over $N_c = 5$ cycles. We used the subspace method to estimate unknown time delays. As already pointed out in Section 4.2, the signal poles (and thus the unknown time delays) can be estimated by choosing $L = 3$ eigenvalues closest to the unit circle. Once the time delays of the pulses have been estimated, the corresponding pulse shapes are obtained by polynomial approximation of the DFT coefficients. In this case, we used a polynomial of degree $R = 20$, which clearly yields a very good approximation of the received waveforms. However, by increasing the sampling rate, the performance of the method does not necessarily improve, since we try to fit more coefficients from frequency bands where noise dominates the signal. This effect can be seen in Figure 4.10(e). In order to

overcome this problem, an exponential weighting of the estimated DFT coefficients is carried out, as discussed in Section 4.2. This can significantly improve the accuracy of the reconstruction, as can be seen in Figure 4.10(f).

4.7 Application to CDMA systems

The techniques for channel estimation developed in this chapter can be also used in other systems with bandwidth expansion, such as code division multiple access (CDMA) systems [88]. Bandwidth expansion in direct sequence (DS) CDMA systems is accomplished by means of a spreading code, often called a signature sequence, whose chip rate is much higher than the information signal bandwidth [20]. While the problems of high sampling rates and the complexity of channel estimation algorithms in DS-CDMA systems are not as critical as it was the case with UWB systems, we will show that one can obtain high-resolution estimates of the channel parameters by sampling the received signal below the traditional chip rate.

4.7.1 Channel estimation

Consider the simple case of a DS-CDMA system with a single user, operating over a multipath fading channel with at most L propagation paths. We assume that the channel varies slowly, i.e. it is considered constant over a channel estimation window. A received baseband signal $y(t)$ can be thus represented as a sum of multiple copies of an attenuated and delayed transmitted signals and noise,

$$y(t) = \sum_{l=1}^L a_l s(t - t_l) + \eta(t), \quad (4.47)$$

where $s(t)$ is a signature sequence of length N assigned to the user, t_l denotes the delay of the signal received along the l -th path, a_l is the corresponding complex propagation coefficient that includes channel attenuation and a phase offset along the l -th path, and $\eta(t)$ denotes additive white Gaussian noise.

Note that the above expression for the received signal is the same one we had in the case of UWB signals (4.2), except that in this case $s(t)$ corresponds to the signature sequence assigned to the user. Therefore, the DFT coefficients of the received signal are given by

$$Y[m] = \sum_{l=1}^L a_l S[m] e^{-jm\omega_0 t_l} + N[m], \quad \omega_0 = 2\pi/T_s, \quad (4.48)$$

where $S[m]$ and $N[m]$ denote the DFT coefficients of the signature sequence and noise respectively. Since the $S[m]$'s in (4.48) are assumed to be known coefficients, the problem of estimating the unknown parameters t_l and a_l from the set of coefficients $Y[m]$ is now equivalent to the problem of channel estimation in UWB systems, already discussed in this chapter. Since the received signal has only $2L$ degrees of freedom, in the noiseless case, it suffices to use only $2L$ coefficients $Y[m]$ to estimate all the unknown parameters. In the noisy case, the sampling rate should be increased above the critical rate, and the choice

of the sampling rate depends on a signal-to-noise ratio and the desired estimation precision. However, we will show that for the values of SNR encountered in practice, the sampling rate required for estimating the time delays with a sub-chip precision is still below the chip rate.

4.7.2 Joint time delay and angle estimation

One can further extend the above results to the problem of joint delay and angle estimation using antenna arrays, in order to simultaneously exploit the space and time domain structure of received multipath signals [64]. Namely, the use of antenna arrays improves the performance of CDMA receivers in the spatial domain, by steering beams toward desired users and thus decreasing the interference power level, while the RAKE receiver attempts the same goal through temporal operations by coherently combining multipath signals from a desired user [44] [64] [70] [76].

Consider a uniform linear antenna array system consisting of S omnidirectional elements with equal interelement spacing Δ . We will assume that the carrier frequency is relatively high compared to the bandwidth of the transmitted signal⁴ and that a channel is slowly varying. The direction of arrival θ_l of the signal received along the l -th path is assumed to be the same for all antennas in the array. However, there will be a fixed phase difference between signals received at each two consecutive elements of the array, given by $e^{j\omega_c \frac{\Delta \sin \theta_l}{c}} = e^{j\phi_l}$, where ω_c denotes the angular frequency of the carrier. The same phase difference will thus appear between corresponding DFT coefficients of signals received at each two consecutive elements.

Consider next a set of the DFT coefficients of the received signal, estimated separately at each antenna, and denote them as $Y_1[m], Y_2[m], \dots, Y_S[m]$. If we denote by A_g the antenna gain (assumed to be the same for all antennas), the coefficients $Y_s[m]$ can be expressed as

$$Y_s[m] = \sum_{l=1}^L a_l e^{-jm\omega_0 t_l} A_g e^{-j(s-1)\phi_l}, \quad (4.49)$$

that is, a linear combination of two-dimensional complex exponentials. Note that the above equation can be also written in the form

$$Y_s[m] = \sum_{l=1}^L A_l e^{-jm\omega_0 t_l} e^{-js\phi_l}, \quad (4.50)$$

where $A_l = a_l A_g e^{-j\phi_l}$. Therefore, the problem of estimating the delays and direction of arrivals can be considered as a special case of 2-D harmonic retrieval problem. In the case of a separable problem (i.e. when the delays t_l are different or when all the angles ϕ_l are different), it would be possible to solve uniquely for all the unknown parameters by considering the outputs of only two antennas in the system and using 1-D subspace methods [65] [39]. However, such an approach may suffer from poor numerical performance for low signal-to-noise ratios and cannot be used in the non-separable case. Therefore, given

⁴Note that this assumption is not valid in the case of ultra-wideband signals.

that the coefficients $Y_s[m]$ have the form of a linear combination of 2-D complex exponentials, a more sensible approach is to use 2-D subspace algorithms for harmonic retrieval (such as MEMP, ACMP, 2-D ESPRIT etc.), which have better performance, yet at the expense of higher computational complexity. In Chapter 5, we will discuss the problem of 2-D harmonic retrieval in more detail and describe the ACMP (Algebraic Coupling of Matrix Pencils) algorithm, which belongs to the class of high-resolution subspace algorithms. At this point, it is important to note that in order to apply 2-D subspace algorithms successfully, the number of antennas S in the array cannot be chosen arbitrarily. The minimum number of sensors S_{min} required for a unique solution by most 2-D methods is $S_{min} = 2L$, that is, it depends only on the number of multipaths.

4.7.3 Channel estimation in W-CDMA systems: simulation results

In the following, we present simulation examples that illustrate the performance of the channel estimation algorithm in CDMA systems. Figure 4.11 illustrates the timing synchronization performance of our method for an additive white Gaussian noise channel, where the spreading is achieved with pseudo-random sequences of length 511. Figure 4.11 shows a root mean square error of time delay estimation (normalized to the chip duration T_c) versus the sampling rate. The error obviously decays fast as the sampling rate increases, and it is thus unnecessary to resort to chip or fractional sampling rates to obtain precise estimates (within a fraction of the chip duration) of the relative time delays. For example, by sampling the received signal at one fourth of the chip rate, the average estimation error is less than one tenth of the chip duration (for $E_b/N_0 \geq 7dB$), and by further increasing the sampling rate the performance does not considerably improve. The time delay error in multipath fading channels is illustrated in Figure 4.11(b), where we assumed that the signal is made up of 3 components having equal power. The estimation error is somewhat higher than in the non-fading channel case, however, it is interesting to note that if there is only one dominant component (with 70% of the total power), the estimation error is almost the same as in the non-fading channels. This result also implies that our algorithm is robust to model mismatch. In other words, it is possible to estimate the parameters of dominant paths precisely as long as the strongest signal components are incorporated in the system model.

We next consider the performance of our scheme in the case of a joint angle and delay estimation, where we used a 2-D subspace based algorithm for harmonic retrieval, the ACMP algorithm to jointly estimate time delays and direction-of-arrivals of all users. Figures 4.12(a) and 4.12(b) show normalized delay and angle estimation errors. It is obvious that by increasing the number of sensors, the angle estimation error decays faster, while by increasing the sampling rate the delay estimation error is improved. Such a behavior is due to the fact that by increasing the number of antennas we add more information about the spatial domain structure of the signal, whereas by increasing the sampling rate we include more information about the time-domain signal structure. The same conclusions hold for multipath channels, yet all the estimation errors are somewhat higher.

4.8 Conclusion

We have presented several methods for subspace parameter estimation in ultra-wideband systems, which are based on the sampling results for certain classes of parametric non-bandlimited signals, presented in Chapters 2 and 3. Our approach takes advantage of well-known spectral estimation techniques, requires lower sampling rate and, therefore, lower complexity and power consumption compared to existing digital solutions. Besides, it leads to faster acquisition and allows for identification of more realistic channel models without resorting to complex algorithms. We specifically considered the application to indoor wireless networks, where low rates and low power consumption are required. The developed algorithms can also be used in other UWB applications, primarily for synchronization and channel characterization purposes, as well as in other wideband systems, such as wideband CDMA.

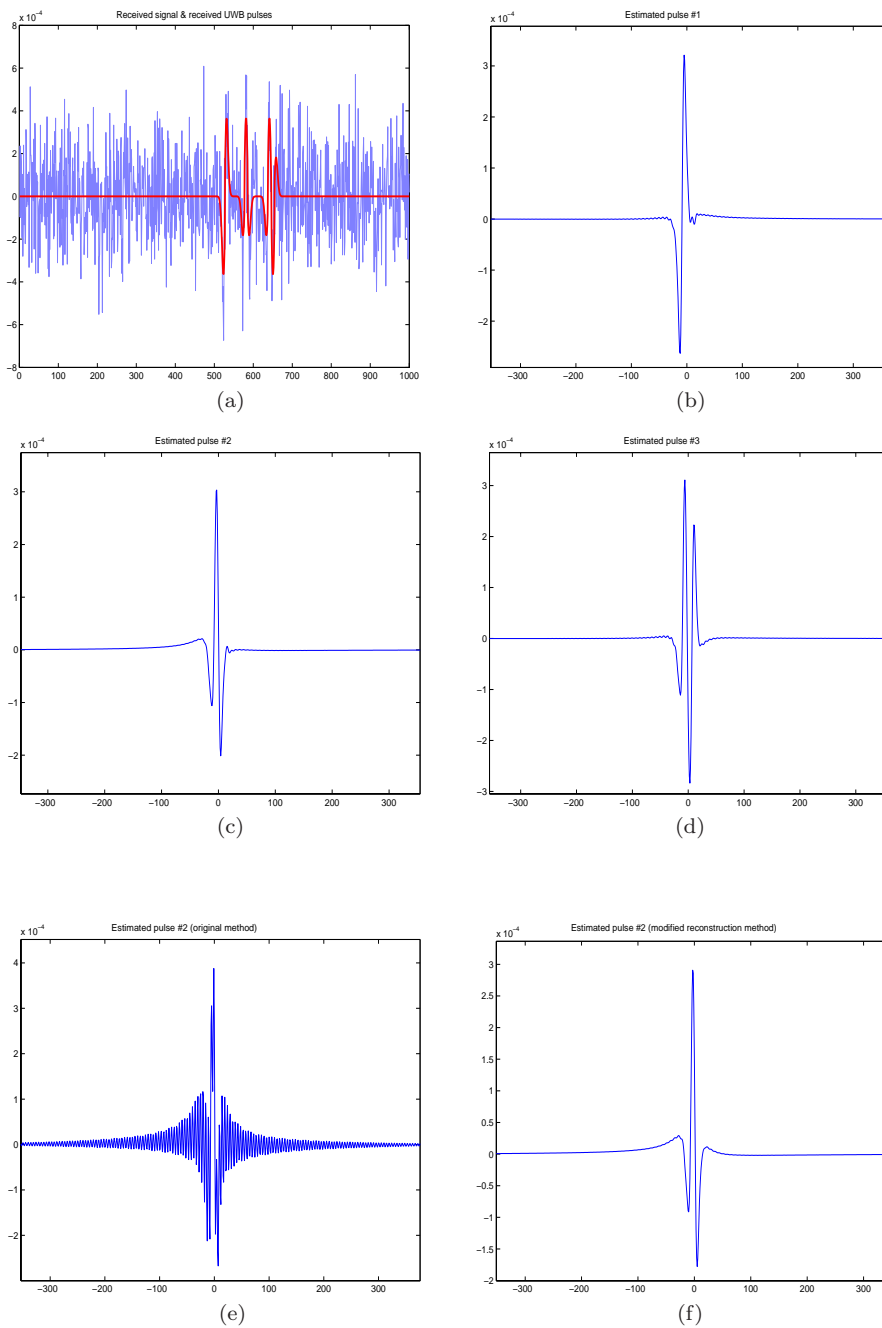


Figure 4.10: Joint pulse shape and delay estimation (a) Received noisy signal (blue) and the noiseless signal made up of three short pulses having different shapes (red). (b) Estimated shape of the first pulse. (c) Estimated shape of the second pulse. (d) Estimated shape of the third pulse. The received signal is sampled at one fifth the Nyquist rate ($N_s = N_n/5$). We used a polynomial of order $R = 20$ to approximate the DFT coefficients of the received signal. (e) Estimated second pulse in the case when the sampling rate is increased to $N_n = N_n/3$. No spectral extrapolation is used. (f) Estimated second pulse from (e) using spectral extrapolation along with the exponential weighting of the approximated DFT coefficients.

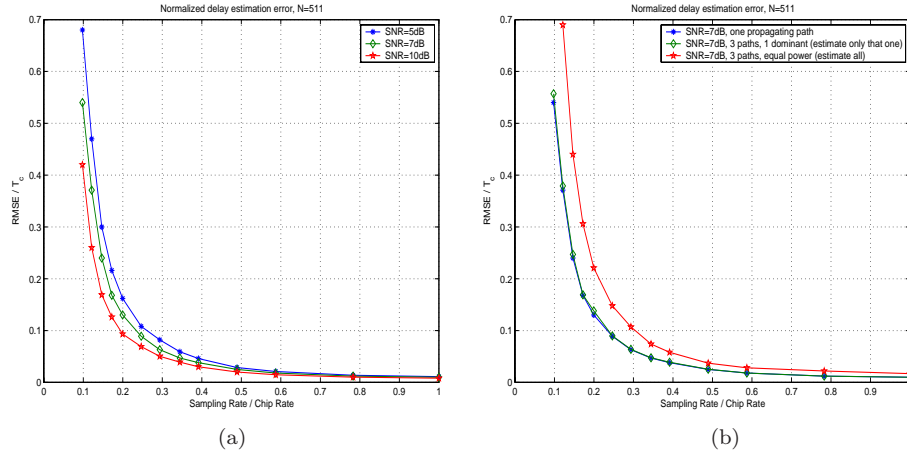


Figure 4.11: Channel estimation in CDMA systems Average timing synchronization error (normalized to T_c) in the multiuser case vs. sampling rate. We assumed a non-fading channel. The signature sequence is of length 511. (d) Comparison of timing estimation errors in single-path and multipath channels (3 received components of equal power).

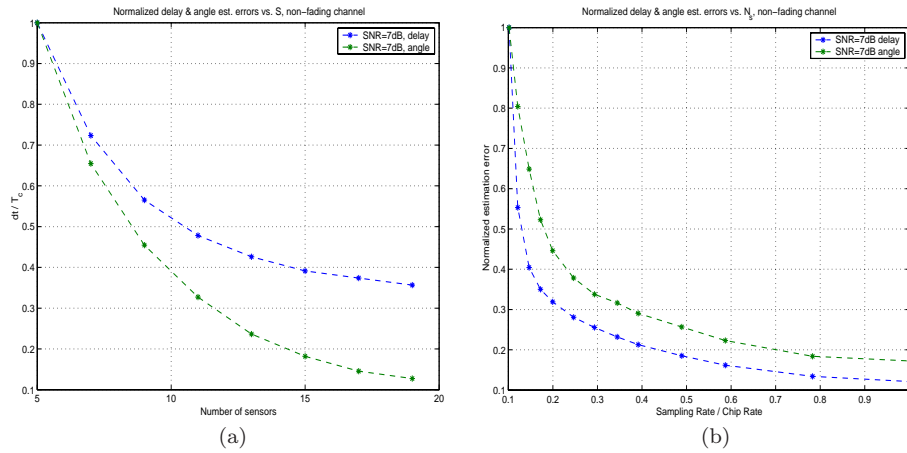


Figure 4.12: Channel estimation in CDMA systems - Joint angle and delay estimation (a) Normalized angle and delay estimation errors vs. number of sensors in the antenna array S . The signature sequence assigned to a user is of length 511. (b) Normalized angle and delay estimation errors vs. sampling rate.

Chapter 5

Sampling Methods for Classes of Periodic Non-Bandlimited 2-D Signals

In this chapter, we consider possible extensions of our sampling framework to classes of periodic non-bandlimited 2-D signals that have a finite number of degrees of freedom, that is, signals with *finite complexity*. We show that it is possible to develop exact sampling schemes and reconstruction formulas for certain classes of such signals, including sets of 2-D Diracs, lines or bilevel polygons. Similarly to the problem from the 1-D case, the space of signals we analyze is not a shift-invariant vector space, but rather a union of shift-invariant spaces of finite dimension [45]. Therefore, we focus on developing exact sampling schemes for signals with M degrees of freedom that require on the order of M samples (or at most $\mathcal{O}(M^2)$ samples), and algorithms that can recover such signals with high numerical precision.

The outline of the chapter is as follows. In Section 5.1, we review classes of non-bandlimited two-dimensional signals that will be of interest in the sequel. In Section 5.2, we consider the problem of sampling a periodic set of M weighted 2-D Diracs and propose a sampling scheme which, in the separable case, allows for perfect reconstruction from only $\mathcal{O}(M)$ samples of the signal. In Section 5.3, we extend the analysis to the non-separable case, and develop a “true” 2-D method that can perfectly reconstruct the signal from $\mathcal{O}(M^2)$ samples. A possible extension of these results to the problem of sampling some simple objects, such as sets of lines or polygons, is addressed in Section 5.4. In Section 5.5, we analyze the problem of estimating the model order and discuss numerical performance of our methods as well as robustness to model mismatch and noise. Simulation results that indicate desirable properties both in the deterministic case and in the presence of noise are given in Section 5.6. Finally, we give a brief summary of our results in the concluding remarks.

5.1 Problem Statement

In the first two chapters of this thesis, we have shown that one can develop sampling schemes for a large class of parametric non-bandlimited signals, namely, certain signals of a finite rate of innovation. Examples include streams of Diracs, non-uniform splines and piecewise polynomials, and the common feature of such signals is that they allow for a parametric representation with a finite number of degrees of freedom and can be perfectly reconstructed from a finite set of samples. The proposed methods were intended for one-dimensional signals, but when going to higher dimensions, the problem becomes more involved and does not necessarily allow for direct extension of 1-D results. We will thus consider the problem of developing exact sampling schemes and reconstruction formulas for certain classes of parametric non-bandlimited 2-D signals that have a finite number of degrees of freedom. The sampling setup we are using is shown in Figure 5.1, where the original 2-D signal $g(x, y)$ is filtered with a smoothing kernel $\varphi(x, y)$, and a uniform set of samples is taken from the filtered version $g_f(x, y) = g(x, y) * \varphi(x, y)$, that is,

$$g_s(p, q) = \langle g(x, y), \varphi(x - pT_{sx}, y - qT_{sy}) \rangle, \quad p, q \in \mathbb{Z}. \quad (5.1)$$

The above setup is typical for acquisition devices encountered in practice and the key question is under what conditions one can reconstruct $g(x, y)$ from $g_s(p, q)$. This question is fundamental in multidimensional signal processing, however, similarly to the 1-D case, the problem we consider differs from standard problems in 2-D sampling theory in the sense that classes of signals we analyze do not belong to a single linear space, but rather to a union of linear spaces of finite dimension.

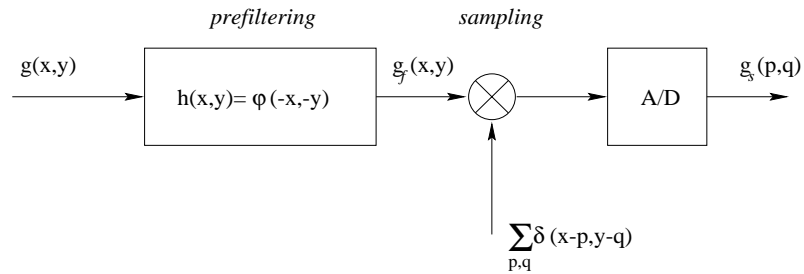


Figure 5.1: Sampling Setup Analog signal $g(x, y)$ is prefiltered with $h(x, y) = \varphi(-x, -y)$ (anti-aliasing step). The sampled signal is given by $g_s(p, q) = \sum_{p, q \in \mathbb{Z}} g_f(x, y) \delta(x - p, y - q)$.

There are several important issues that will be addressed in this chapter. We investigate if it is possible to develop a sampling scheme for a signal with M degrees of freedom that requires on the order of M samples, and what kernels $\varphi(x, y)$ allow for such schemes. Another important point is the numerical performance of the algorithms, that is, we will be interested in developing techniques that can recover the signal from a set of its samples with high numerical precision, regardless of the signal complexity (e.g. the value of the parameter M) or signal structure. And finally, we expect the algorithms to be computationally efficient and, if possible, robust to noise and model mismatch. We will show that, under certain conditions, one can develop methods that satisfy all of the

above requirements. Some of the techniques we will be using are encountered in spectral analysis [28]-[39] [69] [74] [81]-[84], or in error correction coding [5] [6] [53]. The proposed methods, while being more complex than the existing schemes for bandlimited signals, still offer efficient algorithmic implementations. We will analyze in detail the case of a signal made up of 2-D Diracs, and discuss some extensions of the results to the problem of sampling some simple objects, such as lines and polygons.

5.1.1 2-D Signals of Finite Complexity

A class of signals of finite complexity can be informally defined as a class of 2-D signals that have a parametric representation with a finite number of degrees of freedom. Similarly to the 1-D case, where we focused on signals of finite rate of innovation, the main reason why we consider the sampling problem for such a class of signals is the fact that one can expect to relate the number of degrees of freedom of the signal to the minimum sampling density ρ (or the minimum number of samples) that allows for perfect reconstruction. For example, consider the simple case of a two-dimensional bandlimited real signal $g(x, y)$, with a Fourier transform that is nonzero over a finite region R in the frequency space. If we let $2B_x$ and $2B_y$ represent the widths in the f_x and f_y directions of the smallest rectangle that encloses the region R , then appropriately spaced samples can perfectly represent the signal, i.e.

$$g(x, y) = \sum_{m=-\infty}^{\infty} \sum_{n=-\infty}^{\infty} g(mX, nY) \text{sinc}(x/X - m, y/Y - n), \quad (5.2)$$

where X and Y are such that $X \leq \frac{1}{2B_x}$ and $Y \leq \frac{1}{2B_y}$. The above relation implies that we can think of the bandlimited signal as having $1/X$ and $1/Y$ degrees of freedom per unit of length in the x and y direction respectively, which correspond to minimum sampling densities ρ_x and ρ_y . A more general form of (5.2) is given by

$$g(x, y) = \sum_{m=-\infty}^{\infty} \sum_{n=-\infty}^{\infty} c_{mn} \varphi\left(\frac{x - x_m}{X}, \frac{y - y_n}{Y}\right), \quad (5.3)$$

where x_m and y_n are arbitrary shifts. For example, when $\varphi(x, y) = \delta(x, y)$ and both $x_n - x_{n-1}$ and $y_n - y_{n-1}$ are i.i.d. random variables with exponential density, then $g(x, y)$ describes a separable 2-D Poisson process. Other examples of signals of finite complexity include simple lines and polygonal lines, planar parametric curves as well as some parametric signals whose boundaries have a finite number of degrees of freedom. We will thus try to exploit the finite number of degrees of freedom property and develop sampling schemes that allow for a perfect reconstruction from a finite number of samples.

5.2 Periodic Set of 2-D Diracs in Continuous Space

5.2.1 Fourier series

One of the most basic forms of non-bandlimited signals of finite complexity is a set of Diracs, that is, one particular realization of a 2-D Poisson process.

Although this signal has a simple parametric representation, the problem of extracting its parameters from a set of samples is a more involved task than in the one-dimensional case. In this section, we present sampling methods for a periodic set of Diracs in continuous space. Specifically, we will show that a lowpass approximation of the signal, that is, a projection of the signal onto the subspace of proper dimension, provides sufficient information for perfect reconstruction.

Let $g(x, y)$ be a periodic 2-D signal given by

$$g(x, y) = \sum_{p, q} \sum_{k=0}^{M-1} c_k \delta(x - pT_x - x_k, y - qT_y - y_k), \quad (5.4)$$

where M is assumed to be known and $T_x = T_y = T$. Consider the Fourier series representation of $g(x, y)$

$$g(x, y) = \sum_{m=-\infty}^{\infty} \sum_{n=-\infty}^{\infty} G[m, n] e^{jm\omega_0 x} e^{jn\omega_0 y}, \quad (5.5)$$

where $\omega_0 = \frac{2\pi}{T}$ and $G[m, n]$ are the Fourier series coefficients given by

$$\begin{aligned} G[m, n] &= \frac{1}{T^2} \int_0^T \int_0^T g(x, y) e^{-jm\omega_0 x} e^{-jn\omega_0 y} dx dy \\ &= \frac{1}{T^2} \int_0^T \int_0^T \sum_{k=0}^{M-1} c_k \delta(x - x_k, y - y_k) e^{-jm\omega_0 x} e^{-jn\omega_0 y} dx dy \\ &= \sum_{k=0}^{M-1} \frac{1}{T^2} \int_0^T \int_0^T c_k \delta(x - x_k, y - y_k) e^{-jm\omega_0 x} e^{-jn\omega_0 y} dx dy \\ &= \sum_{k=0}^{M-1} \frac{1}{T^2} c_k e^{-jm\omega_0 x_k} e^{-jn\omega_0 y_k} \\ &= \sum_{k=0}^{M-1} a_k e^{-jm\omega_0 x_k} e^{-jn\omega_0 y_k}, \end{aligned}$$

that is, a linear combination of M complex exponentials. We will first analyze the case where the set of Diracs has no common components along one direction, that is, all x_k are distinct (or alternatively all y_k have different values), and present a method that can perfectly recover the signal from $\mathcal{O}(M)$ samples.

5.2.2 Annihilating filter approach: the separable case

Consider the Fourier Series coefficients $G[m, 0]$, and $G[m, 1]$, given by equation (5.6),

$$G[m, 0] = \sum_{k=0}^{M-1} a_k e^{-jm\omega_0 x_k}, \quad (5.6)$$

$$G[m, 1] = \sum_{k=0}^{M-1} a_k e^{-jm\omega_0 x_k} e^{-j\omega_0 y_k} = \sum_{k=0}^{M-1} A_k e^{-jm\omega_0 x_k}, \quad (5.7)$$

where $A_k = a_k e^{-j\omega_0 y_k}$, and define a filter $H(z)$ of order M , having zeros at $z_k = e^{-j\omega_0 x_k}$

$$H(z) = \prod_{k=0}^{M-1} (1 - z^{-1} z_k) = \sum_{i=0}^M h_i z^{-i}. \quad (5.8)$$

Let $H = \text{coeff}(H(z)) = [1 \ h_1 \ h_2 \dots \ h_M]$. Since $G[m, 1]$ has the form of a weighted sum of exponentials, i.e. $G[m, 1] = \sum_{k=0}^{M-1} \alpha_k z_k^m$, the following relation must be satisfied

$$H * G[m, 1] = 0, \quad m \in \mathbb{Z}. \quad (5.9)$$

In other words, each exponential in $G[m, 1]$ is being zeroed out by one of the roots of $H(z)$, thus the filter $H(z)$ is the annihilating filter for $G[m, 1]$, and its zeros uniquely define the set of locations $\{x_k\}$. A more detailed analysis of the annihilating filters is given in Chapter 2 and in [74] and [85]. Therefore, we will only outline the basic steps of the algorithm in the two-dimensional case.

5.2.3 Algorithm outline

- Find the Fourier series coefficients $G[m, 0]$ and $G[m, 1]$, $m \in [-M, M]$, from a set of samples

$$y_s[p, q] = \langle g(x, y), \varphi(x - pT_{sx}, y - qT_{sy}) \rangle, \quad \begin{aligned} p &\in [0, T/T_{sx} - 1], \\ q &\in [0, T/T_{sy} - 1], \end{aligned}$$

where $\varphi(x, y)$ is a 2-D sinc sampling kernel¹ of bandwidth $[-M\omega_0, M\omega_0] \times [-\omega_0, \omega_0]$, while the sampling periods T_{sx} and T_{sy} are chosen such that $N_{sx} = T/T_{sx} \geq 2M + 1$ and $N_{sy} = T/T_{sy} \geq 2 \cdot 1 + 1$, with $\{N_{sx}, N_{sy}\} \in \mathbb{N}$. Namely, the sample values $y_s[p, q]$ are given by

$$\begin{aligned} y_s[p, q] &= \sum_m \sum_n G[m, n] \langle \varphi(x - pT_{sx}, y - qT_{sy}), e^{jm\omega_0 x} e^{jn\omega_0 y} \rangle \\ &= \sum_m \sum_n G[m, n] \Phi(m\omega_0, n\omega_0) e^{jm\omega_0 p T_{sx}} e^{jn\omega_0 q T_{sy}} \\ &= \sum_{m=-M}^M \sum_{n=-1}^1 G[m, n] e^{jm\omega_0 p T_{sx}} e^{jn\omega_0 q T_{sy}}, \end{aligned}$$

where $\Phi(\omega_x, \omega_y)$ is the Fourier transform of $\varphi(x, y)$ which satisfies

$$\Phi(\omega_x, \omega_y) = \begin{cases} 1, & |\omega_x| \leq M\omega_0, |\omega_y| \leq \omega_0 \\ 0, & \text{otherwise.} \end{cases} \quad (5.10)$$

If the sampling periods T_{sx} and T_{sy} satisfy the above requirements, this system of equations is invertible and will yield a unique solution for $G[m, 0]$ and $G[m, 1]$, $m \in [-M, M]$.

- Find the filter coefficients h_i , $i = 1, 2, \dots, M$, from a system of equations

$$H * G[m, 1] = \sum_{i=0}^M h_i G[m - i, 1] = 0. \quad (5.11)$$

¹Note that $\varphi(x, y)$ does not necessarily have to be a periodic function.

If we let $m = 1, 2, \dots, M$, the above system reduces to

$$h_0 G[m, 1] + \sum_{i=1}^M h_i G[m-i, 1] = 0. \quad (5.12)$$

Assuming without loss of generality that $h_0 = 1$, the filter coefficients h_i can be computed from the Yule-Walker system

$$\sum_{i=1}^M h_i G[m-i, 1] = -G[m, 1], \quad m = 1, 2, \dots, M, \quad (5.13)$$

which has a unique solution if the x_k 's are distinct. If that condition is satisfied, the Fourier series coefficients $G[m, 1]$, $m \in [-M+1, M]$ provide sufficient information to solve uniquely for the filter coefficients h_i , and hence for the set $\{x_i\}$ by factorization.

- Solve for the set of pairs (x_k, y_k) and corresponding weights a_k .
Consider the expressions for $G[m, 0]$ and $G[m, 1]$, $m \in [0, M-1]$ in matrix form

$$\begin{pmatrix} G[0, 0] \\ G[1, 0] \\ \vdots \\ G[M-1, 0] \end{pmatrix} = \begin{pmatrix} 1 & \dots & 1 \\ e^{-j\omega_0 x_0} & \dots & e^{-j\omega_0 x_{M-1}} \\ \vdots & \ddots & \vdots \\ e^{-j(M-1)\omega_0 x_0} & \dots & e^{-j(M-1)\omega_0 x_{M-1}} \end{pmatrix} \cdot \begin{pmatrix} a_0 \\ a_1 \\ \vdots \\ a_{M-1} \end{pmatrix}. \quad (5.14)$$

The above system is a Vandermonde system which yields a unique solution for the weights a_i , provided $x_i \neq x_j$ when $i \neq j$. By a similar argument, $A_i = a_i e^{-j\omega_0 y_i}$ can be found from the coefficients $G[m, 1]$

$$\begin{pmatrix} G[0, 1] \\ G[1, 1] \\ \vdots \\ G[M-1, 1] \end{pmatrix} = \begin{pmatrix} 1 & \dots & 1 \\ e^{-j\omega_0 x_0} & \dots & e^{-j\omega_0 x_{M-1}} \\ \vdots & \ddots & \vdots \\ e^{-j(M-1)\omega_0 x_0} & \dots & e^{-j(M-1)\omega_0 x_{M-1}} \end{pmatrix} \cdot \begin{pmatrix} a_0 e^{-j\omega_0 y_0} \\ a_1 e^{-j\omega_0 y_1} \\ \vdots \\ a_{M-1} e^{-j\omega_0 y_{M-1}} \end{pmatrix}. \quad (5.15)$$

Equations (5.13), (5.14) and (5.15), yield a unique solution for the set $\{(x_k, y_k, a_k)\}$, thus we can state:

Proposition 5.1: Let $g(x, y)$ be a periodic set of M weighted 2-D Diracs of periods $T_x = T_y = T$ in the x and y directions, and assume that $g(x, y)$ does not contain common components along the x direction. Denote by $\varphi(x, y)$ the 2-D sinc sampling kernel of bandwidth $[-M\omega_0, M\omega_0] \times [-\omega_0, \omega_0]$, and choose the sampling periods T_{sx} and T_{sy} such that $N_{sx} = T/T_{sx} \geq 2M+1$ and $N_{sy} = T/T_{sy} \geq 2 \cdot 1 + 1$, where $\{N_{sx}, N_{sy}\} \in \mathbb{N}$. Then the samples

$$y_s[p, q] = \langle g(x, y), \varphi(x - pT_{sx}, y - qT_{sy}) \rangle, \quad p \in [0, N_{sx} - 1] \quad q \in [0, N_{sy} - 1],$$

are a sufficient representation of $g(x, y)$.

In the case when the coordinates of the Diracs are distinct along the y direction but not along the x direction, the algorithm remains virtually the same. The only difference is the use of an alternative sinc sampling kernel of bandwidth $[-\omega_0, \omega_0] \times [-M\omega_0, M\omega_0]$, while the signal parameters can be found from the Fourier Series coefficients $G[0, n]$ and $G[1, n]$, $n \in [-M, M]$. The presented method thus yields a unique solution by taking only $\mathcal{O}(M)$ samples of the signal, but its numerical stability typically degrades as the number of Diracs increases, due to the root finding part of the algorithm. Another disadvantage is that the method fails when the Diracs have common components along both directions, which also points to numerical instability if the coordinates are very close.

It is worth noting that it is also possible to solve for the signal parameters from the same set of the Fourier series coefficients using one-dimensional subspace methods for harmonic retrieval, as discussed in Chapter 2. However, the same necessary condition for the success of these methods holds, namely, the set of Diracs must have no common components along the x or the y direction. If such is not the case, one possible way of handling this problem is discussed in the next section.

5.3 Sampling schemes in the non-separable case

The algorithm we described is based on the idea of reducing the two-dimensional sampling problem to one dimension and using 1-D methods for harmonic retrieval. However, we have seen that such an approach imposes certain constraints in terms of the locations of the Diracs in the set, i.e. the necessary condition is that the problem is separable in the x , or alternatively, y direction. In order to avoid this constraint, it seems natural to try to extend the idea of annihilating filters to two-dimensions. In other words, if we can find an FIR filter $H(z_1, z_2)$ having M zeros at $(z_{1k}, z_{2k}) = (e^{-j\omega_0 x_k}, e^{-j\omega_0 y_k})$, which satisfies $H[m, n] * G[m, n] = 0$, then the problem would essentially be equivalent to the one we discussed in the 1-D case. Yet, it turns out that this approach cannot be used. The main reason is that in the two-dimensional case, there is no general relationship between the degree of a bivariate polynomial and the number of its zeros. For example, consider a filter $H(z_1, z_2) = \prod_{k=0}^{M-1} (1 - z_1^{-1} e^{-j\omega_0 x_k} z_2^{-1} e^{-j\omega_0 y_k})$ which is a 2-D counterpart of the annihilating filter defined in Section 5.2. $H(z_1, z_2)$ is a polynomial in z_1^{-1} and z_2^{-1} of degree $2M$, and satisfies the relation $H[m, n] * G[m, n] = 0$, but has an infinite number of zeros over the complex field, located at hyperbolas $z_1 z_2 = e^{-j\omega_0(x_k + y_k)}$. Clearly, the problem in two dimensions is more involved and a simple extension of the method from the 1-D case will not lead to the solution.

An alternative way to estimate the locations and weights of Diracs is to use 2-D subspace methods. Two-dimensional subspace-based algorithms have been studied extensively in the context of harmonic retrieval, typically for distinguishing and tracking signals of interest and extracting relevant information from noisy measurements. In that particular framework, subspace methods are used with the aim to estimate the signal parameters from noisy data and a model that approximately fits all the available information is more desirable. We will prove that in the deterministic case, 2-D subspace methods can be adapted in

such a way that the exact values of the parameters x_i , y_i and a_i , can be found from only $\mathcal{O}(M^2)$ samples of the signal $g(x, y)$.

5.3.1 Subspace-based approach

Consider again the Fourier series coefficients $G[m, n]$, given by (5.6),

$$G[m, n] = \sum_{k=0}^{M-1} a_k e^{-jm\omega_0 x_k} e^{-jn\omega_0 y_k}. \quad (5.16)$$

To make the notation simpler, we can write the above system as

$$G[m, n] = \sum_{k=0}^{M-1} a_k w_k^m z_k^n, \quad (5.17)$$

where $w_k = e^{-j\omega_0 x_k}$ and $z_k = e^{-j\omega_0 y_k}$. If we let $0 < m \leq P-1$ and $0 < n \leq Q-1$, equation (5.17) can be written as $G = WAZ$, with matrices W , A , and Z defined as

$$W = \begin{pmatrix} 1 & 1 & 1 & \dots & 1 \\ w_1 & w_2 & w_3 & \dots & w_M \\ \vdots & & & & \\ w_1^{P-1} & w_2^{P-1} & w_3^{P-1} & \dots & w_M^{P-1} \end{pmatrix}, \quad (5.18)$$

$$A = \text{diag}(a_1 \ a_2 \ a_3 \ \dots \ a_M), \quad (5.19)$$

$$Z = \begin{pmatrix} 1 & z_1 & z_1^2 & \dots & z_1^{Q-1} \\ 1 & z_2 & z_2^2 & \dots & z_2^{Q-1} \\ \vdots & & & & \\ 1 & z_M & z_M^2 & \dots & z_M^{Q-1} \end{pmatrix}. \quad (5.20)$$

If the projections of the set of Diracs on the x and the y directions are distinct, then the rank of the matrix G is equal to M and the values w_i and z_i can be obtained from the principal left or right singular vectors of G . If this condition is not satisfied, the algorithm fails due to the rank deficiency of G . Among the earliest spectral estimation techniques that addressed this problem was the MEMP algorithm (Matrix Enhancement and Matrix Pencil) [34]. The method introduces so-called “enhanced matrices”, both of rank M , from which the sets $\{w_i\}$ and $\{z_i\}$ could be obtained, yet an additional step is required to form the correct pairs (w_i, z_i) . This often involves a costly minimization procedure, making this algorithm unattractive due to its computational cost. In response to that, there has been a lot of work toward developing high-resolution methods that would link the estimation problems in both dimensions [28] [69] [81]-[84]. We will show how one such method, the ACMP algorithm (Algebraic Coupling of Matrix Pencils), can be efficiently applied to our sampling problem. A more detailed discussion of the method can be found in [81].

5.3.2 Outline of the ACMP algorithm

Let the $K(P-L) \times L(Q-K)$ enhanced matrix J be defined as

$$J = \begin{pmatrix} G^{(1,1)} & G^{(2,1)} & \dots & G^{(L,1)} \\ G^{(1,2)} & G^{(2,2)} & \dots & G^{(L,2)} \\ G^{(1,K)} & G^{(2,K)} & \dots & G^{(L,K)} \end{pmatrix}, \quad (5.21)$$

where the (k, l) -th block component of J is given by

$$J_{kl} = G^{(l,k)} = \begin{pmatrix} G[l, k] & \dots & G[l, Q - K - 1 + k] \\ G[l + 1, k] & \dots & G[l + 1, Q - K - 1 + k] \\ \vdots & & \\ G[P - L - 1 + l, k] & \dots & G[P - L - 1 + l, Q - K - 1 + k] \end{pmatrix}. \quad (5.22)$$

The matrix J can be written as

$$J = W'AZ', \quad (5.23)$$

where W' and Z' are generalized Vandermonde matrices

$$W' = (W_{P-L}^T \quad Z_d W_{P-L}^T \quad Z_d^2 W_{P-L}^T \quad \dots \quad Z_d^{K-1} W_{P-L}^T), \quad (5.24)$$

$$Z' = (Z_{Q-K}^T \quad W_d Z_{Q-K}^T \quad W_d^2 Z_{Q-K}^T \quad \dots \quad W_d^{L-1} Z_{Q-K}^T). \quad (5.25)$$

W_d and Z_d are $M \times M$ diagonal matrices $W_d = \text{diag}\{e^{i\omega_0 x_k}\}$, $Z_d = \text{diag}\{e^{i\omega_0 y_k}\}$, while W_{P-L} and Z_{Q-K} are given by

$$W_{P-L} = \begin{pmatrix} 1 & 1 & 1 & \dots & 1 \\ w_1 & w_2 & w_3 & \dots & w_M \\ \vdots & & & & \\ w_1^{P-L-1} & w_2^{P-L-1} & w_3^{P-L-1} & \dots & w_M^{P-L-1} \end{pmatrix}, \quad (5.26)$$

$$Z_{Q-K} = \begin{pmatrix} 1 & z_1 & z_1^2 & \dots & z_1^{Q-K-1} \\ 1 & z_2 & z_2^2 & \dots & z_2^{Q-K-1} \\ \vdots & & & & \\ 1 & z_M & z_M^2 & \dots & z_M^{Q-K-1} \end{pmatrix}. \quad (5.27)$$

Define next a top-left matrix J_{tl} , obtained by omitting the last row and the last column of the block components of J , i.e. the top-left matrix J_{tl} has block components

$$J_{tl, kl} = \underline{G}^{(l,k)} = G_{l:P-L-2+l, k:Q-K-2+k}, \quad (5.28)$$

where $(\cdot)|$ denotes the operation of deleting the last column of (\cdot) , while $\underline{(\cdot)}$ denotes the operation of deleting the last row of (\cdot) . Define in a similar way top-right and bottom-left matrices J_{tr} and J_{bl} . The outline of the ACMP algorithm is then

- Compute the singular value decomposition of J_{tl} .

$$J_{tl} = USV^H \quad (5.29)$$

- Find C_{tr} , C_{tl} , C_{bl} and C_{br} from

$$U^H (J_{tr} - \mu J_{tl}) V = F(Z_d - \mu I) G = C_{tr} - \mu C_{tl}, \quad (5.30)$$

$$U^H (J_{bl} - \mu J_{tl}) V = F(W_d - \lambda I) G = C_{bl} - \lambda C_{tl}. \quad (5.31)$$

- Compute the eigenvalue decomposition of a matrix $C_{tl}^{-1}(\beta C_{tr} + (1 - \beta)C_{bl})$

$$C_{tl}^{-1}(\beta C_{tr} + (1 - \beta)C_{bl}) = G^{-1}TG, \quad (5.32)$$

where β is a scalar introduced with the aim of avoiding multiple eigenvalues.

- Apply the eigentransformation T to $C_{tl}^{-1}C_{tr}$ and $C_{tl}^{-1}C_{bl}$ to find Z_d and W_d , i.e.

$$T(C_{tl}^{-1}C_{bl})T^{-1} = W_d, \quad (5.33)$$

$$T(C_{tl}^{-1}C_{tr})T^{-1} = Z_d. \quad (5.34)$$

Since the same transformation is used to diagonalize both matrices, w_i and z_i correspond to the same sinusoidal component. A necessary condition for this property to hold is that all the matrices involved in the two matrix pencils, $J_{tr} - \mu J_{tl}$ and $J_{bl} - \lambda J_{tl}$, can be written as the product of the same left and right matrices, with possibly a different matrix in the middle. On the other hand, a sufficient condition for Y' and Z' to have the full rank M is

$$P - L \geq M \quad K, L \geq M \quad Q - K \geq M. \quad (5.35)$$

Equation (5.35) implies that if we set $L = K = M$, the sufficient condition for having a unique solution is $P \geq 2M$, $Q \geq 2M$. In other words, it suffices to know $G[m, n]$, $m, n \in [-M, M]$ ², therefore, only $\mathcal{O}(M^2)$ samples of $g(x, y)$ will yield a unique solution for the set of pairs (w_i, z_i) . Note that $G[m, n]$ do not necessarily have to correspond to the lowpass version of the signal and it is possible to obtain a perfect reconstruction from any subspace of the same dimension³.

Finally, the corresponding set of weights $\{a_i\}$ can be found from equation (5.23), i.e. $A = W'^+ J Z'^+$, where $(\cdot)^+$ denotes a pseudoinverse of (\cdot) . Since both W' and Z' are of rank M , the above system will have a unique solution for the matrix of coefficients A . This leads us to the following proposition.

Proposition 5.2: Consider a periodic set of M weighted 2-D Diracs $g(x, y)$, having periods $T_x = T_y = T$ in the x and y directions, and let $\varphi(x, y)$ be the 2-D sinc sampling kernel of bandwidth $[-M\omega_0, M\omega_0] \times [-M\omega_0, M\omega_0]$. If the sampling periods T_{sx} and T_{sy} are such that $N_{sx} = T/T_{sx} \geq 2M + 1$ and $N_{sy} = T/T_{sy} \geq 2M + 1$, where $\{N_{sx}, N_{sy}\} \in \mathbb{N}$, then in the general case, the samples

$$y_s[p, q] = \langle g(x, y), \varphi(x - pT_{sx}, y - qT_{sy}) \rangle, \quad p \in [0, N_{sx} - 1] \quad q \in [0, N_{sy} - 1],$$

are a sufficient characterization of $g(x, y)$.

In our analysis, we specifically considered the sinc sampling kernel because it allows for a straightforward computation of the Fourier series coefficients of the signal from the set of samples. However, we can use any bandlimited

²In our case $G[m, n]$ are the Fourier series coefficients of $g(x, y)$.

³While this is true for deterministic signals, in the presence of noise it is desirable to use oversampled schemes and estimate the signal parameters from a frequency band where SNR is highest.

kernel whose spectrum Φ is nonzero over the same region $[-M\omega_0, M\omega_0] \times [-M\omega_0, M\omega_0]$, assuming that the inverse of Φ over that frequency range exists and is numerically stable. That is, the only modification is that the Fourier series coefficients of the sampled signal have to be divided by the corresponding Fourier series coefficients of the sampling kernel before running the estimation algorithm. This allows us to use the same approach based on the shift-invariant subspace property together with a much wider class of anti-aliasing filters.

5.4 Extension to Lines and Polygons

The results we derived so far can be applied to a larger class of two-dimensional signals, such as simple lines, polygonal lines, as well as some simple 2-D objects. As we will see, the extensions are not straightforward and typically become more intricate as we increase the complexity of the model.

5.4.1 Line of finite length

Consider a periodic signal $g(x, y)$, represented within one period as

$$g(x, y) = \begin{cases} \delta(y - (ax + b)), & x_1 \leq x \leq x_2 \\ 0, & \text{otherwise} \end{cases} \quad (5.36)$$

The above notation assumes that the line is not vertical, otherwise a similar expression can be written by swapping x and y . The Fourier series coefficients of $g(x, y)$ are given by

$$\begin{aligned} G[m, n] &= \frac{1}{T^2} \int_0^T \int_0^T g(x, y) e^{-jm\omega_0 x} e^{-jn\omega_0 y} dx dy \\ &= \frac{1}{T^2} \int_{x=x_1}^{x=x_2} e^{-jm\omega_0 x} \left(\int_0^T \delta(y - (ax + b)) e^{-jn\omega_0 y} dy \right) dx \\ &= \frac{1}{T^2} \int_{x=x_1}^{x=x_2} e^{-jm\omega_0 x} e^{-jn\omega_0(ax+b)} dx \\ &= \frac{e^{-jm\omega_0 x_1} e^{-jn\omega_0 y_1} - e^{-jm\omega_0 x_2} e^{-jn\omega_0 y_2}}{j2\pi T^2(m + na)}. \end{aligned} \quad (5.37)$$

Clearly, $G[m, n]$ has no longer the form of a linear combination of complex exponentials, since both m and n appear in the denominator. Therefore, neither the annihilating filter method nor the subspace methods can be used directly with the set of the Fourier series coefficients. Yet, the problem can be handled in the following way. Consider the coefficients $G[m, 0]$

$$G[m, 0] = \frac{e^{-jm\omega_0 x_1} - e^{-jm\omega_0 x_2}}{j2\pi T^2 m}, \quad (5.38)$$

and define $\tilde{G}[m] = j2\pi T^2 m G[m, 0] = e^{-jm\omega_0 x_1} - e^{-jm\omega_0 x_2}$. Since $x_1 \neq x_2$ ⁴, we can solve for the set $\{x_1, x_2\}$ by using the 1-D annihilating filter $H(z)$ with zeros $z_1 = e^{-j\omega_0 x_1}$ and $z_2 = e^{-j\omega_0 x_2}$. The filter coefficients $H[m] = \text{coeff}(H(z))$

⁴We assumed that the line is not vertical, otherwise we have to consider the coefficients $G[0, n]$

can be found from the system of equations $H[m] * \tilde{G}[m] = 0$, $m \in [-2, 2]$. Next, consider the coefficients $G[m, 1]$

$$G[m, 1] = \frac{e^{-jm\omega_0 x_1} e^{-j\omega_0 y_1} - e^{-jm\omega_0 x_2} e^{-j\omega_0 y_2}}{j2\pi T^2(m+a)}. \quad (5.39)$$

There are three unknowns y_1 , y_2 and a , that can be found from $G[m, 1]$, $m \in [-2, 2]$. Along with the set $\{x_1, x_2\}$, this uniquely defines the line.

5.4.2 Polygonal line

A straightforward extension of the previous result is the case of a 2-D signal $g(x, y)$ made up of a periodic pattern of a polygonal line, that is, a closed curve made up of a finite number of linear pieces. Let the vertices be located at points (x_i, y_i) , $i = 1, 2, \dots, M$. Since we can think of $g(x, y)$ as being composed of M lines, the Fourier series coefficients $G[m, n]$ can be found using equation (5.37),

$$\begin{aligned} G[m, n] = & \frac{e^{-jm\omega_0 x_1} e^{-jn\omega_0 y_1}}{j2\pi T^2} \left[\frac{1}{m+na_1} - \frac{1}{m+na_M} \right] + \\ & + \frac{e^{-jm\omega_0 x_2} e^{-jn\omega_0 y_2}}{j2\pi T^2} \left[\frac{1}{m+na_2} - \frac{1}{m+na_1} \right] + \dots \\ & + \frac{e^{-jm\omega_0 x_M} e^{-jn\omega_0 y_M}}{j2\pi T^2} \left[\frac{1}{m+na_M} - \frac{1}{m+na_{M-1}} \right] \end{aligned}$$

The above relation holds if there are no vertical segments in the signal and is obtained after grouping the terms with the same denominator. Consider the set of coefficients $G[0, n]$, $n \in [-M, M]$:

$$\begin{aligned} G[0, n] = & \frac{e^{-jn\omega_0 y_1}}{j2\pi T^2} \left[\frac{1}{na_1} - \frac{1}{na_M} \right] + \frac{e^{-jn\omega_0 y_2}}{j2\pi T^2} \left[\frac{1}{na_2} - \frac{1}{na_1} \right] + \dots \\ & \dots + \frac{e^{-jn\omega_0 y_M}}{j2\pi T^2} \left[\frac{1}{na_M} - \frac{1}{na_{M-1}} \right]. \end{aligned} \quad (5.40)$$

Let $\tilde{G}[n] = j2\pi T^2 n G[0, n]$:

$$\tilde{G}[n] = \sum_{k=1}^N c_k e^{-j\omega_0 n y_k} \quad n \in \mathbb{Z}, \quad (5.41)$$

where $c_k = 1/a_k - 1/a_{k-1}$. Since $\tilde{G}[n]$ has the form of a weighted sum of complex exponentials, the sets $\{y_i\}$ and $\{c_i\}$ can be found from the coefficients $\tilde{G}[n]$, $n \in [-M, M]$ using the annihilating filter method. In order to obtain a unique solution, two conditions need to be satisfied. Namely, all y_i must be different and none of the coefficients c_i should be equal to zero. The second condition is always satisfied, given the fact that the adjacent segments of the polygonal line must have different slopes (a_{k-1} and a_k). On the other hand, the first condition poses further constraints on the location of the vertices.

Next, consider a set of coefficients $G[1, n]$ $n \in [-M, M]$, given by

$$\begin{aligned} G[1, n] = & \frac{e^{-j\omega_0 x_1} e^{-jn\omega_0 y_1}}{j2\pi T^2} \left[\frac{1}{1+na_1} - \frac{1}{1+na_M} \right] + \dots \\ & \dots + \frac{e^{-j\omega_0 x_M} e^{-jn\omega_0 y_M}}{j2\pi T^2} \left[\frac{1}{1+na_M} - \frac{1}{1+na_{N-1}} \right]. \end{aligned} \quad (5.42)$$

This is a system of $2M$ nonlinear equations with $2M$ unknowns that can be solved for $z_i = e^{-j\omega_0 x_i}$ and a_i . Together with the corresponding values y_i , this uniquely defines the polygonal line.

While all the signal parameters can be extracted from the above set of samples, the described method includes solving the system of nonlinear equations (5.42), which may yield a mediocre numerical precision and high complexity. One possible way to overcome this problem is to solve separately for the x and the y coordinates of vertices, and then use a combinatorial approach, that is, find a set of pairs (x_i, y_i) that best matches the lowpass approximation obtained from the samples. Although this solution requires twice the number of samples compared to the previous method and involves an optimization procedure as well, its numerical precision is typically much better. Clearly, both methods yield a solution by taking $\mathcal{O}(M)$ samples, however, the necessary condition for their success is that the vertices of the polygonal line have no common components along the x and y directions.

5.4.3 Bilevel 2-D signals

A further extension of the previous results includes the case of a bilevel signal $g(x, y)$ made up of a periodic pattern of polygons. As in the previous case, assume that $g(x, y)$ doesn't contain vertical lines. Under this assumption, we can take a partial derivative with respect to y and by denoting $g_y(x, y) = \frac{\partial g(x, y)}{\partial y}$, we get

$$\begin{aligned} \frac{\partial g(x, y)}{\partial y} &= \sum_{m=-\infty}^{\infty} \sum_{n=-\infty}^{\infty} G[m, n] j n \omega_0 e^{j m \omega_0 x} e^{j n \omega_0 y} \\ &= \sum_{m=-\infty}^{\infty} \sum_{n=-\infty}^{\infty} G_y[m, n] e^{j m \omega_0 x} e^{j n \omega_0 y}. \end{aligned} \quad (5.43)$$

Since $g_y(x, y)$ is a signal made up of a polygonal line, its Fourier series coefficients are given by

$$G_y[m, n] = j \omega_0 n G[m, n]. \quad (5.44)$$

Therefore, instead of taking a derivative of the signal itself, the derivation can be done on the Fourier series coefficients and the values $G_y[m, n]$ should be used in the algorithm developed in Section 5.2.

5.5 Numerical Performance and Algorithms in the Presence of Noise

So far we have assumed deterministic signals and considered the possibility of developing the sampling schemes that allow for perfect reconstruction from as few samples as possible. Questions that naturally arise from this approach are related to numerical precision and stability of the developed algorithms as well as to their performance in the presence of noise.

5.5.1 Complexity

In Section 5.1.1, we proved that in the noiseless, separable case, the annihilating filter algorithm leads to perfect reconstruction from only $\mathcal{O}(M)$ samples. However, in the presence of noise, this approach has several disadvantages. Namely, the annihilating filter method is basically a 1-D approach, that is, the coordinates of Diracs along one direction are estimated by finding the roots of the annihilating filter, while the corresponding coordinates along the other direction are then found by solving a Vandermonde system (i.e., the information is extracted from a set of weighting coefficients). In general, the root finding part of the algorithm is more robust to noise than the estimation of the weighting coefficients, which then results in a different numerical precision in the x and y directions. Besides, even in the case of noiseless data, the numerical accuracy of the method decreases if there are closely spaced Diracs in the set (particularly for large values of M), due to the root finding part of the algorithm. The approach based on 2-D subspace methods exploits the shift-invariance property and relies only on a right deployment of matrix manipulations. It avoids the problem of different precision in x and y and typically yields better performances, yet, at the expense of a higher computational complexity. The major computational requirement of the annihilating filter method is associated to the root finding part of the algorithm, so that the overall computational order is $\mathcal{O}(M^2 \log M)$. The computational requirement of the ACMP algorithm is dominated by the singular value decomposition of the $M^2 \times M^2$ matrix J_{tl} , which results in the overall order of $\mathcal{O}(M^6)$.

5.5.2 Noisy case

In the case of noisy signals, critically sampled schemes typically result in poor numerical accuracy. In practice, this problem can be dealt with by using oversampling and truncation of the singular value decomposition (SVD) of certain matrices. For example, we can exploit this idea to modify the ACMP algorithm presented in Section 5.2. Since the presence of noise destroys the low rank property of the matrix J_{tl} , defined in (5.28), we have to truncate the singular value decomposition of J_{tl} explicitly to rank M , i.e.

$$J_{tl} = U_s S_s V_s^H + U_n S_n V_n^H, \quad (5.45)$$

with S_s being a full-rank $M \times M$ matrix. The presence of noise thus necessarily degrades the performance of the algorithm, due to the fact that the eigentransformation T will no longer perfectly diagonalize both matrix pencils.

The same approach can be used to modify the annihilating filter method, that is, we should consider an extended system of equations (5.13)

$$\sum_{i=1}^M h_i G[m-i, 1] = -G[m, 1], \quad m = 1, 2, \dots, M_1 \quad M_1 > M, \quad (5.46)$$

and decompose a matrix of coefficients \mathbf{G} as

$$\mathbf{G} = \begin{pmatrix} G[0, 1] & G[-1, 1] & \cdots & G[1-M, 1] \\ G[1, 1] & G[0, 1] & \cdots & G[2-M, 1] \\ \vdots & \vdots & \ddots & \\ G[M_1-1, 1] & G[M_1-2, 1] & \cdots & G[M_1-M, 1] \end{pmatrix}$$

$$= U_s S_s V_s^H + U_n S_n V_n^H, \quad (5.47)$$

where the first term corresponds to the best (in the Frobenius-norm sense) rank M approximation of the matrix \mathbf{G} . The filter coefficients H are then computed as

$$H = -V_s S_s^{-1} U_s^H \cdot \begin{pmatrix} G[1, 1] \\ G[2, 1] \\ \vdots \\ G[M_1, 1] \end{pmatrix}. \quad (5.48)$$

5.5.3 Estimation of the model order and model mismatch

In all the methods presented so far, we required prior knowledge of the model order M . Therefore, an obvious question is how can one know in advance the number of unknown parameters of the signal? This question is at the core of a model-based approach to nonlinear estimation problems encountered in signal and data analysis [26] [39]. For example, if we use the ACMP algorithm, M can be estimated as the number of dominant singular values of J_{tl} , which is a very good estimate of the model order if the smallest singular value of the original, low-rank matrix J_{tl} , is not dominated by the noise variance. On the other hand, for low values of signal-to-noise ratio, it is often difficult to discriminate between small singular values corresponding to the signal from extraneous ones due to noise and, typically, only dominant signal components can be reliably estimated. That is, in such a case, overmodeling the signal can give rise to spurious poles which can be incorrectly identified as signal poles. Similarly, if the annihilating filter algorithm is used, the number of dominant singular vectors of the extended matrix \mathbf{G} (assuming that the number of columns is greater than M) should be used as an estimate of the model order. A more detailed treatment of this problem can be found in [26].

Another interesting question is how well we can reconstruct the signal if the number of samples is less than the minimum number theoretically required for perfect reconstruction? Intuitively, if the signal has only $K < M$ dominant components, one might expect to extract only these components from the undersampled signal, provided that the number of samples is still sufficient for that. This turns out to be true, as we will demonstrate in the next section, which points to some robustness of the algorithms to model mismatch.

5.6 Simulation Results

We illustrate the performance of the proposed sampling schemes with some simulation examples. A noiseless periodic signal made up of $M = 9$ weighted Diracs, that have common components along the y direction but not along the x direction, is presented in Figure 5.2(a). The signal is filtered with the sinc sampling kernel of bandwidth $[-M\omega_0, M\omega_0] \times [-\omega_0, \omega_0]$, shown in Figure 5.2(b), leading to the lowpass approximation in Figure 5.2(c). All the signal parameters are estimated using the annihilating filter method, and the reconstructed signal is illustrated in Figure 5.2(d). The algorithm provides almost perfect reconstruction in this case, with an RMSE of less than 10^{-12} .

Figure 5.3(a) illustrates a noiseless signal consisting of $M = 9$ weighted Diracs that have common components in both directions. Since the annihilating

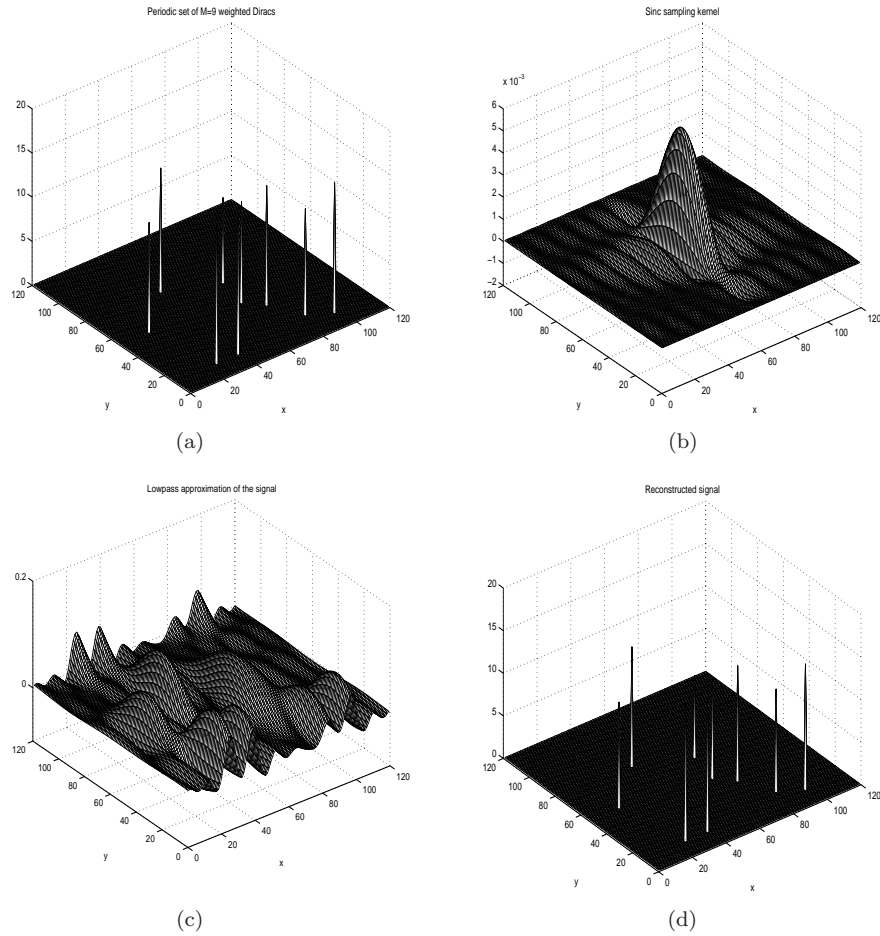


Figure 5.2: The Annihilating Filter Method. (a) Two-dimensional signal made up of $M = 9$ weighted Diracs (b) 2-D sinc sampling kernel of bandwidth $[-M\omega_0, M\omega_0] \times [-\omega_0, \omega_0]$ (c) Lowpass approximation obtained by convolving the signal with the sinc function (d) Reconstructed signal.

filter method would fail in this case, we will use the ACMP algorithm to recover the signal from its lowpass approximation. The signal is sampled with the sinc sampling kernel, shown in Figure 5.3(b), and reconstructed with an RMSE of less than 10^{-13} . However, as opposed to the annihilating filter method, the numerical precision of this algorithm is not considerably affected by the spacing of Diracs in the set. This is shown in Figure 5.4, where a reconstruction error is plotted as a function of average spacing D of the Diracs in the set. Clearly, for small values of D , the performance of the annihilating filter method degrades as the number of Diracs increases, while the ACMP method retains good numerical properties even for large values of M .

We next analyze robustness of the algorithms to model mismatch, in particular, how well they perform if the signal is undersampled. Figure 5.5(a) shows a signal made up of $M = 8$ weighted Diracs, with $K = 5$ of them being dominant. The locations of the Diracs are randomly chosen according to a uniform

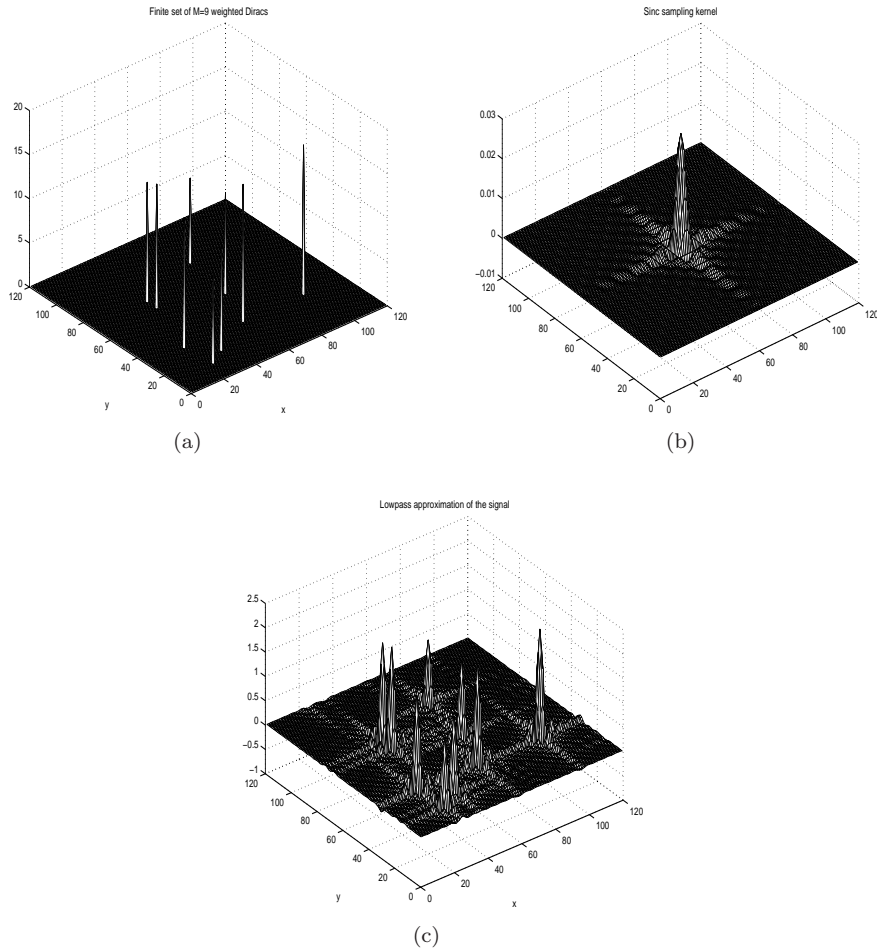


Figure 5.3: The ACMP algorithm. (a) Signal made up of $M = 9$ weighted Diracs that have common components along both directions (b) Sinc sampling kernel of bandwidth $[-M\omega_0, M\omega_0] \times [-M\omega_0, M\omega_0]$ used in the algorithm (c) Lowpass approximation of the signal.

distribution over $[1, 150] \times [1, 150]$. The signal is sampled with the sinc kernel of bandwidth $[-K\omega_0, K\omega_0] \times [-K\omega_0, K\omega_0]$ and the ACMP method is used to find the signal parameters from its lowpass approximation. In Figure 5.5(b) we show a reconstructed signal where only the dominant components have been extracted, while the precision with which we can estimate them depends on the number of non-dominant components and their overall power, as illustrated in Figure 5.5(c).

Figure 5.6 shows the behavior of the ACMP algorithm in the presence of noise. We considered the signal made up of 8 Diracs, this time having equal weights, embedded in additive white Gaussian noise. The method was tested for different values of a signal-to-noise ratio (SNR) and different values of the sampling kernel bandwidth B_s . For each value of the SNR, as well as B_s , we plotted an average RMSE over 50 different realizations of the signal. The results clearly indicate that the numerical precision of the method is improved

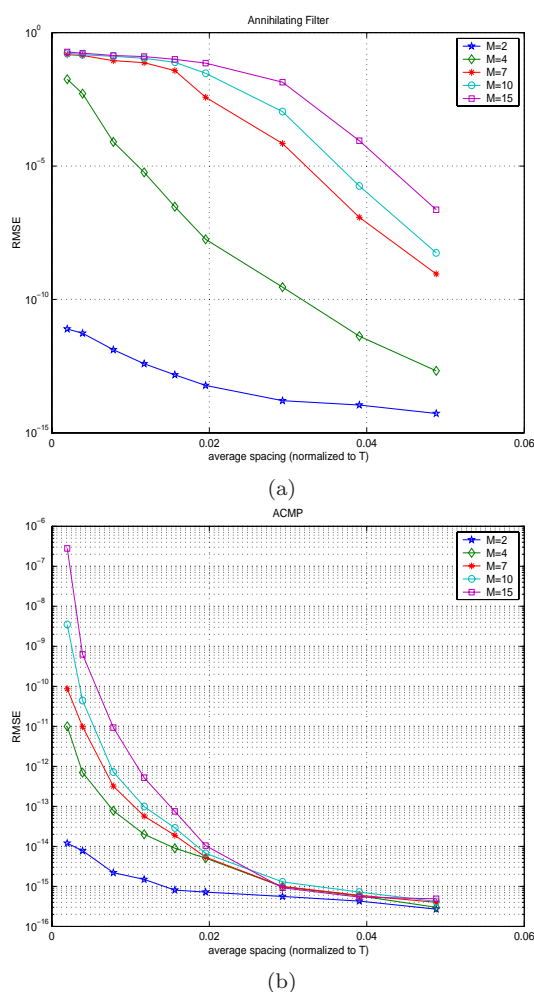


Figure 5.4: Numerical Performance vs. Average Spacing of the Diracs. The numerical behavior of the algorithms is tested for different values of the average spacing (normalized to one period) of M Diracs in the set, as well as for different values of M . (a) Average reconstruction error for the annihilating filter algorithm (b) Average reconstruction error for the ACMP algorithm.

by increasing the bandwidth of the sampling kernel and estimating the signal parameters from a larger set of samples. Roughly speaking, in order to reduce the RMSE by a factor of K_s , the bandwidth of the sampling kernel has to be increased K_s times.

Some extensions of the developed sampling schemes to simple objects are considered next. One example is presented in Figure 5.7, which demonstrates the performance of the algorithm when applied to a set of two finite lines. The signal is filtered with the sinc kernel of bandwidth $[-4\omega_0, 4\omega_0] \times [-\omega_0, \omega_0]$, leading to a lowpass approximation shown in Figure 5.7(b). A set of lines is almost perfectly reconstructed by using the annihilating filter method (see Figure 5.7(c)). Another example is illustrated in Figure 5.8(a), that is, sampling

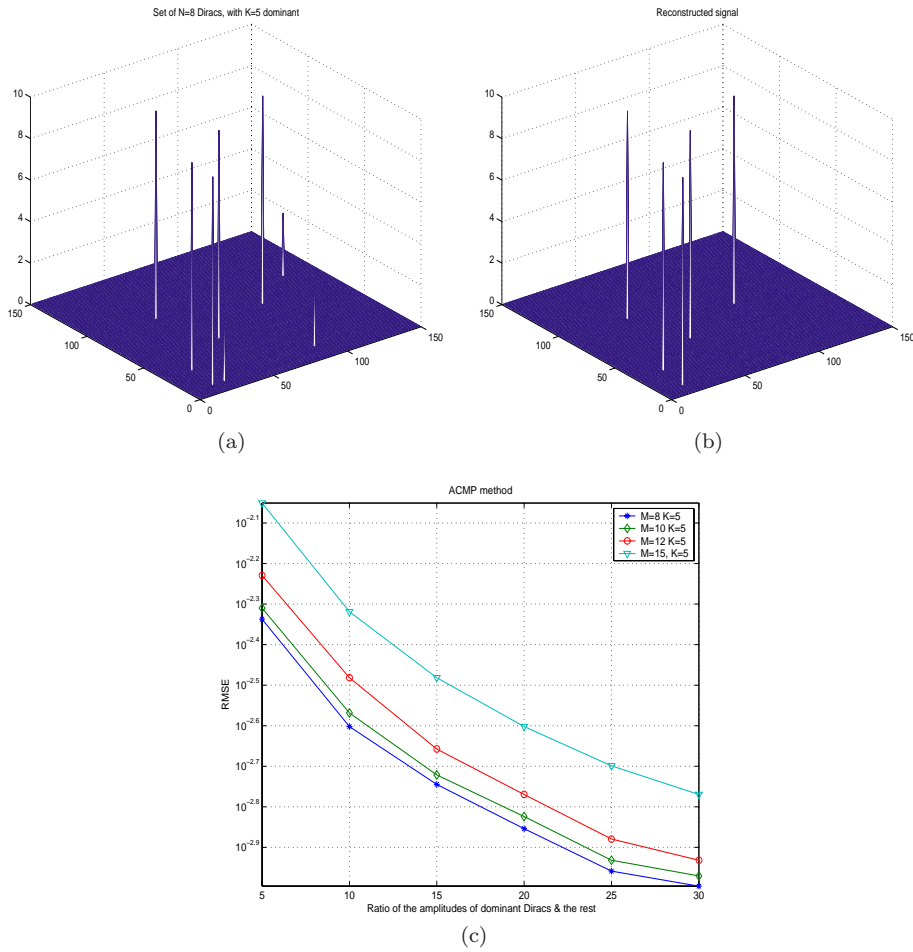
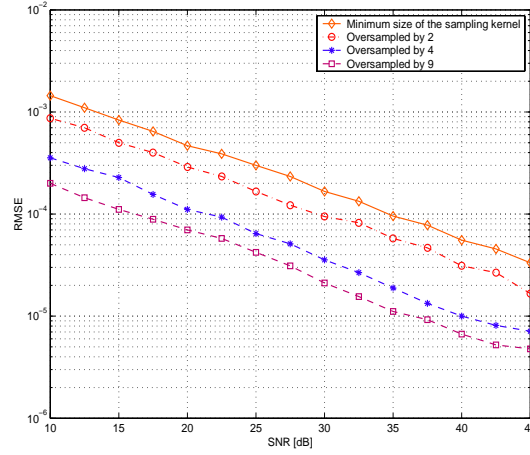


Figure 5.5: Model mismatch (a) Set of $M = 8$ weighted Diracs with $K = 5$ Diracs being dominant, all having the same weights $a_n = 10$, while the rest have weights $a_n = 3$. (b) Reconstructed signal. We assumed that the model order is $M = 5$ and used the ACMP algorithm to reconstruct the signal. Only the dominant components are extracted, with the reconstruction error of $RMSE=0.006$. (c) Average reconstruction error for different values of the ratio of amplitudes $\frac{A_{\text{dominant}}}{A_{\text{non-dominant}}}$ as well as for different number of non-dominant components in the set for the ACMP method

a bilevel pentagon. The signal is first filtered with a sinc kernel of bandwidth $[-2M\omega_0, 2M\omega_0] \times [-\omega_0, \omega_0]$ (where $M = 5$), and a set of samples is taken from a lowpass approximation shown in Figure 5.8(b). Although the signal is completely specified by this set of samples, we extracted only the x coordinates of vertices from the given set, while the y coordinates are found from sample values taken with the sinc kernel of bandwidth $[-\omega_0, \omega_0] \times [-2M\omega_0, 2M\omega_0]$. The reason for doing this is to avoid solving the system of nonlinear equations (5.42), which typically results in less numerical precision than the above approach. The corresponding pairs (x_i, y_i) are then found by using a combinatorial method, that is, by choosing a set that corresponds to a signal with a lowpass version that best matches the lowpass approximation from Figure 5.8(b). Figure 5.8(c)



(b)

Figure 5.6: Performance in the presence of noise. *RMSE versus SNR for different values of the oversampling factor. We consider the signal made up of 8 Diracs with equal weights. The method was tested for different values of SNR and different values of the bandwidth of the sampling kernel B_s .*

shows the polygonal line reconstructed using the annihilating filter method, whereas in Figure 5.8(d) a 1-D subspace method (the state space approach from Chapter 2) is applied, which clearly performs better.

5.7 Conclusion

We have presented several algorithms for sampling certain classes of 2-D signals that are not bandlimited, but have a finite number of degrees of freedom. Our approach differs from standard multidimensional sampling schemes, since we tried to develop methods that can perfectly reconstruct such signals from a finite set of samples. We analyzed in detail the signal made up of 2-D Diracs, whose algebraic structure gives a good insight into the basic principles inherent in all our algorithms, and discussed possible extensions of the results to more complex classes of signals. In order to derive exact sampling formulas, we used some techniques already encountered in the context of spectral estimation. Although the sampling results were derived under the noise-free assumption, the case of noisy data was considered as well. The methods have desirable numerical properties, for a good choice of parameters and sufficient oversampling. We are currently looking into one application to super-resolution videogrammetry, where the position of 3-D objects can be determined with sub-pixel precision by locating some clearly marked features, such as points or edges, using a set of 2-D images taken from various angles [14]. In the next chapter, we will investigate alternative sampling techniques, such as Radon transform sampling, which are applicable to more general classes of signals.

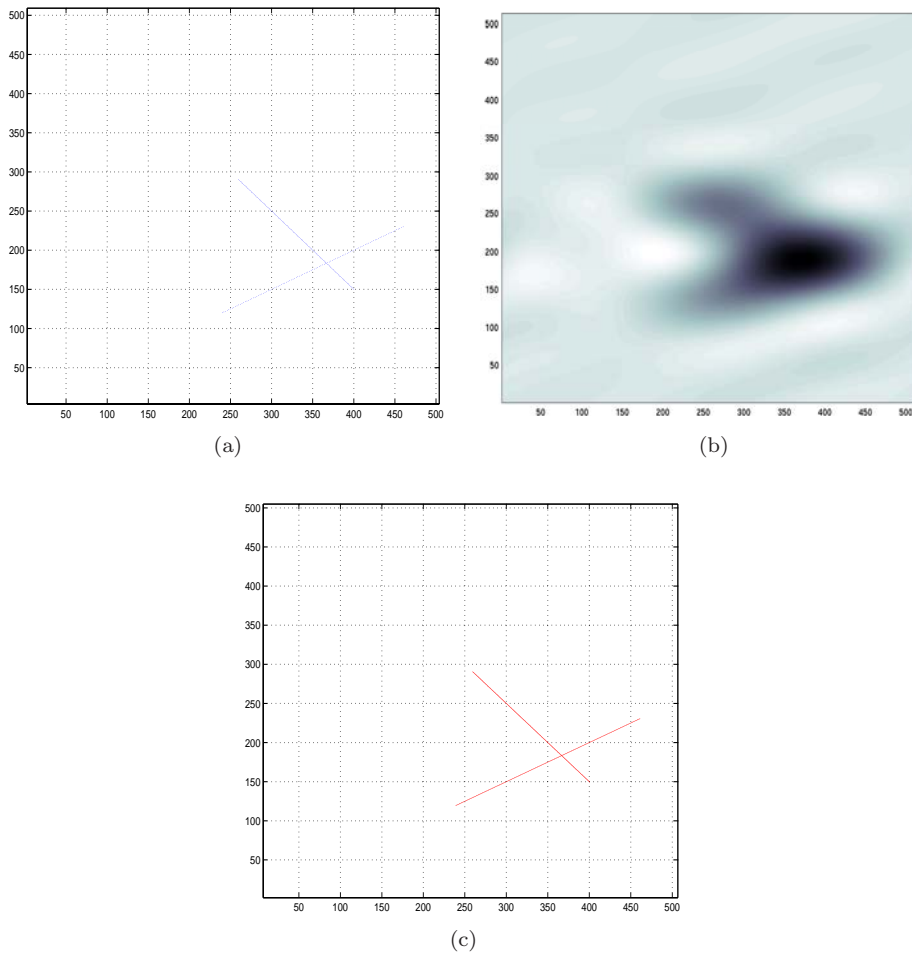


Figure 5.7: Set of Finite Lines. (a) Signal made up of two finite lines (b) Lowpass approximation obtained by convolving the signal with the sinc kernel of bandwidth $[-4\omega_0, 4\omega_0] \times [-\omega_0, \omega_0]$ (c) Reconstructed set of lines.

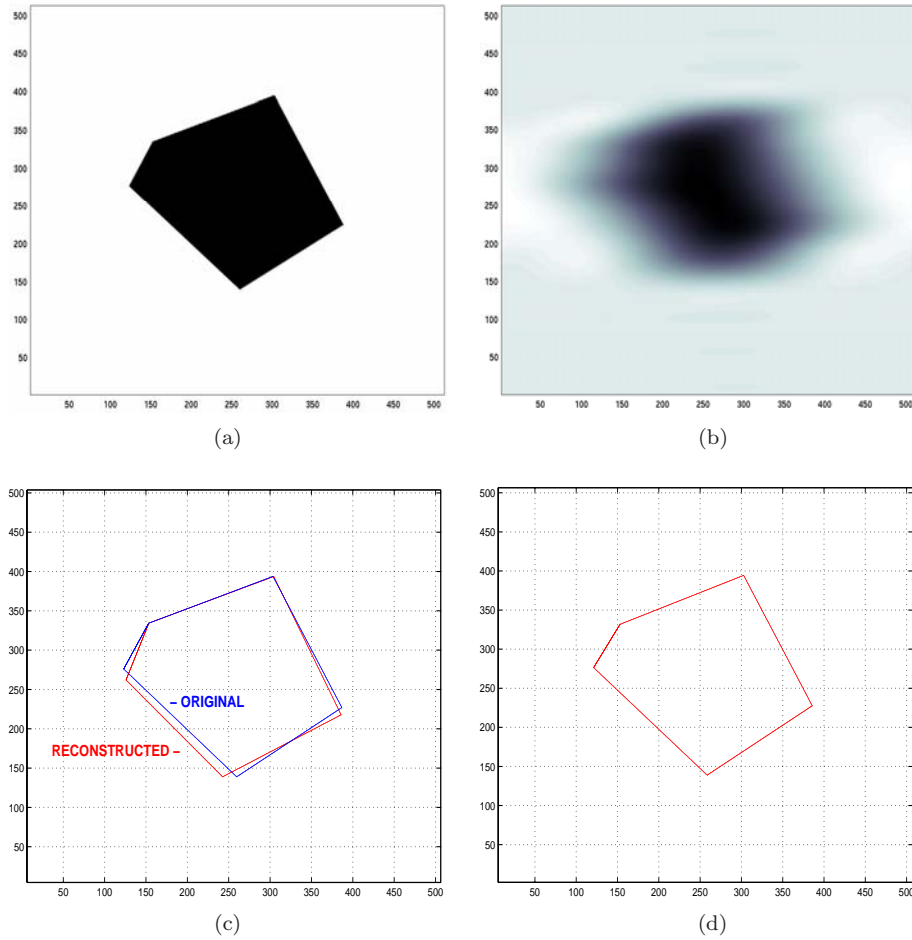


Figure 5.8: Bilevel Polygon. (a) *Bilevel pentagon. The signal has $2M = 10$ degrees of freedom* (b) *Lowpass approximation obtained by convolving the signal with the sinc kernel of bandwidth $[-2M\omega_0, 2M\omega_0] \times [-\omega_0, \omega_0]$* (c) *Polygonal line reconstructed with the annihilating filter method and the original polygonal line.* (d) *Polygonal line reconstructed with the state space method. In this case the line is reconstructed with an RMSE of less than 10^{-4} .*

Chapter 6

Extension to Aperiodic and Radon Transform Case

In the previous chapter, we have considered the problem of sampling periodic non-bandlimited signals of *finite complexity*, that is, 2-D signals that have a parametric representation with a finite number of degrees of freedom. We have first analyzed a periodic set of M weighted Diracs and proved that in the absence of noise, such a signal can be perfectly reconstructed from $\mathcal{O}(M)$ samples in the separable case, or $\mathcal{O}(M^2)$ samples if the problem is non-separable. However, we have seen that extending the results to more complex classes of signals is far from trivial. For example, even for the very simple case of a bilevel polygon, the problem of reconstructing such a signal from a set of its Fourier series coefficients becomes quite involved. Furthermore, the Fourier analysis can be formally used only in the case of periodic signals. Therefore, an important and challenging question is whether it is possible to come up with practical methods for sampling aperiodic 2-D signals with a finite complexity, which yield perfect reconstruction from a finite set of samples.

In this chapter, we consider the problem of developing sampling schemes and reconstruction formulas for certain classes of such signals, such as sets of 2-D Diracs, polygons and bilevel signals with piecewise polynomial boundaries. We first develop a sampling scheme based on a Gaussian kernel, and point to potentials and limitations of such an approach. We then investigate an alternative approach, based on sampling the Radon transform of such signals. In particular, we show that by taking a finite number of “filtered” line integrals, the problem can be reduced to its one-dimensional equivalent, which is more convenient for algorithmic implementation.

The outline of the chapter is as follows. In Section 6.1, we consider the case of a finite set of Diracs, and derive sampling theorems using a Gaussian kernel. In Section 6.2, we focus on the problem of reconstructing the signal from a finite number of samples of its Radon transform. That is, we analyze a set of M 2-D Diracs and prove that the signal can be uniquely reconstructed by taking at least $2M$ samples along $M + 1$ distinct directions. In Section 6.3, we extend the result to more complex classes of signals, such as bilevel polygons, or bilevel signals with piecewise polynomial boundaries. Finally, in Section 6.4, we conclude with a summary of the key results.

6.1 Gaussian Sampling Scheme

The sampling results for a set of 2-D Diracs, presented in the previous chapter, have been derived under the assumption that the signal is modeled as a periodic pattern of Diracs, so that the relevant parameters can be extracted from the appropriate set of the Fourier series coefficients. In this section, we analyze the problem of sampling two-dimensional signals made up of a finite number of weighted Diracs.

Let a signal $g(x, y)$ be given by

$$g(x, y) = \sum_{i=0}^{M-1} a_i \delta(x - x_i, y - y_i). \quad (6.1)$$

Consider the samples obtained by filtering the signal with the Gaussian kernel, $\varphi_g(x, y) = e^{-(x^2+y^2)/2\sigma^2}$, taken at (mT, nT)

$$\begin{aligned} g[m, n] &= \sum_{i=0}^{M-1} a_i e^{-((x_i-mT)^2+(y_i-nT)^2)/2\sigma^2} \\ &= \sum_{i=0}^{M-1} a_i e^{-(x_i^2+y_i^2)/2\sigma^2} e^{(mx_i+ny_i)/\sigma^2} e^{-(m^2+n^2)T^2/2\sigma^2} \end{aligned} \quad (6.2)$$

Extending a technique from Section 3.3, denote by $\tilde{g}[m, n] = g[m, n]e^{(m^2+n^2)T^2/2\sigma^2}$ and $c_i = a_i e^{-(x_i^2+y_i^2)/2\sigma^2}$. Then, (6.2) reduces to:

$$\tilde{g}[m, n] = \sum_{i=0}^{M-1} c_i e^{mx_i/\sigma^2} e^{ny_i/\sigma^2}. \quad (6.3)$$

The set of modified samples $\tilde{g}[m, n]$ can be thus expressed as a linear combination of real exponentials. Therefore, in order to determine a_i and (x_i, y_i) in the general, non-separable case, one can use the ACMP method described in the previous chapter. Thus, we have the following proposition:

Proposition 6.1: Consider a finite set of M weighted 2-D Diracs $g(x, y)$, and let $\varphi_g(x, y)$ be the Gaussian sampling kernel $\varphi_g(x, y) = e^{-(x^2+y^2)/2\sigma^2}$. If $N_{sx} \geq 2M + 1$ and $N_{sy} \geq 2M + 1$, then the $N_{sx}N_{sy}$ sample values

$$y_s[p, q] = \langle g(x, y), \varphi_g(x - pT, y - qT) \rangle, \quad p \in [0, N_{sx} - 1] \quad q \in [0, N_{sy} - 1]$$

are sufficient to reconstruct the signal.

In Figure 6.1(a), we illustrate a noiseless signal made up of $M = 17$ weighted Diracs. The signal is filtered with the Gaussian kernel shown in Figure 6.1(b), and a set of uniform samples is taken from a filtered version shown in Figure 6.1(c). The reconstructed signal is presented in Figure 6.1(d), and the reconstruction error is less than 10^{-8} . As already discussed in Chapter 2, the width of the Gaussian kernel (i.e. the value of the parameter σ) must be chosen carefully in order to ensure the good numerical performance of the method, as illustrated is Figure 6.2.

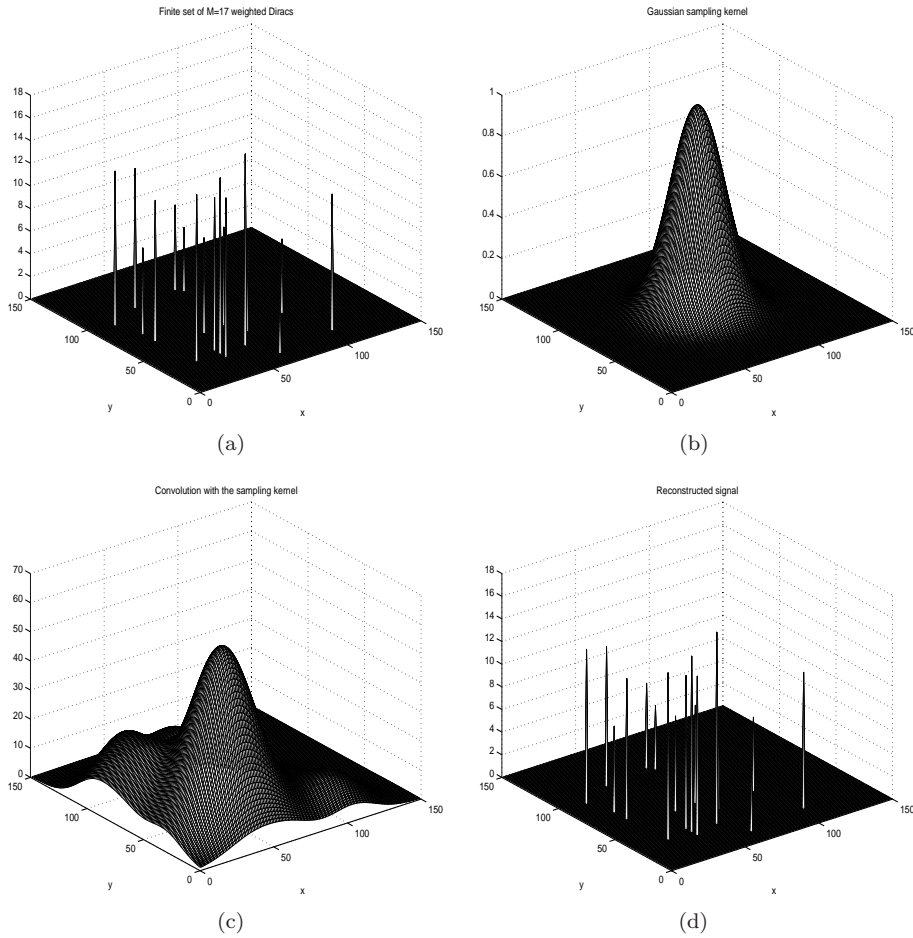


Figure 6.1: Finite Set of 2-D Diracs. (a) Two-dimensional signal made up of $M = 17$ weighted Diracs (b) Gaussian sampling kernel (c) Convolution of the signal with the sampling kernel (d) Reconstructed signal with an RMSE of less than 10^{-8} .

6.1.1 Point spread function

The previous result can be directly extended to the case of signals modeled as a “blurred” version of the set of Diracs, or more precisely, as a convolution of the signal $g(x, y)$ with a point spread function (PSF). This case is of interest to the field of optical astronomy, where the image formation, without noise, can be modeled as a convolution of the object being made up of point sources (i.e. stars) with the PSF, which may be a result of the imperfections of imaging optics, atmospheric processes etc.

There is no exact expression describing the shape of the PSF, however, many authors [56] [68] prefer to model the blurring process due to the atmospheric turbulence by a Gaussian function of the form:

$$h(x, y) \propto e^{-\frac{(x^2+y^2)}{2\sigma_s^2}}, \quad (6.4)$$

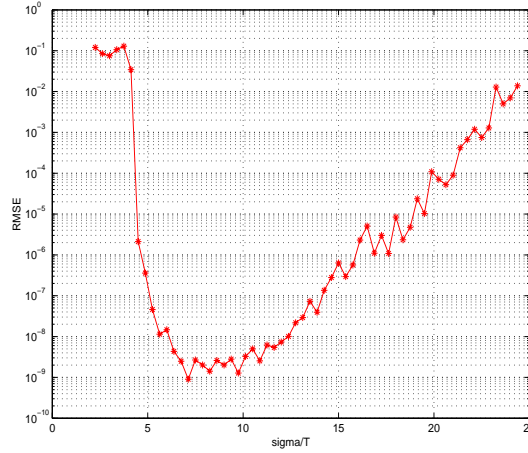


Figure 6.2: Numerical Precision vs. Width of the Gaussian Kernel. The signal from Figure 6.1(a) is sampled with the Gaussian kernel $e^{-\frac{x^2+y^2}{2\sigma^2}}$. The parameter σ is varied between $0.03T$ and $25T$, where T denotes the spacing between adjacent samples. The reconstruction error is plotted as a function of $\frac{\sigma}{T}$, indicating a strong sensitivity to the choice of the width σ .

or, equivalently, in the frequency domain as

$$H(f_x, f_y) \propto e^{-\pi^2(f_x^2 + f_y^2)2\sigma_s^2}, \quad (6.5)$$

which turns out to be a good approximation in the case of aberration-free imaging optics.

Following the approach from the previous section, the blurred version of the set of Diracs $g(x, y) * h(x, y)$ is convolved with the Gaussian kernel $\varphi_g(x, y) = e^{-(x^2+y^2)/2\sigma^2}$ prior to sampling. Due to the associativity of the convolution operator, this is equivalent to convolving the set of Diracs $g(x, y)$ with a Gaussian kernel of different width¹, that is,

$$\varphi_g^{(s)}(x, y) = e^{-\frac{(x^2+y^2)}{2(\sigma^2+\sigma_s^2)}}.$$

As a result, a set of samples can be expressed as a linear combination of 2-D exponentials, which was studied in the previous section. Note that since σ_s is supposed to be known (or can be estimated prior to sampling the signal), the only difference compared to the previous case is that the “effective” width of the sampling kernel is given by $(\sigma^2 + \sigma_s^2)^{1/2}$. This is illustrated in Figure 6.3, where we show the case of a noiseless signal made up of $K = 17$ Diracs, convolved with a Gaussian PSF (Figure 6.3(a)), and critically sampled. The signal is filtered with a Gaussian kernel, shown in Figure 6.1(b). The reconstructed set of Diracs is shown in Figure 6.3(b), where the RMSE of reconstruction is less than 10^{-7} .

6.1.2 Noisy case

Similarly to the 1-D case, the sampling scheme based on a Gaussian kernel can be ill-conditioned in the presence of noise, due to the weighting of signal samples

¹The analytic expression for the new kernel can be obtained in the frequency domain, by multiplying Fourier transforms of $\varphi_g(x, y)$ and $h(x, y)$.

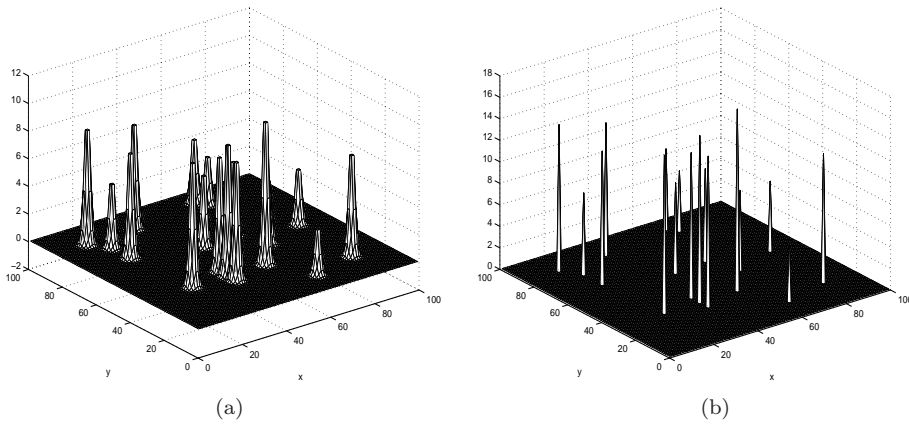


Figure 6.3: Point spread function. (a) *Two-dimensional signal made up of $M = 17$ weighted Diracs, convolved with a Gaussian PSF.* (d) *Reconstructed signal with an RMSE of less than 10^{-7} .*

with exponentially increasing terms. In order to improve the conditioning of the system, one can use the technique discussed in Chapter 3, where a data matrix is properly weighted prior to estimating the signal parameters, as described in Section 3.3.1. The performance of such a method in the two-dimensional case is illustrated in Figure 6.4, where we show the RMSE of location estimates versus SNR, and this for a local reconstruction method (i.e., the size of a sampling window is comparable to the width of the sampling kernel). In particular, we consider the signal made up of $K = 5$ Diracs with equal weights, randomly distributed over $[1, 50] \times [1, 50]$, yet assuming that their average spacing (in both the x and the y direction) is $T_s = 8$. The signal is sampled with a 2-D Gaussian kernel with parameter $\sigma = 5$, and the method was tested for different values of the oversampling factor. As expected, by increasing the sampling density, RMSE decreases, however, by comparing the RMSE obtained in this case with an RMSE obtained in the case of periodic signals (shown in Figure 5.6), we can see that the Gaussian scheme is less robust to noise. Furthermore, as already discussed in the 1-D case, the width of the kernel must be chosen carefully, otherwise, the performance of the method can degrade significantly.

Still, one of the main problems associated with the Gaussian scheme is that it cannot be directly extended to more complex classes of 2-D signals. Namely, unlike in the case of periodic signals, where it was possible to generalize the result on 2-D Diracs to signals such as sets of lines and polygons, in the case of finite-length signals, similar approach cannot be used. In particular, even though in the finite-length case the samples can be expressed as a sum of weighted exponentials as well, the weights c_i depend on the x and y coordinates of the Diracs. That is, $c_i = a_i e^{-(x_i^2 + y_i^2)/2\sigma^2}$ (see (6.3)), and it is no longer possible to extend the result to other classes of signals using the approach from Section 5.4.

In the rest of the chapter, we will consider an alternative approach to sampling aperiodic 2-D signals of finite complexity, which exploits the properties of the signal in the Radon transform domain [9] [18]. The concept we present offers the possibility of decomposing the problem into a set of 1-D equivalents, which is more convenient for algorithmic implementation and can be extended

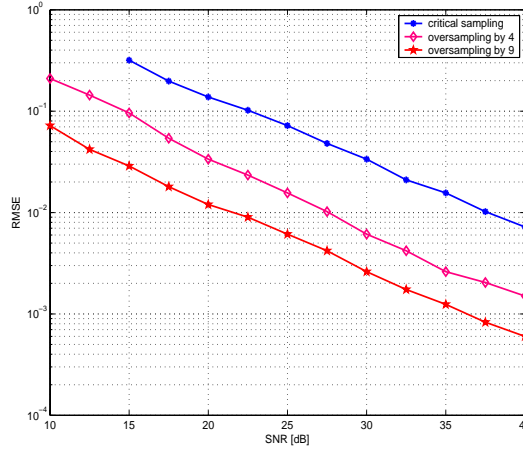


Figure 6.4: Performance of the 2-D Gaussian sampling scheme. *RMSE of location estimates versus SNR for different values of the oversampling factor. We consider the signal made up of 8 Diracs with equal weights, randomly distributed over $[1, 100] \times [1, 100]$, sampled with the 2-D Gaussian kernel, with parameter $\sigma = 7$. The method was tested for different values of SNR and different values of the oversampling factor.*

to a wider class of signals.

6.2 Sampling the Radon transform

We start the analysis by considering the same signal $g(x, y)$, made up of M weighted Diracs. As already mentioned, the signal $g(x, y)$ is given by

$$g(x, y) = \sum_{k=0}^{M-1} c_k \delta(x - x_k, y - y_k).$$

Let $Rg(p, \theta)$ denote the Radon transform [18] of $g(x, y)$

$$Rg(p, \theta) = \int g(x, y) \delta(p - x \cos(\theta) - y \sin(\theta)) dx dy, \quad (6.6)$$

that is, the integral of g over the line $l_{p, \theta}$, defined by $p(\theta) = x \cos(\theta) + y \sin(\theta)$. The key is to observe that for any given angle θ_0 , the Radon transform $Rg(p, \theta_0)$ can be represented as a weighted sum of $M_0 \leq M$ 1-D Diracs, that is,

$$Rg(p, \theta_0) = \sum_{k=0}^{M_0-1} a_{0k} \delta(p - p_{0k}). \quad (6.7)$$

The reason for having $M_0 \leq M$ is that there can be more than one Dirac spike on the path of integration. For the case of a signal made up of 2-D Diracs, this is illustrated in Figure 6.5.

This fact can be exploited in an elegant way to tackle the problem in the 2-D case. Since the signal consisting of M 1-D Diracs can be perfectly recovered from a set of $2M$ samples, by sampling the signal with the Gaussian kernel, one can take advantage of that result to develop a sampling scheme for 2-D signals

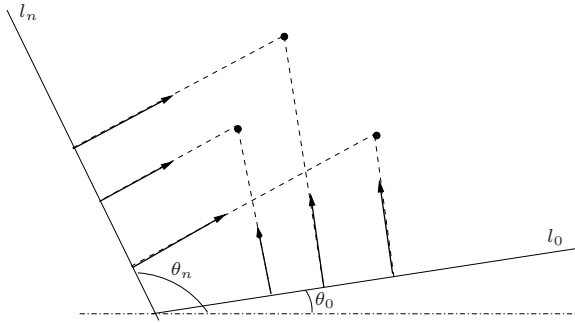


Figure 6.5: Radon transform of the set of Diracs *The projection of a set of M weighted 2-D Diracs onto an arbitrary line is a stream of at most M weighted 1-D Diracs.*

as well. Namely, instead of taking the line integral in the equation (6.6), we can replace the δ function with the appropriate kernel, such as the Gaussian kernel $\varphi_g(x) = e^{-x^2/2\sigma^2}$. In other words, we can consider the filtered projection $\tilde{R}g(p, \theta)$ of the signal $g(x, y)$

$$\tilde{R}g(p, \theta) = \int g(x, y) \varphi(p - p_\theta) dx dy,$$

where $p_\theta = x \cos(\theta) + y \sin(\theta)$. An interesting property that emerges from this formulation is that for any angle θ_0 , the projection $\tilde{R}g(p, \theta_0)$ of $g(x, y)$ becomes a convolution of its Radon transform $Rg(p, \theta_0)$ (that is, a stream of 1-D Diracs) and the Gaussian sampling kernel, i.e.

$$\tilde{R}g(p, \theta_0) = Rg(p, \theta_0) * \varphi_g(p). \quad (6.8)$$

The above equation implies that the locations p_k and weights a_k of the 1-D Diracs, defined by (6.7), can be obtained from $N \geq 2M_0$ samples of $\tilde{R}g(p, \theta_0)$, that is, $p_n(\theta_0) = \tilde{R}g(p - nT_p, \theta_0)$, $n = 0, \dots, N - 1$. Alternatively, one can use a bandlimited kernel, such as the sinc kernel, however, in this case, the problem of reconstructing the signal is more complex [85]. While the set of locations $\{p_{0k}\}$ does not itself define $g(x, y)$, in the following, we will prove that the projections of $g(x, y)$ onto $M + 1$ lines entirely specify the signal.

Assume that we find the projections of $g(x, y)$ onto $M + 1$ lines with different slopes, determined by angles $\theta_0, \theta_1, \dots, \theta_M$. Using the method described above, we can solve for the coordinates p_{mk} and weights a_{mk} , $m = 0, 1, \dots, M$ of the set of 1-D Diracs along each line, and thus uniquely specify the set of “projecting” lines l_{p_{mk}, θ_m} . Clearly, for any point that belongs to the set of 2-D Diracs, exactly $M + 1$ projecting lines must intersect. A reverse statement, that the points where $M + 1$ projecting lines intersect must belong to the set, can be proved by counterexample. Namely, assume that exactly $M + 1$ such lines intersect at some point A . If A does not belong to the set of Diracs, then there must exist at least one point from the set located at each of the lines l_{p_{mk}, θ_m} , $m = 0, 1, \dots, M$, which implies that $g(x, y)$ is made up of at least $M + 1$ Diracs, which obviously contradicts our basic assumption.

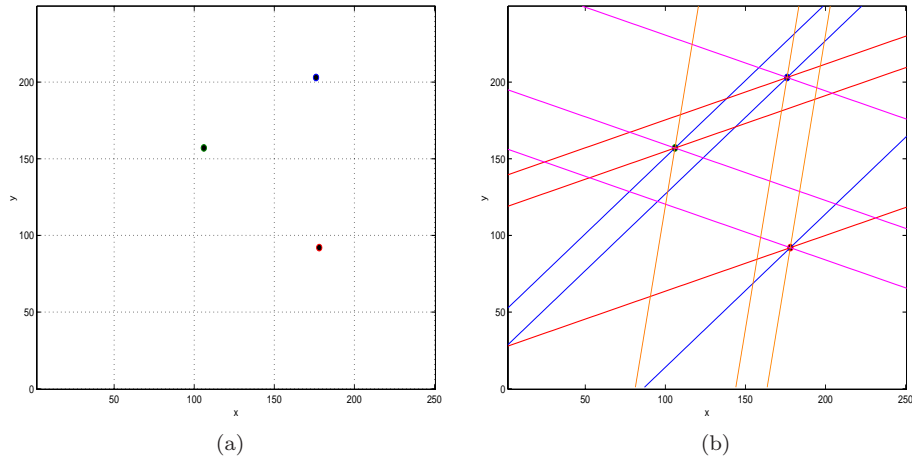


Figure 6.6: Reconstruction of the Set of 2-D Diracs. (a) 2-D signal consisting of $M = 3$ weighted Diracs (b) Reconstruction of the signal from projecting lines obtained by sampling the Radon transform of the signal with a Gaussian kernel. Points where exactly $M + 1 = 4$ lines intersect correspond to the Diracs in the set.

Once the locations of Diracs have been found, the corresponding weights c_k can be estimated by solving the system of at least M linear equations, that we can choose out of $(M + 1)2M$ equations available from the set of projections of $g(x, y)$. Thus, we can state:

Theorem 6.2 Consider a finite set of M weighted 2-D Diracs and let $\varphi_g(p)$ be the 1-D Gaussian sampling kernel, given by $\varphi_g(x) = e^{-x^2/2\sigma^2}$. If $N \geq 2M$ then the N sample values of the filtered Radon transform

$$\langle Rg(p, \theta_m), B_p \varphi_g(p - nT_p) \rangle \quad n = 1, \dots, N$$

taken along each of the $M + 1$ different directions $\theta_0, \theta_1, \dots, \theta_M$, uniquely specify the signal.

In Figure 6.6, we illustrate the basic principle behind the proposed method with a simulation example. In Figure 6.6(a), we show a set of $M = 3$ Diracs in the 2-D plane. The filtered projections of the signal are taken along four different directions, and in each direction, we take a set of $2M = 6$ measurements. The reconstructed signal is shown in Figure 6.6(b), where the locations of Diracs are found from a set of points where exactly $M + 1 = 4$ projecting lines intersect.

As can be seen from the above analysis, in the general case, the algorithm yields a unique solution by taking on the order of M^2 samples of the Radon transform. However, in practice, taking samples in more than three directions is often not necessary, thus, one can often take on the order of M samples, and still be able to reconstruct the signal. In [9] and [29], the authors even argue that in “most cases” encountered in practice, two projections are sufficient for a unique reconstruction, however, in such a case, the reconstruction algorithm is based on a combinatorial approach. Finally, we would like to note that as opposed to other reconstruction methods that require as many measurements in the radial direction as possible [2], our approach assumes that the number of

samples in each direction is related to the number of degrees of freedom of the signal.

6.3 Extension to More Complex Classes of Signals

After the somewhat “synthetic” case study in the previous section, we will next explore possible extensions of this result to more complex classes of signals. In the first example, we will consider the problem of sampling a bilevel polygon, for which traditional sampling schemes turn out to be quite inefficient, although it represents a simple example of a non-bandlimited 2-D signal of finite complexity. The second example is related to bilevel signals with piecewise polynomial boundaries. Unlike in the periodic case, where the problem of reconstructing such signals from an appropriate set of the Fourier series coefficients is quite complex, by sampling the Radon transform of such signals we can solve the problem using simpler techniques.

6.3.1 Bilevel polygon

Consider a signal $g(x, y)$ which is a bilevel polygon, and let vertices be at points (x_i, y_i) , $i = 1, 2, \dots, M$. Obviously, this signal has $2M$ degrees of freedom, since it is uniquely specified by the coordinates of its vertices. In the previous chapter, we have seen that developing an exact sampling result in the case of a periodic signal, which takes advantage of the frequency domain representation of the signal, is quite complicated. Besides, it imposes some constraints in terms of the location of vertices, namely, we required that the boundary contains no vertical or horizontal lines. An alternative way to solve for the coordinates (x_i, y_i) is to take advantage of the fact that the projection of $g(x, y)$ on an arbitrary line is a piecewise linear signal. We can therefore use the same approach as in the previous section, and incorporate the sampling schemes for such 1-D signals into our algorithm, by replacing the δ function from (6.7) by a proper kernel. Namely, a 1-D piecewise linear signal $f(p)$ with M pieces, can be uniquely represented by its $2M$ samples $\langle f(p), \varphi_g^{(2)}(p - nT_p) \rangle$, where $\varphi_g^{(2)}(p)$ is the second derivative Gaussian sampling kernel. Due to the associativity of the convolution operator, a convolution of the signal $f(p)$ with $\varphi_g^{(2)}(p)$ is equivalent to the convolution of the second derivative $f^{(2)}(p)$ (i.e. a stream of Diracs) with the Gaussian kernel, thus the problem can be reduced to the one we have already analyzed in the previous section. In other words, the sampling scheme in 2-D should be modified such that the δ function in (6.7) is replaced by $\varphi_g^{(2)}(p)$. In that case, taking at most $2M$ samples from each of the $M + 1$ projections, and applying the same techniques described in Section 6.2, will uniquely specify the coordinates of vertices. Therefore, we have the following proposition.

Proposition 6.3 Given a bilevel polygon with M vertices and the second derivative Gaussian sampling kernel $\varphi_g^{(2)}(p)$, then the $N \geq 2M$ samples

$$\langle Rg(p, \theta_m), \varphi_g^{(2)}(p - nT_p) \rangle \quad n = 1, \dots, N$$

taken along each of the $M + 1$ directions $\theta_0, \theta_1, \dots, \theta_M$, are a sufficient representation of the signal.

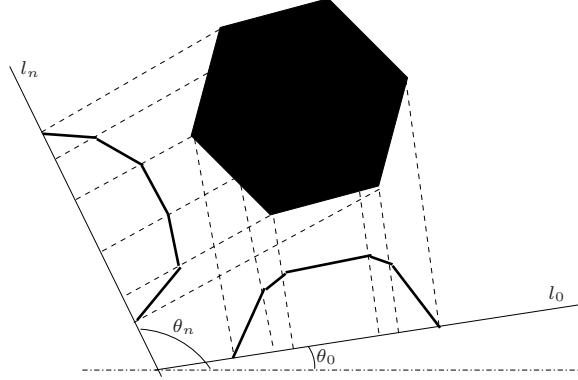


Figure 6.7: Bilevel polygon The projection of a bilevel polygon is a piecewise linear signal. For the signal with M vertices, $2M$ sample values of the Radon transform taken from each of its $M + 1$ different projections uniquely define the signal.

Equivalently, one can use the approach from Section 3.3.3, and sample the signal with the Gaussian kernel $\varphi_g(p)$. In this case, the n -th derivative Gaussian kernel can be approximated as a linear combination of shifted versions of $\varphi_g(p)$, using the relation (3.35), that is,

$$\varphi_g^{(n)}(p) \approx \frac{2}{\sigma} (\varphi_g^{(n-1)}(p - \sigma/4) - \varphi_g^{(n-1)}(p + \sigma/4)), \quad n = 2, 3, 4, \dots \quad (6.9)$$

In particular, the second derivative Gaussian kernel $\varphi_g^{(2)}(p)$, can be computed as a weighted sum of three shifted versions of $\varphi_g(p)$, namely,

$$\varphi_g^{(2)}(p) \approx \left(\frac{2}{\sigma}\right)^2 (\varphi_g(p - \sigma/2) - 2\varphi_g(p) + \varphi_g(p + \sigma/2)). \quad (6.10)$$

We illustrate the method with an example of a bilevel triangle, shown in Figure 6.8(a). The projections of the signal are taken in $M + 1 = 4$ different directions. The reconstructed boundary and the boundary of the original signal are shown in Figure 6.8(b), indicating desirable properties of our method.

6.3.2 Bilevel signal with piecewise polynomial boundary

Another class of signals well-suited for the application of the presented method, is a class of bilevel signals with piecewise polynomial boundaries. That is, for a signal whose boundary is a piecewise polynomial with K pieces of maximum degree R , it is possible to obtain a perfect reconstruction by taking only $O(RK)$ samples of its Radon transform. To prove this result, define a bilevel signal with a piecewise polynomial boundary (with respect to the x axis) as

$$g(x, y) = \begin{cases} 1 & y \leq p(x) \\ 0 & \text{otherwise.} \end{cases} \quad (6.11)$$

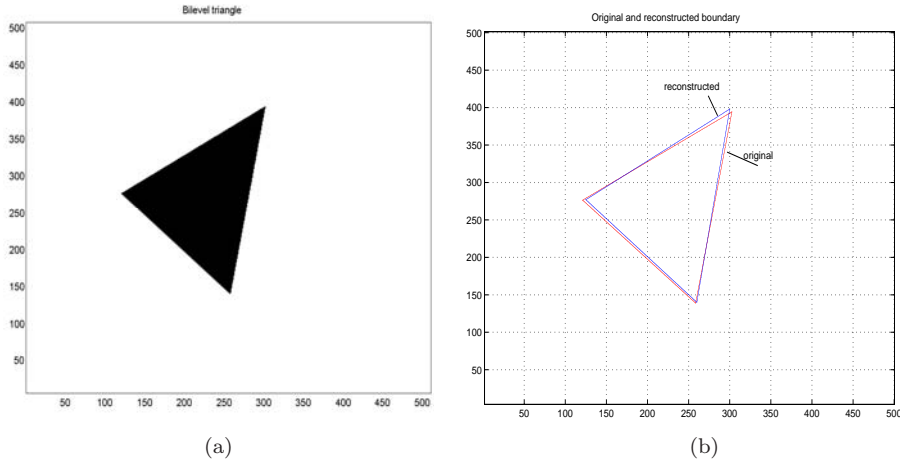


Figure 6.8: Reconstruction of a bilevel triangle. (a) *Bilevel triangle* (b) *Reconstructed (and original) boundary.* The reconstructed boundary is obtained by taking a set of filtered projections with a Gaussian kernel along $M + 1 = 4$ different directions.

where $p(x)$ is a piecewise polynomial signal having K pieces of maximum degree R . Therefore, one can extend the result from the 1-D case, and take the samples of the projection of $g(x, y)$ on the x -axis using the $(R + 1)$ -th derivative Gaussian kernel $\varphi_g^{(R+1)}(x)$. Note that the $(R + 1)$ -th derivative $p^{(R+1)}(x)$ is a sum of K differentiated Diracs, i.e.

$$p^{(R+1)}(t) = \sum_{k=0}^{K-1} \sum_{r=0}^R c_{k,r} \delta^{(r)}(t - t_k),$$

that is, there are K degrees of freedom corresponding to the locations of discontinuities and $(R + 1)K$ degrees of freedom corresponding to weights. Therefore, it suffices to take at least $(R + 2)K$ samples with the kernel $\varphi_g^{(R+1)}(x)$ to be able to reconstruct the signal. We can thus state the following proposition:

Proposition 6.4 Consider a bilevel signal with a piecewise polynomial boundary $p(x)$ having K pieces of maximum degree R . Then, the set of $N \geq (R + 2)K$ samples of its Radon transform,

$$\langle Rg(p, \theta_x), \varphi^{(R+1)}(p - nT_p) \rangle \quad n = 1, \dots, N$$

taken along the x direction, uniquely represents the signal.

Equivalently, one can use the approach from Section 3.3.3, and take samples with the Gaussian kernel $\varphi_g(x)$. In this case, one should increase the sampling density $(R + 2)$ times, given that the $(R + 1)$ -th derivative Gaussian kernel $\varphi_g^{(R+1)}(x)$ can be computed as a linear combination of $(R + 2)$ shifted versions of $\varphi_g(x)$, that is, $(R + 2)^2 K$ samples of the Radon transform will uniquely specify the signal.

6.4 Conclusion

We have developed algorithms for sampling certain classes of aperiodic 2-D signals that are not bandlimited, and yet have a finite number of degrees of freedom. We have first considered the case of a finite set of Diracs, and derived a sampling theorem using a Gaussian kernel. We next focused on an alternative approach, and proposed sampling schemes lead to perfect reconstruction from a finite number of samples of the Radon transform. The proposed algorithms are very convenient in terms of computational efficiency, and are potentially of impact in certain signal processing applications, such as reconstruction from projections. Finally, we believe that a larger class of sampling problems can be analyzed within the proposed framework, opening up an area for further investigation.

Chapter 7

Conclusion

7.1 Summary

Sampling theory has recently experienced a strong research revival, due in part to the connections made with wavelet theory, which led to a generalization of Shannon's original theory and development of more advanced formulations with immediate relevance to signal processing and communications. For example, it is well-known that the standard sampling paradigm for the representation of bandlimited functions can be extended to certain classes of non-bandlimited signals that belong to shift-invariant spaces, such as uniform splines. While this result is valid for signals that live on a subspace spanned by a generating function and its uniform shifts, it cannot be extended to the general case, and typically, only the projection of the signal onto that specific subspace can be reconstructed.

In recent work by Vetterli et al. [85], it was shown that one can develop exact sampling schemes for a larger class of signals that are neither bandlimited nor live on a subspace, namely, certain signals of *finite rate of innovation*. A common feature of such signals is that they allow for a parametric representation with a finite number of degrees of freedom and can be perfectly reconstructed from a finite number of samples. The key in all constructions is to identify the innovative part of a signal using model-based methods for parameter estimation, commonly encountered in high-resolution spectral analysis.

In this thesis, we have revisited the sampling problem for signals of finite rate of innovation, and developed improved, more robust sampling schemes that allow for stable and precise reconstruction in the presence of noise. We have also explored applications of the new sampling results to communication problems and extended the results to the two-dimensional case. The main contributions of the thesis are summarized below.

Sampling theory and model-based signal analysis

We have considered the sampling problem for signals made up of 1-D Diracs and generalized the results to more complex classes of signals. In particular, we developed a subspace approach to signal reconstruction, which converts a nonlinear estimation problem into the simpler problem of estimating the parameters of a linear model. This provides an elegant and robust framework

for solving a large class of sampling problems, while offering more flexibility than the traditional scheme for bandlimited signals. For classes of periodic signals, such as piecewise polynomials and nonuniform splines, we proposed novel algebraic approaches that solve the sampling problem in the Laplace domain, after appropriate windowing. Building on the results for periodic signals, we extended our analysis to finite-length signals and developed sampling schemes based on a Gaussian kernel.

Most of the schemes we proposed use algebraic transformations to convert a set of samples into a sum of complex exponentials. As a result, the problem of signal reconstruction can be reduced to the one of estimating the parameters of multiple superimposed sinusoids. For such a problem, model-based methods provide an elegant tool for exposing the structure of an underlying signal. Such methods assume that the signal satisfies a generating model of known functional form, and then proceed in estimating the parameters of the assumed model.

We have developed high-resolution model-based algorithms that extend classical harmonic retrieval techniques and are applicable to more general classes of parameter estimation problems. One example, relevant to ultra-wideband (UWB) systems, is the problem of estimating time delays and pulse shapes of multipath components, which cannot be solved using models and methods used in conventional communication systems. We have shown that by considering the problem in the frequency domain and exploiting the structure of the signal subspace, one can jointly estimate the unknown pulse shapes and time delays, using linear techniques and fast algorithms.

Another problem we investigated in the context of model-based spectral estimation is the possibility of improving the resolution performance in the case when the signal contains closely spaced frequencies. This problem arises in applications such as time delay estimation in multipath channels, where the estimation performance of parametric methods can degrade significantly if a received signal has closely spaced components. We proposed techniques that can improve the resolution capability of existing methods, without increasing the computational complexity. Namely, since the performance of parametric methods depends strongly on the eigenstructure of an associated data matrix, we proposed alternative ways for constructing such a matrix from the same data set. While such techniques are of general interest to high-resolution spectral estimation, they are particularly useful in communication applications.

Applications to wideband communications

We have considered applications of our results to certain nonlinear estimation problems encountered in wideband communication systems, most notably ultra-wideband (UWB) systems, where the bandwidth used for transmission is much larger than the bandwidth or rate of information being sent. We have developed several frequency domain methods for channel estimation and synchronization in ultra-wideband systems, which yield high-resolution estimates of all relevant channel parameters by sampling a received signal below the Nyquist rate. Furthermore, we have proposed algorithms that are suitable for identification of more realistic UWB channel models, where a received signal is made up of pulses with different pulse shapes. Our approach can be generalized to the case when the channel parameters are estimated from multiple frequency bands with highest signal-to-noise ratio, which allows one to maximize the estimation per-

formance, given a constraint on the acceptable sampling rate in a system. We have also considered a multiresolution version of such schemes, which provides unique advantages over existing techniques in terms of computational complexity and acquisition speed.

Multidimensional sampling theory

We have considered possible extensions of our sampling results to the two-dimensional case and developed exact sampling schemes and reconstruction formulas for some classes of parametric non-bandlimited signals, such as sets of 2-D Diracs, polygons or signals with piecewise polynomial boundaries. We focused on developing sampling schemes for signals with M degrees of freedom that require on the order of M (or at most M^2) samples, and algorithms that can recover such signals with high numerical precision. We analyzed in detail a periodic set of 2-D Diracs and extended the results to more complex objects such as lines and polygons. Unlike most multidimensional sampling schemes, the methods we propose perfectly reconstruct such signals from a finite number of samples in the noiseless case. Similarly to the 1-D case, some of the techniques we used were already encountered in the context of high-resolution harmonic retrieval. In particular, SVD-based methods and the annihilating filter approach are both explored as inherent parts of the developed algorithms. We have also considered an alternative sampling approach, which exploits the properties of a signal in the Radon transform domain. We showed that by taking a finite number of “filtered” line integrals, the problem can be reduced to its one-dimensional equivalent, which is much more convenient for algorithmic implementation. Such an approach allowed us to develop exact sampling results for 2-D Diracs, polygons or signals with piecewise polynomial boundaries. That is, we showed that one can perfectly reconstruct these signals from a finite set of samples of their Radon transform. This led to simpler reconstruction algorithms compared to “true” 2-D schemes, and is applicable to more general classes of finite complexity signals.

7.2 Future Research

In this thesis, we explored both theoretical and practical aspects of sampling theory for classes of parametric non-bandlimited signals. We tried to point to potentials and limitations of the new framework, however, the topics we considered are far from being exhausted. In the following, we describe possible directions for future theoretical work and some areas for practical contributions.

Jitter analysis, model mismatch and filter design issues

As a follow-up to our work on problems in sampling theory, there are several interesting topics that one can explore further. Namely, in all our constructions, we assumed perfect acquisition devices and focused primarily on noise analysis. In practice, one has to take into account imperfections of the anti-aliasing filter, quantization issues or the presence of jitter in the sampling process. For example, in the absence of noise, a uniform set of samples taken at the rate of innovation is sufficient for perfect reconstruction of a signal. In practice, one

must use oversampled schemes in order to improve robustness to noise, however, whether oversampling is sufficient to compensate for the effects of jitter is still not well understood. Similarly, in our analysis, we have only briefly touched upon the problem of model mismatch. Therefore, it is of interest to develop better mathematical understanding of the effect of jitter and filter imperfections (in particular, phase distortion) on the reconstruction performance. Also, it would be important to consider more realistic classes of anti-aliasing filters and develop a formal framework for analyzing model mismatch.

Local reconstruction schemes with a Gaussian kernel

The problem of developing sampling schemes for aperiodic signals with finite rate of innovation turned out to be more challenging than we had originally assumed. While in the simple case of a set of Diracs we were able to derive exact formulas using the Gaussian sampling kernel, we had to modify original schemes to overcome the problem of numerical ill-conditioning in the presence of noise and develop techniques for extending the results to more complex classes of signals. Despite all these modifications, we have seen that the Gaussian schemes are very sensitive to the choice of the width (σ) of the sampling kernel. Specifically, we showed that the optimal width of the kernel depends on the size of the reconstruction window and the average spacing between the Diracs. In this context, it would be interesting to investigate novel, multiresolution reconstruction algorithms, akin to those presented in Section 4.5, where one would first obtain a coarse approximation of the signal and then perform precise reconstruction by windowing the signal and estimating the parameters locally (i.e. in each window separately). Somewhat related to that is the problem of developing iterative reconstruction methods, where one could obtain a coarse estimate of the signal in the first step, and then perform successive refinement in each iteration. This problem is relevant to the 2-D case as well.

Extending the results to other classes of signals

So far, we have focused on developing exact sampling schemes for some specific classes of signals with finite rate of innovation, such as non-uniform splines and piecewise polynomials, where the innovation is contained in discontinuities (either in the signal itself or in its derivatives). In such a case, we were able to convert a set of samples into a sum of exponentials and identify the innovative part of a signal using harmonic retrieval methods. Thus a natural question that arises is the following: what other types of innovation can be identified and what are appropriate reconstruction methods? For example, frequency-modulated signals (where the modulating signal is of finite rate of innovation) also belong to the class of parametric non-bandlimited signals, yet one cannot use the presented approach to reconstruct the signal. Therefore, it would be interesting to generalize our results to other classes of parametric non-bandlimited signals and investigate alternative computational tools that could possibly allow for simpler reconstruction algorithms. Yet, one of the most challenging problems is the development of new two-dimensional representations for images. This is closely related to the sampling problem for 2-D signals, since the latter can also be viewed as the problem of signal representation through a set of samples. In this

context, one possible research direction is to further investigate the possibility of exploiting the signal structure in the Radon transform domain.

Applications to communications and wireless sensor networks

Along with theoretical research in sampling theory, it is of interest to further explore its applications to communication problems. As we have argued throughout this thesis, one of the most promising application areas is UWB technology, still there are several open problems that one can investigate next. One topic of interest is to investigate the possibility of having some kind of hybrid synchronization schemes that would combine the advantages of various techniques. For example, subspace methods can acquire a received signal much faster than the schemes based on matched filters, however, matched filters are more robust in estimating multiple closely spaced signal components. Therefore, one can use subspace methods for coarse (and fast) synchronization, and then use the approach based on matched filters in order to obtain precise estimates of multipath components. Besides, it would be interesting to investigate applications to high-speed communications and explore novel methods for systems with non-impulsive signaling (such as multiband OFDM). Another application area is wireless sensor networks, where it is of interest to investigate algorithmic foundations for real-time distributed signal processing, in particular, under limited communication and computation resources. For example, one could further investigate problems of distributed and non-uniform sampling by taking advantage of the correlation among sensed data, and explore multiresolution sampling schemes, among other topics.

Bibliography

- [1] A. Aldroubi and K. Grochenig, “Non-uniform sampling in shift-invariant spaces,” *SIAM Rev.*, vol. 43, pp. 585-620, 2001.
- [2] S. Basu and Y. Bresler, “ $\mathcal{O}(N^2 \log_2 N)$ Filtered backprojection reconstruction algorithm for tomography,” *IEEE Transactions on Image Processing*, Vol. 9, No. 10, October 2000.
- [3] J. J. Benedetto and P. J.S.G. Ferreira, *Modern Sampling Theory: Mathematics and Applications*, Birkhauser, Boston, 2001.
- [4] S. E. Bensley and B. Aazhang, “Subspace-based channel estimation for code division multiple access communication systems,” *IEEE Transactions on Communications*, Vol. 44, No. 8., p.p. 1009-1020, August 1996.
- [5] E. R. Berlekamp, *Algebraic Coding Theory*, McGraw-Hill, New York, 1968.
- [6] R. E. Blahut, *Theory and Practice of Error Control Codes*, Addison-Wesley, Reading, MA, 1983.
- [7] T. Blu, P. Thévenaz, M. Unser, “Linear interpolation revitalized,” *IEEE Transactions on Image Processing*, Vol. 13, No. 5, pp. 710-719, May 2004.
- [8] T. Blu, P. Thévenaz, M. Unser, “Complete parameterization of piecewise-polynomial interpolation kernels,” *IEEE Transactions on Image Processing*, Vol. 12, No. 11, pp. 1297-1309, November 2003.
- [9] Y. Bresler, “Model-based estimation techniques for 3-D reconstruction from projections,” PhD dissertation, Department of Electrical Engineering, Stanford University, Stanford, CA, 1985.
- [10] Y. Bresler and A. Macovski, “Exact maximum likelihood parameter estimation of superimposed exponential signals in noise,” *IEEE Trans. Acoust., Speech, Signal Processing*, Vol. 34, pp. 1081-1089, Oct. 1986.
- [11] J. L. Brown Jr. and S. D. Cabrera, “On well-posedness of the Papoulis generalized sampling expansion,” *IEEE Trans. on Circuits and Systems*, Vol. 38, No. 5, pp. 554-556, 1991.
- [12] <http://bwrc.eecs.berkeley.edu>
- [13] D. Cassioli, M. Z. Win, A. F. Molisch, “The ultra-wide bandwidth indoor channel: From statistical model to simulations,” *IEEE J. Select. Areas Commun.*, vol. 20, pp. 1247-1257, December 2002.

-
- [14] A. Chebira, P. L. Dragotti, L. Sbaiz, M. Vetterli, "Sampling and interpolation of the plenoptic function," in *Proc. IEEE International Conference on Image Processing*, Vol. 2, pp. 917-920, Sept. 2003.
- [15] T. Cho, D. Cline, C. Conroy and P. Gray, "Design considerations for high-speed low-power low-voltage CMOS analog-to-digital converters," *Digest of Technical papers*, Advanced Analog Integrated Circuit Symposium, March 1994.
- [16] R. J. Cramer, R. A. Scholtz and M. Z. Win, "Evaluation of an Ultra-Wideband Propagation Channel," *IEEE Trans. on Antennas and Propagation*, Vol. 50, No. 5, pp 561-570, May 2002.
- [17] P. J. Davis, *Interpolation and Approximation*, Dover Publications, 1975.
- [18] S. R. Deans and R. Moses, *The Radon Transform and Some of Its Applications*, Willey, 1993.
- [19] J. W. Demmel, *Applied Numerical Linear Algebra*, SIAM, Philadelphia, PA, 1997.
- [20] R. C. Dixon, *Spread Spectrum Systems with Commercial Applications*, Wiley, New York, NY, 1994.
- [21] I. Djokovic and P. P. Vaidyanathan, "Generalized sampling theorems in multiresolution spaces," *IEEE Transactions on Signal Processing*, Vol. 45, pp. 583-599, March 1997.
- [22] I. O' Donnell, M. Chen, S. Wang and R. Brodersen, "An Integrated, Low-Power, Ultra-Wideband Transceiver Architecture for Low-Rate Indoor Wireless System," *IEEE CAS Workshop on Wireless Communications and Networking*, September 2002.
- [23] E. Ertin, U. Mitra and S. Siwamogsatham, "Maximum-likelihood-based multipath channel estimation for code-division multiple-access systems," *IEEE Transactions on Communications*, Vol. 49, No. 2, pp. 290-302, February 2001.
- [24] R. Fleming, C. Kushner, "Spread Spectrum Localizers," U.S. Patent 5,748,891, May 5, 1998.
- [25] R. Fleming, C. Kushner, G. Roberts and U. Nandiwada, "Rapid Acquisition for Ultra-Wideband Localizers," in *Proc. IEEE Conf. on UWB Systems and Technologies*, May 2002.
- [26] J. J. Fuchs, "Estimating the number of sinusoids in additive white noise," *IEEE Transactions on Acoust., Speech, Signal Processing*, Vol. ASSP-36, pp. 1846-1853, December 1998.
- [27] G. H. Golub, C. F. Van Loan, *Matrix Computations*, The Johns Hopkins University Press, 1989.
- [28] M. Haardt, M. D. Zoltowski, C. P. Mathews and J. A. Nosssek, "2D Unitary Esprit for efficient 2D parameter estimation," *IEEE International Conference on Acoustics, Speech, and Signal Processing*, Vol. 3, pp. 2096-2099, 1995.

-
- [29] G. Herman and A. Kuba, *Discrete Tomography: Foundations, Algorithms and Applications*, Birkhauser, Boston, 1999.
- [30] E. Homier and R. Scholtz, "Rapid Acquisition of UWB Signals in a Dense Multipath Channel," in *Proc. IEEE Conf. on UWB Systems and Technologies*, May 2002.
- [31] Y. Hua, M. Nikpour and P. Stoica, "Optimal reduced rank estimation and filtering," *IEEE Trans. on Signal Processing*, Vol. 49, No. 3, pp. 457-468, March 2001.
- [32] Y. Hua and T. Sarkar, "Matrix pencil method for estimating parameters of exponentially damped/undamped sinusoids in noise," *IEEE Transactions on Acoustics, Speech and Signal Processing*, Vol. 38, No. 5, pp. 814-824, May 1990.
- [33] Y. Hua and T. Sarkar, "On SVD for estimating generalized eigenvalues of singular matrix pencil in noise," *IEEE Transactions on Signal Processing*, Vol. 39, No. 4, April 1991.
- [34] Y. Hua, Estimating two-dimensional frequencies by matrix enhancement and matrix pencil, *IEEE Transactions on Signal Processing*, Vol. 40, pp. 2267-2280, September 1992.
- [35] A. J. Jerri, "The Shannon sampling theorem—Its various extensions and applications: A tutorial review," *Proc. of IEEE*, Vol. 65, pp. 1565-1579, 1977.
- [36] V. A. Kotel'nikov, "On the transmission capacity of "ether" and wire in electrocommunications," *Izd. Red. Upr. Svyazzi RKKK (Moscow)*, 1933.
- [37] V. A. Kotel'nikov, "Reprint: On the transmission capacity of "ether" wire in electrocommunications," in *Modern Sampling Theory: Mathematics and Applications*, J. J. Benedetto and P. J. S. G Ferreira, Eds. Boston, MA; Birkhauser, 2000.
- [38] M. Kristensson, M. Jansson and B. Ottersten, "Further results and insights on subspace based sinusoidal frequency estimation," *IEEE Trans. on Signal Processing*, Vol. 49, No. 12, pp. 2962-2974, December 2001.
- [39] S. Y. Kung, K. S. Arun and D. V. Bhaskar Rao, "State-space and singular-value decomposition-based approximation methods for the harmonic retrieval problem," *Journal of the Optical Society of America*, Vol. 73, No. 12, pp. 1799-1811, December 1983.
- [40] J. Kusuma, I. Maravic and M. Vetterli, "Sampling with finite innovation rate: channel and timing estimation in UWB and GPS," *In Proc. of ICC*, Vol. 5, pp. 3540-3544, May 2003.
- [41] J. Y. Lee and R. Scholtz, "Ranging in a dense multipath environment using an UWB radio link," *IEEE Journal on Selected Areas in Communications*, Vol. 20, No. 9, pp. 1677-1683, December 2002.

-
- [42] H. B. Lee, "Eigenvalues and eigenvectors of covariance matrices for signals closely spaced in frequency," *IEEE Trans. on Signal Processing*, Vol. 40, No. 10, pp. 2518-2535, October 1992.
- [43] D. A. Linden, "A discussion of sampling theorems," in *Proc. IRE*, Vol. 47, pp. 1219-1226, 1959.
- [44] H. Liu and M. Zoltowski, "Blind equalization in antenna array CDMA systems", *IEEE Transactions on Signal Processing*, Vol. 45, pp 161-172, Jan. 1997.
- [45] Y. Lu and M. Do, "A geometrical approach to sampling signals with finite rate of innovation," in *Proc. ICASSP*, May 2004.
- [46] S. Mallat, *A Wavelet Tour of Signal Processing*, San Diego, CA: Academic, 1998.
- [47] I. Maravic and M. Vetterli, "Exact sampling results for classes of parametric non-bandlimited 2-D signals," *IEEE Trans. on Signal Processing*, Vol. 5, No. 1, pp. 175-189, Jan. 2004.
- [48] I. Maravic and M. Vetterli, "A sampling theorem for the Radon transform of finite complexity objects," in *Proc. IEEE International Conference on Acoustics, Speech, and Signal Processing*, Vol. 2, pp. 1197-1200, May 2002.
- [49] I. Maravic, M. Vetterli and K. Ramchandran, "High-resolution methods for channel estimation and synchronization in UWB systems," to be submitted to *IEEE Trans. on Signal Processing*.
- [50] I. Maravic, M. Vetterli and K. Ramchandran, "High-resolution acquisition methods for wideband communication systems," *In Proc. of ICASSP*, Vol. 4, pp. 133-136, April 2003.
- [51] I. Maravic and M. Vetterli, "Low-complexity subspace methods for channel estimation and synchronization in ultra-wideband systems," *In Proc. of IWUWB*, June 2003.
- [52] P. Marziliano, *Sampling Innovations*, PhD thesis, EPFL, 2001.
- [53] J. L. Massey, "Shift register synthesis and BCH decoding," *IEEE Transactions on Information Theory*, Vol. IT-15, pp. 122-127, January 1969.
- [54] J. L. Massey, "Toward an information theory of spread-spectrum systems," in *Code Division Multiple Access Communications*, S. G. Glisic and P. A. Leppanen, Eds. Boston, MA: Kluwer, 1995, pp. 29-46.
- [55] S. Matej and I. Bajla, "A high-speed reconstruction from projections using direct Fourier method with optimized parameters—An experimental analysis," *IEEE Trans. on Medical Imaging*, Vol. 9, No. 4, pp. 421-429, 1990.
- [56] R. Molina, J. Nunez, F. J. Cortio and J. Mateos, "Image restoration in astronomy," *IEEE Signal Processing Magazine*, Vol. 18, No. 2, pp. 11-29, March 2001.

-
- [57] A. V. Oppenheim and R. W. Schaffer, *Discrete-Time Signal Processing*, Prentice Hall, 1989.
- [58] R. Roy and T. Kailath, "ESPRIT estimation of signal parameters via rotational invariance techniques," *IEEE Trans. on Acoustics, Speech and Signal Processing*, vol. 37, No.7, pp. 984-995, July 1989.
- [59] A. Papoulis, "Generalized sampling expansion," *IEEE Transactions on Circuits and Systems*, Vol. 24, pp. 652-654, November 1977.
- [60] J. A. Parker, R. V. Kenyon and D. E. Troxel, "Comparison of interpolation methods for image resampling," *IEEE Transactions on Medical Imaging*, Vol. MI-2, No. 1, pp. 31029, 1981.
- [61] A. Paulraj, B. Khalaj and T. Kailath, "2-D RAKE receivers for CDMA cellular systems," in *Proc. IEEE GLOBECOM*, Vol. 1, San Francisco, CA, Dec. 1994, pp. 400-404.
- [62] J. G. Proakis, *Digital Communications*, McGraw-Hill, New York, 1995.
- [63] G. R. B. de Prony, "Essai Experimentale et Analytique," *Paris Journal de L'Ecole Polytechnique*, Vol. 1, No. 2, pp. 24-76, 1775.
- [64] J. Ramos and M. Zoltowski, "Low-complexity space-time processor for DS-CDMA communications", *IEEE Transactions on Signal Processing*, Vol. 48, No. 1, January 2000.
- [65] B. D. Rao and K. S. Arun, "Model based processing of signals: A state space approach," *Proceedings of the IEEE*, Vol. 80, No. 2, pp. 283-309, February 1992.
- [66] B. Rao, "Sensitivity analysis of state space methods in spectral estimation," in *Proc. IEEE ICASSP*, April 1987.
- [67] P. A. Rattey and A. G. Lindgren, "Sampling the 2-D Radon transform," *IEEE Trans. on Acoustic, Speech and Signal Processing*, Vol. ASSP-29, No. 5, pp. 994-1002, Oct. 1981.
- [68] R. Molina and B. D. Ripley, "Using spatial models as priors in astronomical image analysis," *Journal of Applied Statistics*, Vol. 16, pp. 193-206, 1989.
- [69] S. Rouquette and M. Najim, "Estimation of frequencies and damping factors by two-dimensional ESPRIT type methods," *IEEE Transactions on Signal Processing*, Vol. 49, No. 1, pp. 237-245, January 2001.
- [70] C. Sengupta, J. Cavallaro and B. Aazhang, "On multipath channel estimation for CDMA systems using multiple sensors", *IEEE Transactions on Communications*, Vol. 49, No. 3, March 2001.
- [71] C. E. Shannon, "Communication in the presence of noise," in *Proc. IRE*, Vol. 37, pp. 10-21, 1949.
- [72] C. E. Shannon, "Classic paper: Communication in the presence of noise," in *Proc. IEEE*, Vol. 86, No. 2, pp. 447-457, 1998.

-
- [73] Q. Spencer, M. Rice, B. Jeffs, M. Jensen, "A Statistical model for the angle-of-arrival in indoor multipath propagation," in *Proc. IEEE Vehicular Technology Conference*, pp. 1415-1419, 1997.
- [74] P. Stoica and R. Moses, *Introduction to Spectral Analysis*, Prentice Hall, 2000.
- [75] E. G. Strom, S. Parkvall, S. L. Miller and B. E. Ottersten, "DS-CDMA synchronization in time-varying fading channels", *IEEE J. Selected Areas in Communications*, vol. 14, pp. 1636-1642, October 1996.
- [76] B. Suard, A. Naguib, G. Xu and T. Kailath, "Performance analysis of CDMA mobile communication systems using antenna arrays", in *Proc. ICASSP*, vol. VI, April 1993, pp. 153-156.
- [77] P. Stoica and A. Nehorai, "MUSIC, maximum likelihood and Cramer-Rao bound," *IEEE Trans. on Acoustics, Speech and Signal Processing*, vol. 37, No. 5, pp. 720-741, May 1989.
- [78] A. L. Swindlehurst, "Time delay and spatial signature estimation using known asynchronous signals," *IEEE Trans. on Signal Processing*, Vol. 46, No. 2, pp. 449-462, February 1998.
- [79] M. Unser and J. Zerubia, "Generalized sampling without bandlimiting constraints," *IEEE Trans. on Circuits and Systems*, Vol. 45, pp. 959-969, Aug. 1998.
- [80] M. Unser, "Sampling—50 years after Shannon," in *Proceedings of the IEEE*, Vol. 88, No. 4, April 2000.
- [81] F. Vanpoucke, M. Moonen and Y. Berthoumieu, "An efficient subspace algorithm for 2-D harmonic retrieval," in *Proc. IEEE International Conference on Acoustics, Speech, and Signal Processing*, Vol. 4, pp. 461-464, 1994.
- [82] R. G. Vaughan, N. L. Scott and D. R. White, "Theory of bandpass sampling," *IEEE Transactions on Signal Processing*, Vol. 39, No. 9, pp. 1973-1984, September 1991.
- [83] A. J. Vanderveen, P. Ober and E. Deprettere, "Azimuth and elevation computation in high resolution DOA estimation," *IEEE Transactions on Signal processing*, Vol. 40, No. 7, pp. 1828-1832, July 1992.
- [84] A. J. Vanderveen, M. C. Vanderveen and A. Paulraj, "Joint angle and delay estimation using shift-invariance techniques," *IEEE Transactions on Signal Processing*, Vol. 46, No. 2, pp. 405-418, February 1998.
- [85] M. Vetterli, P. Marziliano and T. Blu, "Sampling signals with finite rate of innovation," *IEEE Transactions on Signal Processing*, Vol. 50, No. 6, pp. 1417-1428, June 2002.
- [86] M. Vetterli, P. Marziliano and T. Blu, "A Sampling theorem for periodic piecewise polynomial signals," in *Proc. IEEE International Conference on Acoustics, Speech, and Signal Processing*, May 2001.

- [87] M. Vetterli, J. Kovacevic, *Wavelets and Subband Coding*, Englewood Cliffs, NJ: Prentice Hall, 1995.
- [88] A. J. Viterbi, *CDMA - Principles of Spread Spectrum Communication* Reading, MA: Addison-Wesley, 1995.
- [89] L. Yang, Z. Tian and G. Giannakis, "Non-data aided timing acquisition of ultra-wideband transmissions using cyclostationarity," *In Proc. of ICASSP*, April 2003.
- [90] J. L. Yen, "On the nonuniform sampling of bandwidth limited signals," *IRE Trans. Circuit Theory*, Vol. CT-3, pp. 251-257, 1956.
- [91] J. M. Whittaker, "The Fourier theory of the cardinal functions," in *Proc. Math. Soc. Edinburgh*, Vol. 1, pp. 169-176, 1929.
- [92] M. Z. Win, R. A. Scholtz, "Impulse Radio: How it works," *IEEE Commun. Letters*, vol. 2, pp. 36-38, February 1998.
- [93] M. Z. Win, R. A. Scholtz, "On the robustness of ultra-wide bandwidth signals in dense multipath environments," *IEEE Commun. Letters*, vol. 2, pp. 51-53, February 1998.
- [94] M. Z. Win, R. A. Scholtz, "Characterization of ultra-wide bandwidth wireless indoor communication channel: A communication theoretic view," *IEEE J. Select. Areas Commun.*, vol. 20, pp. 1613-1627, December 2002.

Curriculum Vitae

Irena Maravić

Audio-Visual Communications Laboratory
Swiss Federal Institute of Technology in Lausanne (EPFL)
CH-1015 Lausanne, Switzerland
Email: irena.maravic@epfl.ch
Web: <http://lcvwww.epfl.ch/~irena>

Education

- 2001 - 2004 Swiss Federal Institute of Technology in Lausanne, Switzerland
PhD candidate, Department of Computer and Communication Sciences
- 1999 - 2001 California Institute of Technology, Pasadena, California
M.S. in Electrical Engineering, June 2000.
- 1992 - 1997 University of Belgrade, Belgrade, Serbia and Montenegro
B.S. in Electrical Engineering, July 1997.

Research Experience

- 2001 - 2004 **Research Assistant**, Audio-Visual Communications Laboratory, Swiss Federal Institute of Technology in Lausanne, Switzerland
- Summer 2002 **Visiting Scholar**, University of California, Berkeley, USA
- 1999-2001 **Research Assistant**, Optical Information Processing Laboratory, California Institute of Technology, USA
- 1997-1999 **Research Assistant**, Communication Systems Laboratory, University of Belgrade, Serbia and Montenegro

Teaching Experience

Instructor

- Statistical Signal Processing, Computer and Communication Sciences Dept., EPFL, 2003, 2004.

- Optoelectronic Devices and Systems, Dept. of Electrical Eng., Univ. of Belgrade, 1999.

Teaching Assistant

- Statistical Signal Processing, Computer and Communication Sciences Dept., EPFL, 2002.
- Electromagnetic Engineering, Dept. of Electrical Engineering, Caltech, 2001.
- Fourier Optics, Dept. of Electrical Engineering, Caltech, 2000.
- Optical Communications, Dept. of Electrical Engineering, University of Belgrade, 1999.
- Digital Communications, Dept. of Electrical Engineering, University of Belgrade, 1998.

Awards

- Engineering Division Fellowship, California Institute of Technology, 1999-2001.
- University Prize awarded to the highest ranked student in the class, University of Belgrade, 1997.
- Fellowship awarded by the Ministry of Sciences, 1997-1998.
- National Science Foundation Fellowship, 1997.
- Fellowship awarded by the Ministry of Education 1992-1997.

Patents

- I. Maravic and M. Vetterli, "Synchronization and Channel Estimation with Sub-Nyquist Sampling in Ultra-Wideband Communication Systems," US patent application PCT/US04/08871, March 2004.
- I. Maravic, P. L. Dragotti and M. Vetterli, "Sampling Methods, Reconstruction Methods and Devices for Sampling and/or Reconstructing Multidimensional Signals," European patent application PCT/EP02/11862, October 2002.
- I. Maravic, J. Kusuma and M. Vetterli, "Method and Receiver for Decoding Signals Sent Over Bandwidth-Expanding Communication System," European patent application PCT/EP02/62444, March 2002.

Publications

Journal papers and Manuscripts

1. I. Maravic, M. Vetterli, "Exact Sampling Results for Some Classes of Parametric Non-Bandlimited 2-D Signals," *IEEE Transactions on Signal Processing*, Vol. 52, No. 1, pp. 175-189, January 2004.
2. I. Maravic, J. Kusuma and M. Vetterli, "Low-Sampling Rate UWB Channel Characterization and Synchronization," *Journal of Communications and Networks*, special issue on ultra-wideband systems, Vol. 5, No. 4, pp. 319-327, December 2003.
3. I. Maravic and M. Vetterli, "Sampling and Reconstruction Methods for Signals of Finite Rate of Innovation in the Presence of Noise," to appear in *IEEE Transactions on Signal Processing*.
4. I. Maravic, M. Vetterli and K. Ramchandran, "High-Resolution Synchronization and Channel Estimation with Sub-Nyquist Sampling and Application to Ultra-Wideband Systems," to be submitted to *IEEE Transactions on Signal Processing*.
5. C. Moser, I. Maravic, B. Schupp, A. Adibi and D. Psaltis, "Diffraction Efficiency of Localized Holograms in Doubly Doped LiNbO₃ Crystals," *Optics Letters*, Vol. 25, No. 17, pp. 1243-1245, September 2000.

Conference papers

1. I. Maravic, M. Vetterli and K. Ramchandran, "Channel Estimation and Synchronization with Sub-Nyquist Sampling and Application to Ultra-Wideband Systems," invited paper, in *Proc. IEEE Symposium on Circuits and Systems, ISCAS 2004*.
2. I. Maravic, M. Vetterli, "Low-complexity Timing Synchronization in Digital Ultra-Wideband Receivers," In *Proc. of International Workshop on Ultra-Wideband Systems, IWUWB*, June 2003.
3. I. Maravic, M. Vetterli and K. Ramchandran, "High-Resolution Acquisition Methods for Wideband Communication Systems," in *Proc. IEEE Conference on Acoustics, Speech and Signal Processing, ICASSP*, April 2003.
4. J. Kusuma, I. Maravic and M. Vetterli, "Sampling with Finite Rate of Innovation: Channel and Timing Estimation for UWB and GPS," in *Proc. of IEEE Conf. on Communications, ICC*, May 2003.
5. T. Ajdler, R. Cristescu, M. Gastpar, I. Maravic and M. Vetterli, "Distributed Signal Processing and Communications: On the Interaction of Source and Channel Coding," invited paper, In *Proc. of IEEE Conference on Acoustics, Speech and Signal Processing, ICASSP*, April 2003.
6. I. Maravic, M. Vetterli, "Digital DS-CDMA Receiver Working Below the Chip Rate," In *Proc. of Asilomar SSC Conference*, Nov. 2002. Also EPFL Technical Report IC 018/2002.

7. I. Maravic and M. Vetterli, "A Sampling Theorem for the Radon Transform of Finite Complexity Objects," In Proc. of IEEE Conf. on Acoustics, Speech and Signal Processing, ICASSP, May 2002.
8. C. Moser, I. Maravic, B. Schupp and D. Psaltis, "Localized Holographic Recording in Doubly Doped Lithium Niobate," In Proc. of LEOS, November 1999.
9. I. Maravic and A. Marincic, "Precise Methods for Measuring a Laser Beamwidth," In Proc. of ETRAN, November 1998.

Recent Invited Talks

1. "Sampling Methods and High-Resolution Acquisition in Ultra-Wideband Systems," California Institute of Technology, May 2003.
2. "High-Resolution Acquisition Methods for Wideband Communication Systems," University of Michigan, Ann Arbor, May 2003.
3. "Sampling and Bandwidth-Expanding Communication Systems," University of California, Berkeley, September, 2002.
4. "Sampling Signals of Finite Rate of Innovation and Application to Wideband Communication Systems," Berkeley Wireless Research Center, UC Berkeley, August 2002.

THE LITTLE COUSIN SERIES IN MATHEMATICAL SIGNAL PROCESSING

Editor: Martin Vetterli

The Columbia series

1. Karlsson, Gunnar David. *Subband Coding for Packet Video*. CU/CTR/TR 137-89-16, May 1989.
2. Linzer, Elliot Neil. *Arithmetic Complexity and Numerical Properties of Algorithms involving Toeplitz Matrices*. October 1990.
3. Kovačević, Jelena. *Filter Banks and Wavelets: Extensions and Applications*. CU/CTR/TR 257-91-38, September 1991.
4. Uz, Kamil Metin. *Multiresolution Systems for Video Coding*. CU/CTR/TR 313-92-23, May 1992.
5. Radha, Hayder M. Sadik. *Efficient Image Representation using Binary Space Partitioning Trees*. CU/CTR/TR 343-93-23, December 1992.
6. Nguyen, Truong-Thao. *Deterministic Analysis of Oversampled A/D Conversion and Sigma/Delta Modulation, and Decoding Improvements using Consistent Estimates*. CU/CTR/TR 327-93-06, February 1993.
7. Herley, Cormac. *Wavelets and Filter Banks*. CU/CTR/TR 339-93-19, April 1993.
8. Garrett, Mark William. *Contributions toward Real-Time Services on Packet Switched Networks*. CU/CTR/TR 340-93-20, April 1993.
9. Ramchandran, Kannan. *Joint Optimization Techniques in Image and Video Coding with Applications to Multiresolution Digital Broadcast*. June 1993.
10. Shah, Imran Ali. *Theory, Design and Structures for Multidimensional Filter Banks and Applications in Coding of Interlaced Video*. CU/CTR/TR 367-94-14, December 1993.
11. Hong, Jonathan Jen-I. *Discrete Fourier, Hartley, and Cosine Transforms in Signal Processing*. CU/CTR/TR 366-94-13, December 1993.
12. Ortega, Antonio. *Optimization Techniques for Adaptive Quantization of Image and Video under Delay Constraints*. CU/CTR/TR 374-94-21, June 1994.

The Berkeley years

13. Park, Hyung-Ju. *A Computational Theory of Laurent Polynomial Rings and Multidimensional FIR Systems*. Coadv. with Tsit-Yuen Lam, Mathematics, U.C. Berkeley. UCB/ERL M95/39, May 1995.
14. Cvetković, Zoran. *Overcomplete Expansions for Digital Signal Processing*. UCB/ERL M95/114, December 1995.
15. McCanne, Steven Ray. *Scalable Compression and Transmission of Internet Multicast Video*. Coadv. with Van Jacobson, Lawrence Berkeley National Laboratory. UCB/CSD 96/928, December 1996.

16. Goodwin, Michael Mark. *Adaptive Signal Models: Theory, Algorithms, and Audio Applications*. Coadv. with Edward A. Lee, EECS, U.C. Berkeley. UCB/ERL M97/91, December 1997.
17. Goyal, Vivek K. *Beyond Traditional Transform Coding*. UCB/ERL M99/2, September 1998.
18. Chang, Sai-Hsueh Grace. *Image Denoising and Interpolation based on Compression and Edge Models*. Coadv. with Bin Yu, Statistics, U.C. Berkeley. UCB/ERL M99/57, Fall 1998.

The Lausanne time

19. Prandoni, Paolo. *Optimal Segmentation Techniques for Piecewise Stationary Signals*. EPFL 1993(1999), June 1999.
20. Lebrun, Jérôme. *Balancing MultiWavelets*. EPFL 2192(2000), May 2000.
21. Weidmann, Claudio. *Oligoquantization in Low-Rate Lossy Source Coding*. EPFL 2234(2000), July 2000.
22. Balmelli, Laurent. *Rate-Distortion Optimal Mesh Simplification for Communication*. EPFL 2260(2000), September 2000.
23. Marziliano, Pina. *Sampling Innovations*. EPFL 2369(2001), April 2001.
24. Horbelt, Stefan. *Splines and Wavelets for Image Warping and Projection*. EPFL 2397(2001), May 2001.
25. Hasler, David. *Perspectives on Panoramic Photography*. EPFL 2419(2001), July 2001.
26. Do, Minh N. *Directional Multiresolution Image Representations*. EPFL 2500(2001), November 2001.
27. Dragotti, Pier Luigi. *Wavelet Footprints and Frames for Signal Processing and Communications*. EPFL 2559(2002), April 2002.
28. Pecenovic, Zoran. *Integrating Visual and Semantic Descriptions for Effective, Flexible and User-Friendly Image Retrieval*. EPFL 2679(2002), October 2002.
29. Hu, Xiao-Yu. *Low-Delay Low-Complexity Error-Correcting Codes on Sparse Graphs*. EPFL 2681(2002), November 2002.
30. Gastpar, Michael. *To Code Or Not To Code*. EPFL 2687(2002), December 2002.
31. Polotti, Pietro. *Fractal Additive Synthesis*. EPFL 2711(2002), June 2002.
32. Cristescu, Razvan. *Efficient Decentralized Communications in Sensor Networks*, EPFL(2004), March 2004.
33. Shukla, Rahul. *Rate-Distortion Optimized Geometrical Image Processing*., EPFL 2992(2004), May 2004.